ABSTRACT

Title of Document: HIGH REYNOLDS NUMBER VERTICAL UP-FLOW PARAMETERS FOR CRYOGENIC TWO-PHASE HELIUM I

Shouvanik Mustafi, Degree: PhD., 2014

Directed By: Professor Jungho Kim

Department of Mechanical Engineering

The two phase flow characteristics of helium I are of interest since under most operational scenarios this cryogenic fluid exists in both liquid and vapor form because of its extremely low boiling point and latent heat of vaporization. There is a significant knowledge gap in the flow boiling parameters of helium (heat transfer coefficient, pressure drop and dryout heat flux) for high Reynolds number vertical up-flows (Re $=10^5$-10^6). This dissertation fills this gap and helps to expand the use of helium as an inert simulant for hydrogen.

Since no prior correlations for the flow boiling parameters existed for vertical up-flows of helium at these Reynolds numbers, any predictions of these parameters were dependent on correlations that were tested at lower Reynolds numbers, or correlations based on other fluids. The thermophysical properties of helium I are significantly different from most other fluids; therefore the capability of prior correlations in predicting experimental observations was limited. As part of this research new correlations are proposed for the flow boiling parameters. This research begins the

investigation of a new regime for two-phase helium I flows at Reynolds numbers above 3e5. The techniques described will enable future work to address other gaps in knowledge for helium I flows that still remain.

The prior heat transfer coefficient correlation over-predicted the data that was collected for this research. The new correlation improves the agreement with data by a factor of 98. Two prior models for pressure drop, the separated flow model and the homogeneous flow model, under-predict the observed pressure drop. The newer versions of the separated flow and the homogeneous flow correlations improve agreement with the data by about a factor of 3 and by more than a factor of 2 respectively. The previous dryout heat flux correlation considerably over predicts the observed dryout heat flux. The new correlation improves agreement with the data by a factor of 21.

Significant cryogenic challenges were overcome to collect the research data. The strategies described for surmounting the diverse challenges such as thermal acoustic oscillations and low dryout heat flux could be used by future two-phase cryogenic flow researchers.

HIGH REYNOLDS NUMBER VERTICAL UP-FLOW PARAMETERS FOR CRYOGENIC TWO-PHASE HELIUM I

By

Shouvanik Mustafi

Dissertation submitted to the Faculty of the Graduate School of the
University of Maryland, College Park, in partial fulfillment
of the requirements for the degree of
Doctor of Philosophy
2014

Advisory Committee:

Professor Jungho Kim, Chair
Professor Christopher Cadou
Professor Kenneth Kiger
Professor Marino di Marzo
Professor Michael Ohadi

DEDICATION

To those who share their wisdom.

ACKNOWLEDGEMENTS

This dissertation is a culmination of decades of education. Looking back it is clear to me that this body of work would have been impossible without the support and encouragement of the many pillars in my life.

I would like to thank my advisor, Dr. Jungho Kim, for his guidance and for not giving up on me during this lengthy process. I would also like to express my gratitude to the Dissertation Committee and Dr. Radermacher for participating in the review process.

This research was funded by the National Aeronautics and Space Administration (NASA) and the Goddard Space Flight Center (GSFC), and I am grateful to these institutions for recognizing the value of fundamental research in advancing technologies even though these institutions have been operating under challenging budgets during the duration of my research. I would like to express my gratitude to my many colleagues at GSFC who have helped me surmount the challenges that this dissertation presented. I would like to thank Susan Breon and Eric Silk for supporting me and being advocates for me and this body of work. I would like to thank Ed Canavan, John Francis, and Jim Tuttle for their mentorship over many years.

I am fortunate that during various periods in my childhood, Meat Dadu, Babusona Da, Nirmal Kaku, and Anindya Sir shared their wisdom and infected me with a passion for knowledge and the thrill of learning. These four gurus did not have to spend any time challenging a hyperactive child and patiently nurturing his naive curiosity. Yet they found it important to do exactly that – repeatedly and for hours. I strive to pay their gifts forward.

I cherish the support that I received from my friends and extended family to reach this point. It was comforting to have them be welcoming even when I would disappear for months into the depths of my research only to emerge for some fleeting moments.

My parents were my first teachers and they made sure that I realized the value of a good education. My brother was my first rival, my first protector, my first friend, and my first role model. I would like to thank my parents and my brother, and I am grateful that they, along with my Didi, have supported me without any qualms even when I doubted myself.

As the seasons changed and returned and as my hair grayed more permanently, Sudipa shared me with the world of cryogenic research. She did this while braving storms and nourishing souls. Thank you for sharing in my adventures, even the ones that seem foolish.

TABLE OF CONTENTS

LIST OF TABLES

LIST OF FIGURES

NOMENCLATURE

$A_c = \pi d^2/4 \equiv$ Cross Sectional Area [m^2]

$A_t \equiv$ Throat Area of Venturi [m^2]

$Bi = h_{lv} L_c / k \equiv$ Biot Number

$Bo = \dot{q} d_i \Big/ \left(4 \dot{m} L \lambda_{lv} \right) \equiv$ Boiling Number

$Bd = g\left(\rho_l - \rho_g\right) d_h^2 / \sigma \equiv$ Bond Number

$c_{pl} \equiv$ Specific heat at constant pressure of the liquid at saturation [J/(kg.K)]

$c_{pv} \equiv$ Specific heat at constant pressure of the liquid at saturation [J/(kg.K)]

$C_1 \equiv$ Multiplier for Ogato and Sato correlation equation (69)

$C_2 \equiv$ Multiplier for Ogato and Sato correlation equation (69)

$C_D \equiv$ Coefficient of discharge of the venturi

$C_L \equiv$ Multiplier for Ogato and Sato correlation equation (68)

$C_{S1} \equiv$ Term used in definition of Φ_L in equation (16). Defined for both liquid and vapor depending on whether each phase of the flow is laminar or turbulent. See Table 4

$C_{S2} \equiv$ Term used in definition of X in equation (17). Defined for both liquid ($C_{s2,l}$) and vapor ($C_{s2,v}$) depending on the Re_s. See Table 5

$C_{S3} \equiv$ Term used in definition of X in equation (15) and equation (17). Defined for both liquid ($C_{s3,l}$) and vapor ($C_{s3,v}$) depending on the Re_s. See Table 5

$C_{f1} \equiv$ Friction Factor Multiplier used in equation (19)

$C_{f2} \equiv$ Friction Factor Exponent used in equation (19)

$Co = \{(1-x)/x\}^{0.8} \left(\rho_v/\rho_l\right)^{0.5} \equiv$ Convection Number

$d \equiv$ Diameter [m]

$d_h \equiv$ Channel hydraulic diameter [m]

$d_i = 2r_i \equiv$ Inner diameter of heat exchanger [m]

$d_o \equiv$ Outer diameter of the heat exchanger [m]

$d_{PH} \equiv$ Diameter of the pre-heater [m]

$d_{TS} \equiv$ Diameter of the test section [m]

$\mathrm{d}_{\mathrm{VenIn}} \equiv$ Inlet diameter of the venturi [m]

$\mathrm{d}_{\mathrm{VenThroat}} \equiv$ Throat diameter of the venturi [m]

$e \equiv$ Enhancement factor in Chen vorrelation

$E \equiv$ Enthalpy [J/kg]

$E_{PHIn} \equiv$ Pre-heater inlet enthalpy [J/kg]

$\mathrm{f}_{\mathrm{t,l}} \equiv$ Friction Factor if the total flow was liquid

$Fr_{t,l} = 16\dot{m}^2 / \left(\pi^2 d_i^{\,5} \rho_l^{\,2} g \cos\psi\right) \equiv$ Froude Number if the total flow was in the form of a single-phase liquid flowing at the same mass flow rate as the two-phase flow

$f \equiv$ Frequency of oscillation of atom

$g =$ 9.81 m/s^2; Acceleration due to gravity

$G = \dot{m} / A_c \equiv$ Mass Flux [kg/(s. m^2)]

$h_b \equiv$ Heat transfer coefficient due to boiling in the two-phase flow [W/(m^2.K)]

$\mathrm{h}_{\mathrm{correlation}} \equiv$ Heat transfer coefficient calculated by predictive correlation [W/(m^2.K)]

$\mathrm{h}_{\mathrm{experiment}} \equiv$ Heat transfer coefficient measured by experiment [W/(m^2.K)]

$h_l \equiv$ Heat transfer coefficient due to bulk convection in the liquid portion of the two-phase flow [W/(m^2.K)]

$h_{lv} \equiv$ Two-phase liquid vapor heat transfer coefficient that is of interest [W/(m^2.K)]

$h_{t,l}$ ≡ Single-phase heat transfer coefficient if the total flow was in the form of a single - phase liquid flowing at the same mass flow rate as the two-phase flow [W/(m^2.K)]

h_{TS} ≡ Heat transfer coefficient in the test section [W/(m^2.K)]

ħ ≡ Planck's Constant = 6.6e-27erg.s

I ≡ Applied heater current [A]

I_E ≡ Excitation current for Cernox thermometer [A]

Ja ≡ Jacob Number defined in equation (45)

k ≡ Thermal conductivity [W/(m.K)]

L ≡ Length of the heat exchanger [m]

L_c = Volume/ (Surface Area) ≡ Characteristic length of the heat exchanger [m]

L_{TS} ≡ Length of the test section [m]

L_{PH} ≡ Length of the pre-heater [m]

$\dot{m}$ ≡ Total two-phase mass flow rate in heat exchanger [kg/s]

n_1 ≡ Exponent for Ogato and Sato correlation equation (69)

n_2 ≡ Exponent for Ogato and Sato correlation equation (69)

N ≡ Number of data points

P ≡ Pressure [Pa]

P_{TSIn} ≡ Test Section Inlet Pressure [Pa]

$P_{T,Low}$ ≡ Pressure at the Lower Temperature end of the capillary tube [mm of Hg]

$P_{T,High}$ ≡ Pressure at the Higher Temperature end of the capillary tube [mm of Hg]

PH ≡ Pre-heater

P_c ≡ Critical Pressure [Pa]

$P_r = P/P_c \equiv$ Reduced Pressure

$P_{s@T_w} \equiv$ Saturation Pressure at T_w [Pa]

$P_{s@T_f} \equiv$ Saturation Pressure at T_f [Pa]

$Power \equiv$ Power applied to experiment component, eg. pre-heater or test section [W]

$\mathrm{Pr}_l = c_{pl}\mu_l/k_l \equiv$ Prandtl Number of the liquid; Ratio of momentum diffusivity (kinematic viscosity) and thermal diffusivity

$\mathrm{Pr}_v = c_{pv}\mu_v/k_v \equiv$ Prandtl Number of the vapor; Ratio of momentum diffusivity (kinematic viscosity) and thermal diffusivity

$\dot{q} = IV = \mathrm{V}^2/\mathrm{R} \equiv$ Input power [W]

$\dot{\mathrm{q}}_{\mathrm{TS}} \equiv$ Test section heat input [W]

$\dot{\mathrm{q}}_{\mathrm{TS\text{-}Applied}} \equiv$ Test section heater applied power [W]

$\dot{\mathrm{q}}_{\mathrm{TS,Leak}} \equiv$ Test section parasitic heat leak [W]

$\dot{q}'' = \dot{q}/\mathrm{Area} \equiv$ Input heat flux [W/m^2]

$\dot{q}''_{PH} \equiv$ Pre-heater heat flux [W/m^2]

$R \equiv$ Resistance [Ω]

$\mathrm{R}_{\mathrm{PH}} \equiv$ Resistance of pre-heater [Ω]

$\mathrm{R}_{\mathrm{TS}} \equiv$ Resistance of test section heater [Ω]

$\mathrm{R}_0 \equiv$ Atomic separation for a fluid whose properties are dictated by both classical energy and zero-point energy

$\mathrm{R}_0' \equiv$ Atomic separation for a fluid whose properties are dictated only by classical energy

$\mathrm{Re} \equiv$ Reynolds Number

$\mathrm{Re}_{\mathrm{Observe}} \equiv$ Observed Reynolds Number due to fluctuations in flow

$\mathrm{Re}_s \equiv$ Superficial Reynolds Number accounting for portion of the total two-phase flow that is liquid ($\mathrm{Re}_{s,l}$) or a vapor ($\mathrm{Re}_{,v}$).

$\mathrm{Re}_{s,l} = 4\dot{m}(1-x)/(\pi d_i \mu_l) \equiv$ Superficial Liquid Reynolds Number accounting for portion of the two-phase flow that is liquid

$\mathrm{Re}_{s,v} = 4\dot{m}x/(\pi d_i \mu_v) \equiv$ Superficial Vapor Reynolds Number accounting for portion of the two-phase flow that is vapor

$\mathrm{Re}_t \equiv$ Total Reynolds Number if the total two-phase mass flow is in the form of a single –phase liquid ($\mathrm{Re}_{t,l}$) or a single phase vapor ($\mathrm{Re}_{t,v}$).

$\mathrm{Re}_{t,l} = 4\dot{m}/(\pi d_i \mu_l) \equiv$ Reynolds Number if the total flow is in the form of a single-phase liquid flowing at the same mass flow rate as the two-phase flow

$\mathrm{Re}_{t,v} = 4\dot{m}/(\pi d_i \mu_v) \equiv$ Reynolds Number if the total flow is in the form of a single-phase vapor flowing at the same mass flow rate as the two-phase flow

$\mathrm{Re}_{t,v,average} \equiv$ Average $\mathrm{Re}_{t,v}$ for a series of measurements.

$s \equiv$ Suppression Factor in Chen correlation

$S \equiv$ Swirl Number

$t \equiv$ Time [s]

$T \equiv$ Temperature [K]

$\mathrm{T}_{\mathrm{Cernox}} \equiv$ Temperature of Cernox thermometer [K]

$T_{\mathrm{f}} \equiv$ Two-Phase fluid temperature [K]

$T_w \equiv$ Wall temperature of heat exchanger [K]

$\mathrm{T}_{\mathrm{TS\text{-}W}} \equiv$ Test section wall temperature [K]

$\mathrm{T}_{\mathrm{TS\text{-}F\text{-}In}} \equiv$ Fluid temperature at test section Inlet [K]

$TS \equiv$ Test Section

$TT \equiv$ Thermal Transpiration Correction Factor defined in equation (48)

$U \equiv$ Used for Therrmal Transpiration Correction Factor, defined in equation (51)

$V \equiv$ Applied heater voltage [V]

$V_E \equiv$ Excitation voltage for Cernox thermometer [V]

$V_{PH} \equiv$ Voltage of pre-heater [V]

$V_{TS} \equiv$ Voltage of test section heater [V]

$V_{TS\Delta P} \equiv$ Voltage of test section differential pressure gauge [V]

$W \equiv$ Used for Thermal Transpiration correction factor, defined in equation (49)

$x \equiv$ Flow quality = (Vapor Flow Mass)/(Total Flow Mass)

$x_i \geq 0 \equiv$ Inlet flow quality

$x_{mp} = x \text{ at } z = 0.5L \equiv$ Flow quality at the midpoint of the heat exchanger

$x_{\text{Observe}} \equiv$ Observed quality due to fluctuations in flow

$X \equiv$ Martinelli parameter defined in equation (17)

$X_{tt} = \left\{\sqrt{(dP_l/dz)/(dP_v/dz)}\right\}_{tt} \equiv$ Martinelli parameter for turbulent liquid and turbulent vapor flow in a separated flow model of a two-phase flow

$z \equiv$ Axial location along the heat exchanger [m]

$Z \equiv$ Height [m]

$\alpha \equiv$ Void Fraction

$\beta \equiv$ Throat diameter to inlet diameter ratio of venturi

$\kappa \equiv$ Swirl Attenuation Factor

$\delta \equiv$ Accuracy or Uncertainty

$\delta_t \approx k_l/h_{lv} \equiv$ Estimate of thermal boundary layer [m]

$\Delta E_{\text{Subcool To x=0}} \equiv$ Enthalpy gain needed to raise the fluid condition from a subcooled condition to the saturated condition at the inlet [J/Kg]

$\Delta P \equiv$ Differential pressure drop [Pa]

$\Delta P_{TS} \equiv$ Test section pressure drop [Pa]

$\Delta P_{Ven} \equiv$ Venturi pressure drop [Pa]

$\Delta P'_{TS} \equiv$ Test section pressure drop gradient [Pa/m]

$\Delta T = T_W - T_f \equiv$ Temperature difference between wall and flow at heat exchanger [K]

$\gamma_v \equiv$ Ratio of specific heats for the gas; 1.67 for monoatomic gases, 1.4 for diatomic gases, and 1.33 for polyatomic gases

$\lambda_{lv} \equiv$ Latent heat of vaporization [J/kg]

$\mu \equiv$ Viscosity [Pa.s]

$\mu_l \equiv$ Saturated liquid dynamic viscosity [Pa.s]

$\mu_v \equiv$ Saturated vapor dynamic viscosity [Pa.s]

$\upsilon_g \equiv$ Pressure Shifting Factor used in equation (48)

$\rho \equiv$ Density [kg/m^3]

$\rho_l \equiv$ Saturated liquid density [kg/m^3]

$\rho_v \equiv$ Saturated vapor density [kg/m^3]

$\sigma \equiv$ Surface tension of the liquid [N/m]

$\tau_{He} \equiv 2.52$, Contant for thermal transpiration calculation, equation (48)

$\psi \equiv$ Heat exchanger inclination angle from horizontal (positive for up-flow)

$\Phi_L \equiv$ Lockhart Martinelli Correlator defined in equation (16)

$\omega_{He} \equiv$ Used for Thermal Transpiration Correction Factor, defined in equation (50)

1 Introduction:

1.1 Motivation and Knowledge Gap

Helium flowing at a pressure less than its critical pressure (0.23 MPa) almost always flows in a two-phase condition since the boiling point (4.2 K at 1 atm. pressure) and the latent heat of vaporization (20.9 KJ/Kg at 1 atm. pressure) of helium are very low. Helium has the smallest covalent radius of all elements, allowing helium to leak out of or into containment vessels very easily. The combination of these factors has resulted in very limited studies in the flow of helium because of the inherent difficulties and expenses associated in working with helium. Scientists have tended to study helium in the narrow regime of their particular application. Two phase helium flow is most often encountered in liquid helium transfer plumbing between one storage system and another. Two-phase helium is also used as a coolant for superconducting magnet systems such as those found in particle accelerators and Magnetic Resonance Imaging (MRI) machines.

There is a significant gap in knowledge in the flow boiling parameters of helium (heat transfer coefficient, pressure drop and dryout heat flux) for high Reynolds number vertical up-flows ($Re_{t,v}=10^5$-10^6). This dissertation will fill this knowledge gap. The primary reason for this gap has been the lack of need for operations at these high Reynolds numbers and the complexity of making these measurements at these high flow conditions. This research will help to expand the use of helium as an inert simulant for two-phase hydrogen in aerospace applications.

1.2 Application of this Research

One of NASA's applications of helium is as an inert simulant for liquid hydrogen. Both helium and hydrogen are quantum fluids (Section 1.4.1) and hence liquid helium is a reasonable simulant for liquid hydrogen. An effort is underway at NASA to demonstrate subcooling of

liquid hydrogen on the launch pad as a technique for long-term storage of hydrogen. [1] The large quantity of liquid hydrogen that needs to be subcooled in a short duration has prompted the need for heat exchangers that can accommodate high Reynolds number two-phase flows of hydrogen. The flow parameters, such as the heat transfer coefficient and the pressure drop necessary to design a high Reynolds number two phase cryogenic heat exchanger are not available for either hydrogen or helium. This dissertation aids in the design of an appropriate heat exchanger.

The use of cryogenic propellants is crucial for exploration of the solar system because of their superior specific impulse (I_{sp}) capability. Future missions will require vehicles with the flexibility to remain in space for months to years, necessitating long-term storage of these cryogens. One powerful technique for easing the challenge of cryogenic fluid storage is to subcool them below their boiling point at atmospheric pressure prior to launch. Propellants such as liquid hydrogen have large heat capacities. The heating of the chilled cryogens allows them to absorb the energy that leaks into the tank even with the use of the best insulation systems. During this period of heating of the subcooled cryogen there will be minimal need to vent the cryogen, thus extending its in-space vent-free 'hold-time'. This technique can substantially extend the orbital and transit storage of the cryogenic propellants. [2]

It is difficult to chill cryogens while they are in an ambient 300 K environment. In recent years a new technique has been proposed that uses the thermodynamic capabilities of the stored cryogen itself to carry out subcooling using a system known as the Thermodynamic Cryogen Subcooler (TCS). The TCS consists of valves, pumps, compressors and heat exchangers along with insulation enhancements to the subcooled propellant tank and the TCS. The power and footprint requirement will be significantly less than that of previously proposed launch-pad

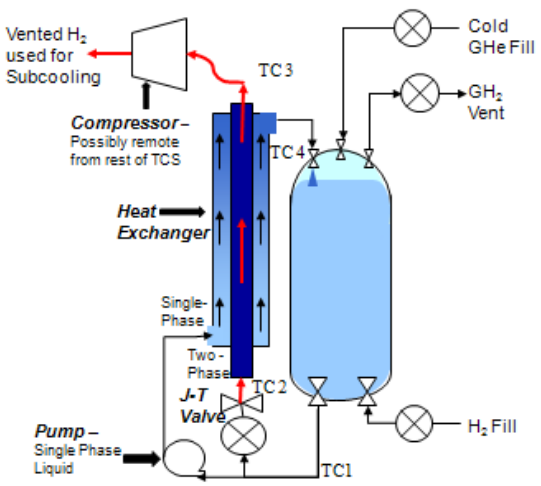

Figure 1: The TCS concept for isobaric subcooling of cryogens on the launch pad.

coolers of various configurations. In addition this system can be used to maintain or further lower the thermodynamic condition of the cryogen that is delivered to the launch pad, even if it has previously been densified or subcooled. There will be minimal addition to the launched mass as the entire TCS will be ground support equipment (GSE).

Figure 1 shows a notional configuration for the TCS that is being proposed for a launch pad subcooling system. The hydrogen that is being subcooled, will be extracted from the tank. Some of this extracted hydrogen will be passed through a Joule-Thomson (J-T) valve that isenthalpicly expands the hydrogen. The hydrogen on the upstream side of the J-T valve, at thermodynamic condition 1 (TC 1), will be at the temperature of the hydrogen in the tank (initially 20.4 K). The hydrogen on the downstream side of the J-T valve (TC 2) will have the same enthalpy as the hydrogen on the upstream side, but at a lower pressure (~0.1 atm.) and substantially lower temperature (~15 K). While going through this expansion the hydrogen at TC 2 becomes a two-phase fluid. Most of the liquid hydrogen extracted from the tank at TC 1 will be pumped into the outside tube of a concentric tube heat exchanger - the single-phase tube. The two-phase hydrogen at TC 2 is passed into the center tube of the concentric tube heat exchanger

— the two-phase tube. Since the hydrogen in the two-phase tube is at a lower temperature than the hydrogen in the single-phase tube it can extract heat from the hydrogen in the single-phase tube and thus subcool the propellant. The two-phase hydrogen will increase in vapor quality along the two-phase tube and is vented (TC 3) to a flare stack through a compressor system. The subcooled hydrogen at the end of the single-phase tube (TC 4) is then fed back into the hydrogen tank. The portion of liquid hydrogen that is expanded through the J-T device and vented will be replaced by a supply of make-up liquid hydrogen to fill and maintain a full tank. As the bulk hydrogen in the tank is subcooled by this process, its density increases so the tank will be backfilled with non-condensable cold helium in order to prevent the tank from experiencing a compressive atmospheric load. The TCS components will be isolated from parasitic heat inputs by using a vacuum outer jacket and multi-layer insulation (MLI). By using the cooling enthalpy available in the cryogen that is being stored the need for a power intensive high-capacity refrigeration system is diminished. [2]

A major component of the TCS is the heat exchanger which will transfer heat from the higher temperature recirculated single-phase liquid cryogen that is being subcooled to the vented lower temperature two-phase cryogen that is performing the cooling. The performance of the heat exchanger will determine the mass and size parameters of the TCS, which are important for the appropriate packaging of this system on the launch pad. An actual TCS would probably consist of a bank of concentric tube heat exchangers that would allow the TCS to be packaged compactly. [2]

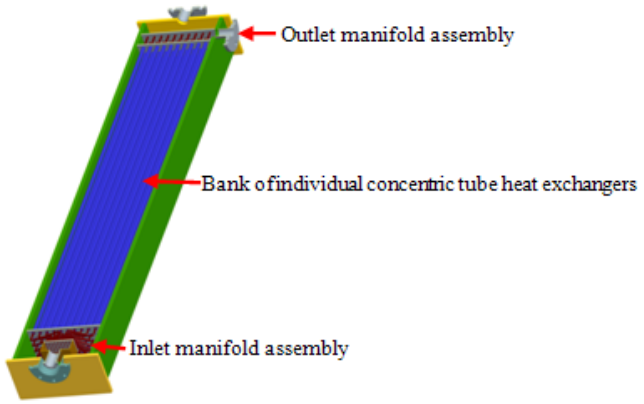

Figure 2: A notional TCS heat exchanger with a bank of concentric tube heat exchangers.

Figure 2 depicts a notional TCS heat exchanger with a bank of individual concentric tube heat exchangers with a manifold splitting the flows near the inlet and another manifold rejoining the flows near the outlet. For a large upper stage sized tank about 35 tons of hydrogen will have to be subcooled within a 12 hour period, leading to the necessity for high Reynolds number flows (10^5 – 10^6) through the heat exchanger to achieve a reasonably compact design. In the future these concentric heat exchangers may provide a baseline for more advanced compact heat exchangers that are difficult to model and scale. [1]

1.3 Objectives and Proposed Work

The focus of this research was the study of two-phase flow parameters necessary to design a high Reynolds number two phase cryogenic heat exchanger. As with most fluids there are many factors that affect the flow boiling characteristics of helium: Reynolds number, vapor quality, flow regime, operating pressure, etc. Studying the effects on flow boiling of these factors is complicated by the thermophysical properties of helium. For example, it is challenging to study flow boiling parameters with the same hardware as a flow-regime visualization experiment, since almost any attempt to perform this visualization will affect the thermodynamic state of the flowing helium. In order to do the flow visualization for two-phase helium the hardware would have to be first characterized to determine the heat flux that is being absorbed

by the flow, since the radiative flux incident on the flow could be on the same order of magnitude as the latent heat of vaporization of the helium. This dissertation serves as the first effort to study vertical up-flows for two-phase helium above $Re_{t,v} > 3x10^5$.

There were three objectives associated with this research:

1. Measure the heat transfer coefficient for high Reynolds number ($Re_{t,v} > 3x10^5$) two-phase vertical flow of cryogenic helium.
2. Measure pressure drop for high Reynolds number ($Re_{t,v} > 3x10^5$) two-phase vertical flow of cryogenic helium.
3. Measure the dryout heat flux for high Reynolds number ($Re_{t,v} > 3x10^5$) two-phase flow of cryogenic helium.

1.4 Background and Theory

1.4.1 Properties of Liquid Helium – The effect of Zero-Point Energy

Property	Helium	Nitrogen	Water
Normal Boiling Point (NBP) Temperature [K]	4.22	77.35	373.12
Density Liquid - NBP [kg/m^3]	124.96	806.08	958.37
Density Vapor - NBP [kg/m^3]	16.70	4.61	0.60
Viscosity Liquid - NBP [kg/(m.s)x10^6]	3.17	160.66	281.66
Viscosity Vapor - NBP [Kg/(m.s)x10^6]	1.24	5.44	12.23
Surface Tension - NBP [N/m]	0.00009	0.00887	0.05892
Heat of Vaporization - NBP [kJ/kg]	20.91	199.18	2256.47
Thermal Conductivity - NBP [mW/(m.K)]	18.65	144.77	679.08
Heat Capacity - Isobaric - NBP (C_p) [kJ/(kg.K)]	5.11	2.04	4.22
Heat Capacity - Isochoric - NBP (C_v) [kJ/(kg.K)]	2.40	1.08	3.77

Table 1: Comparison of Thermophysical properties of helium with other fluids

Table 1 compares the thermophysical properties of helium to nitrogen and water. It is valuable to note the unusually low liquid density, low normal boiling point of helium as well as its unusually low heat of vaporization. The normal boiling point of water is more than 88 times greater than that of helium and the latent heat of vaporization of water is nearly 108 times greater than that of helium. These properties dramatically affect the flow boiling characteristics of liquid helium when compared with other fluids and even other cryogens, such as nitrogen. The thermophysical properties of helium are unusual because of its behavior as a quantum fluid.

According to classical theory the lack of thermal energy at a temperature of absolute zero (0 K) implies that a perfect static balance is achieved between the electromagnetic attractive and repulsive forces on the atoms. This would result in each atom being perfectly motionless and having no kinetic energy. Quantum theory, on the other hand, states that each atom has an irreducible minimum kinetic energy, which is known as the zero-point energy, given by the quantity $(0.5\hbar f)$, where $\hbar$ is Planck's constant, and f is the oscillation frequency of the atom. The

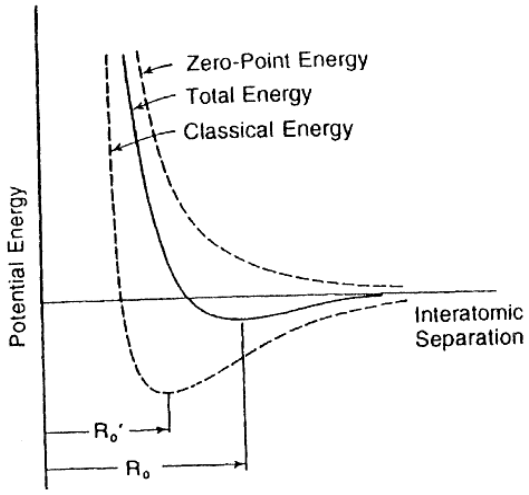

Figure 3: The effect of zero-point energy on atomic separation. [3]

classical energy represents the attractive lattice forming forces of the substance and the zero-point energy represents the repulsive phase altering forces in the substance. The total energy of substances is given by the balance of the classical energy forces and zero-point energy forces. For most substances the classical energy forces dominate the zero-point energy forces. However, for three substances - helium, hydrogen, and neon – at low temperatures the zero-point energy becomes a significant fraction of the total energy. The quantum mechanical, zero-point energy, property of these substances leads to macroscopic effects on their thermophysical properties and are thus referred to as quantum fluids. These fluids do not follow the behavior of normal fluids which are well defined by generalized equations of state. [3]

Figure 3 shows a representative plot of the variation of intermolecular potential energy with interatomic separation. The potential energy is a measure of the temperature. Above the horizontal axis the coulombic repulsive phase-changing forces dominate the interaction between the molecules. Below the horizontal axis, the gravitational attractive lattice forming forces between the molecules dominates. The lower dashed curve represents the property of a fluid under the influence of just the classical energy. The upper dashed curve represents the property of a fluid under the influence of just the zero-point energy. The solid curve represents the actual fluid property and shows the total energy variation with interatomic separation as an average of the classical energy and the zero-point energy properties. R_0' is the atomic separation for a fluid whose properties are dictated only by classical energy. R_0 is the actual atomic separation that results from the addition of the zero point energy to the classical energy. The zero point energy effectively increases the atomic separation that would be observed if only classical energy was governing the atomic separation. As the zero-point energy increases relative to the classical

energy the atomic separation increases as well. This is the reason why quantum fluids have very low densities as liquids. [3]

Figure 3 also shows the effect of zero-point energy in reducing the depth of the potential well of the substance. The “well” region, below the horizontal axis represents the saturation conditions of the fluid. It is only in this region that the fluid can exist in two different densities (interatomic separation) for the same potential energy (temperature). The depth of the potential well is proportional to the latent heat of vaporization or sublimation of the fluid. The zero-point energy effectively decreases the depth of the potential well from what it would be if the fluid properties were dominated by just classical energy. Reducing the depth of the well reduces the temperature range over which saturated conditions are possible by reducing the binding energy between the atoms and thereby reducing the boiling point and latent heat of vaporization of the fluid. The low latent heats of vaporization of quantum fluids are a manifestation of their relatively high zero-point energies. [3]

There are many remarkable effects of zero-point energy on helium apart from its low density and low latent heat of vaporization. Liquid helium demonstrates a high degree of compressibility. Unlike other substances, helium does not have a triple point (the solid-liquid-vapor equilibrium coexistence point). Instead of turning into a solid as the temperature of liquid helium-4 (the most common isotope of helium) is reduced, at 2.17 K, the liquid helium changes into a unique form of liquid. Above 2.17 K, the helium is known as helium I and below 2.17 K, the helium is known as helium II. Helium II has zero viscosity and an anomalously large thermal conductivity which give its remarkable qualities as a superfluid. The large zero-point energy of helium keeps the interatomic separation of helium so large that it does not fall into a solid lattice structure unless it subject to a pressure of 25 atm. [3]

This research has only investigated high Reynolds number flows in liquid helium I. Although the really counterintuitive manifestations of helium's high zero-point energy are observed in helium II, the manifestations of the high zero-point energy in helium I, such as the low density, low boiling point and low latent heat of vaporization also dramatically influences the macroscopic flow parameters that were investigated in this research.

1.4.2 Flow Boiling Regimes

Figure 4 depicts the flow regimes and boiling mechanisms for a typical vertical up-flow. The flow regimes and boiling mechanism are similar to horizontal boiling flows. When the liquid enters the tube at the bottom it is heated up to its saturation temperature at the local pressure by a single phase heat transfer mechanism. As the fluid temperature at the wall rises permitting

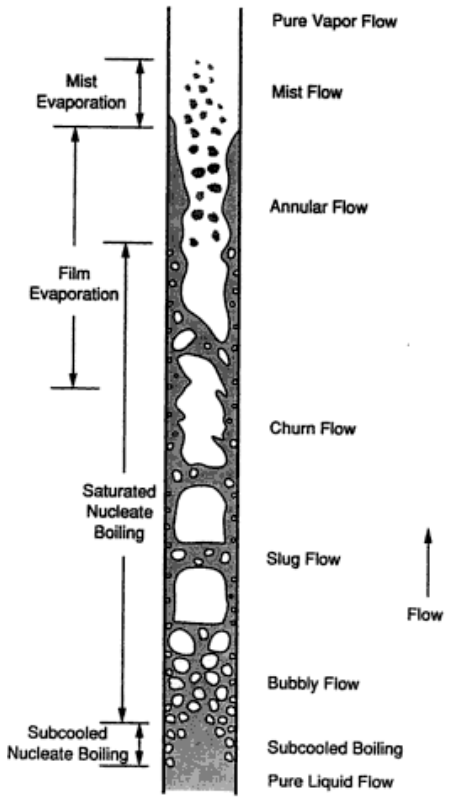

Figure 4: Flow regimes and boiling mechanisms for vertical up-flow boiling. [4]

nucleation, bubbly flow starts as subcooled boiling initiates where the bulk core fluid is still subcooled while fluid near the walls warms up sufficiently to change phase and form bubbles. As the bulk fluid continues to warm to saturation conditions saturated nucleate boiling results in larger bubbles that coalesce to form slug flow and churn flow conditions. With further heating these conditions result in annular flow where a combination of saturated nucleate boiling and film evaporation become important. As the thickness of the annular liquid continues to drop with further evaporation film evaporation becomes dominant. As this vaporization continues, droplets are sheared from the annular film and the film at the wall is dried out leaving an entrained mist of droplets. This condition is known as 'dryout'. Dryout for most liquids happen at moderate to high qualities. Under these conditions it is possible for the vapor around the wall to become superheated while there are droplets of liquid entrained in the vapor. Convection, radiation and droplet collision with the wall eventually result in the mist evaporation in the final stage of vaporization in a vertical tube. [4, 5]

1.4.3 Cryogenic Flow Boiling Heat Transfer and Pressure Drop

In two phase flows there are four different types of flow that are possible: laminar liquid-laminar vapor ($Re_{s,l}<2300$ and $Re_{s,v}<2300$), laminar liquid –turbulent vapor ($Re_{s,l}<2300$ and $Re_{s,v}\geq2300$), turbulent liquid –laminar vapor ($Re_{s,l}\geq2300$ and $Re_{s,v}<2300$), and turbulent liquid – turbulent vapor ($Re_{s,l}\geq2300$ and $Re_{s,v}\geq2300$). This dissertation focused on very high Reynolds number ($Re_{t,v} >3x10^5$) flows where unless the flow quality is extremely close to being completely liquid (x=0) or completely vapor (x=1), the flow will almost always be a turbulent liquid-turbulent vapor type of flow.

1.4.4 Background on cryogenic flow boiling heat transfer correlation at low Reynolds Numbers

In 2001 Van Dresar, Siegwarth, and Hasan proposed correlations specifically for two-phase cryogenic hydrogen and nitrogen flows under horizontal and near horizontal low Reynolds number conditions. They proposed correlations for two flow conditions – laminar liquid/laminar vapor and laminar liquid/turbulent vapor. Equation (1) shows that the fluid quality at the axial location, z, of a heat exchanger can be estimated given a known inlet quality, known input power and a known mass flow rate. [6, 7]

$$x(z) = x_i + \frac{\dot{q}\, z}{\dot{m} L \lambda_{lv}} \tag{1}$$

For the Van-Dresar study, the flow quality at the midpoint of a test section, x_{mp}, was computed by assuming that z is at the midpoint of the test section, and that the fluid at the inlet of the heat exchanger is two-phase (i.e. $x_i \geq 0$). For the Van Dresar experiment the test section was 26 cm long, so a single-point heat transfer coefficient measurement was made at z = 13 cm.

For a laminar liquid/laminar vapor flow Van Dresar correlation is given by equation (2):

$$h_{lv} = 323 \frac{k_l}{d_i} \left[\left(\frac{\rho_v}{\rho_l} \right) \left(\frac{\mu_l}{\mu_v} \right) \left(\frac{1 - x_{mp}}{x_{mp}} \right) \right]^{-0.31} Fr_{t,l}^{0.18} \tag{2}$$

The rms averaged prediction error was within 12% for nitrogen and hydrogen data.

The laminar liquid/turbulent vapor flow Van Dresar correlation is given by equation (3):

$$h_{lv} = 363\frac{k_l}{d_i}\left[\left(\frac{x_{mp}\dot{m}d_i}{\mu_v}\right)\left(\frac{\rho_v}{\rho_l}\right)\left(\frac{\mu_l}{\mu_v}\right)\left(\frac{1-x_{mp}}{x_{mp}}\right)\right]^{-0.14} Fr_{t,l}^{0.07} \quad (3)$$

The rms averaged prediction error for equation (3) was within 15% for nitrogen and hydrogen data. [6, 7]

The Van Dresar horizontal correlations have been validated for nitrogen ($5300 \leq Re_{t,v} \leq 54{,}000$) and hydrogen ($2400 \leq Re_{t,v} \leq 23{,}000$). The correlations for the up-flowing high Reynolds number ($3.27e5 \leq Re_{t,v} \leq 1.51e6$) turbulent liquid - turbulent vapor helium that was studied for this dissertation are significantly different from the Van Dresar correlations. [6, 7]

1.4.5 Background on cryogenic flow boiling heat transfer coefficient at higher Reynolds Numbers

In 1966, Chen proposed that flow-boiling heat transfer coefficients can be thought of as having contributions from the macroscopic heat transfer due to bulk convection of the liquid portion of the two-phase flow, h_l, and the microscopic heat transfer due to boiling of the flow, h_b. Chen introduced an enhancement factor, e >1, to account for increased heat transfer due to higher fluid velocities in two phase flow when compared to single phase liquid flow. In two-phase flow the density of the vapor is lower than the density of the liquid, so to maintain the same mass flow rate as the single phase liquid flow, the two-phase flow has to have a higher velocity. Chen also introduced a suppression factor, s <1, to account for decreased effective superheat in flow boiling when compared to pool nucleate boiling. The Chen correlation is given by equation (4) [4, 9-14]

$$h_{lv} = eh_l + sh_b \tag{4}$$

In equation (4) h_l can be estimated by the Dittus-Boelter equation, given by equation (5) [8-11]

$$h_l = 0.023\left[\mathrm{Re}_{t,l}(1-x)\right]^{0.8} \mathrm{Pr}_l^{0.4}\, k_l / d_i \tag{5}$$

Originally e and s were presented as graphs, but later equations were developed to fit the graphs by Bergles [11]. The boiling heat transfer coefficient, h_b, can be obtained from the Forester-Zuber pool boiling equation which is given by equation (6) [11]

$$h_b = 1.22\times10^{-3} \frac{k_l^{0.79} c_{pl}^{0.45} \rho_l^{0.49}}{\sigma^{0.5} \mu_l^{0.29} \lambda_{lv}^{0.24} \rho_v^{0.24}} \left[\left(T_w - T_\mathrm{f}\right)^{0.24} \left(P_{s@T_w} - P_{s@T_\mathrm{f}}\right)^{0.75}\right] \tag{6}$$

The Chen correlation, which is based on non-cryogenic fluid data, has been reported to greatly under-predict the data for cryogens such as nitrogen, hydrogen and helium [9]. More recent work by Liu-Winterton in 1991 has proposed a variation of the Chen correlation for higher Reynolds number horizontal flows given by equation (7)

$$h_{lv} = \left[\left(eh_l\right)^2 + \left(sh_b\right)^2\right]^{1/2} \tag{7}$$

Steiner has proposed a further variation of this correlation for vertical flows in their asymptotic model given by equation (8). [10]

$$h_{lv} = \left[\left(eh_l \right)^3 + \left(sh_b \right)^3 \right]^{1/3} \tag{8}$$

Other work by Shah [9], Gungor- Winterton [11], and Li-Wu [12] has focused on empirical correlations that are functions of the convection number, the boiling number, the Bond number and the Froude number, and are of the form shown in equation (9). [9, 11, 12]

$$\frac{h_{lv}}{h_{t,l}} \equiv fn\left(Co, Bo, Bd, Fr_{t,l} \right) \tag{9}$$

The convection number correlates to the convection component, the boiling number the boiling component, the Bond number corresponds to the ratio of gravitational forces to surface tension forces and the Froude number corresponds to the flow orientation.

It is important to note that the above correlations by Chen, Gungor-Winterton, Liu-Winterton, Li-Wu, Steiner and Shah are based on curve-fits for a large variety of fluids. These correlations are not specific to vertical up-flows of helium. However, a comparative study of several heat transfer correlations for horizontal flow boiling of two other cryogens, argon and nitrogen, was discussed by Liu-Winterton. [8] A comparison of these correlations is presented in Table 2 to provide an approximate sense of the accuracy of these correlations when describing a real system. Table 2 shows the percentage mean and average deviation of the predicted two-phase cryogenic flow boiling heat transfer coefficient from experimental data as presented by Liu-Winterton. The mean deviation gives an assessment of the average magnitude of the deviation of the data from the correlation, and the average deviation gives an assessment of the

average magnitude of the over-prediction or under-prediction of the correlation. The mean deviation and the average deviation are given by equations (10) and (11) respectively. [8]

$$\text{Mean Deviation} = \frac{1}{N}\sum_{i=1}^{N}\frac{\left|h_{\text{correlation}} - h_{\text{experiment}}\right|}{h_{\text{experiment}}}\times 100\% \tag{10}$$

$$\text{Average Deviation} = \frac{1}{N}\sum_{i=1}^{N}\frac{[h_{\text{correlation}} - h_{\text{experiment}}]}{h_{\text{experiment}}}\times 100\% \tag{11}$$

Although the Shah correlation has the lowest average deviation for argon, the Liu – Winterton correlation has the lowest mean deviation. For nitrogen the Liu-Winterton correlation again has the lowest mean deviation. Unfortunately, none of the correlations seem to be good predictors of either argon or nitrogen flow boiling heat transfer coefficients, although the Liu-Winterton correlation can be considered the best available predictor of horizontal cryogenic flow boiling heat transfer coefficient.

	Argon		**Nitrogen**	
Correlation	**Mean [%]**	**Average [%]**	**Mean [%]**	**Average [%]**
Chen (1966)	76.2	72.5	39.4	3.2
Shah (1984)	28.5	1.6	41	-28.6
Gungor-Winterton (1987)	31.4	10.5	34.4	-21.1
Liu-Winterton (1991)	25.3	9.4	31.7	-4.1

Table 2: Deviations of two-phase cryogenic flow boiling heat transfer coefficients from experiment

The studies highlighted above for argon and nitrogen were in a horizontal orientation. The majority of the published data for higher Reynolds number vertical two-phase helium up-flows was obtained by Keilin [15], and Ogato and Sato [16]. Table 3 shows the published ranges of their data.

Helium Up-flow Data Set	$Re_{t,v}$	x
Keilin (1975)	12,000-62,000	0-0.81
Ogato and Sato (1974)	73,000-185,000	0.02-0.95

Table 3: Range of published higher Reynolds Number helium vertical up-flow data

The Reynolds number range that was investigated in this research is for 3.27e5≤ $Re_{t,v}$≤1.51e6. The most comprehensive study of heat transfer coefficient in vertical up-flows of helium was performed by Ogato and Sato for 7.3e4≤ $Re_{t,v}$≤1.85e5. Their study explored the variation of heat transfer coefficient through the largest range of quality and proposed a relevant model. Ogato and Sato proposed that the heat transfer could be approximated as single phase forced convection for liquids in a low quality regime and for vapor in high quality regimes. In this approximation the heat transfer coefficient is a reduced form of the conventional single phase convection correlation given by equation (12):

$$h_{lv} = 0.015\,\mathrm{Re}^{0.8}\,\mathrm{Pr}^{0.4}\,k/d_i \tag{12}$$

Here, Re = $Re_{s,l}$, k =k_l and Pr = Pr_l for x<0.25 and Re = $Re_{s,v}$, k=k_v and Pr = Pr_v for x>0.75

For the intermediate qualities, $0.25 \leq x \leq 0.75$, Ogato and Sato proposed the correlation in equation (13):

$$h_{lv} = \left(X_{tt}^{-0.66} + 1.5e3Bo^{0.8}\right)h_{t,l} \tag{13}$$

Here, $h_{t,l}$ is derived from equation (12) assuming the entire flow is liquid.

1.4.6 Background on cryogenic flow boiling Pressure Drop at higher Reynolds Numbers

Two-phase liquid-vapor flow has been modeled based on its treatment as either a separated flow or a homogeneous flow. The separated flow model assumes that the two phases are artificially separated into two different streams. The velocities of the vapor and the liquid are not necessarily equal in this model although thermodynamic equilibrium is assumed. The pressure drop and heat transfer in the separated flow model is described by the Lockhart-Martinelli correlations. The separated flow model is generally most accurate for flows with a high-velocity-gas-core surrounded by a liquid film (annular flow). In the homogeneous flow model the two-phase flow is considered to be a single fluid with appropriate mean fluid properties. The vapor and liquid velocities are considered to be equal and the two phases are considered to be in thermodynamic equilibrium. The homogenous model generally is most accurate for very low quality (bubble flow) or high quality flow (mist flow). Both models evaluate the pressure drop as a combination of three pressure drops, the frictional pressure drop, the momentum pressure drop, and the elevation pressure drop, as shown in equation (14). The momentum pressure drop and the frictional pressure drop will vary depending on which model is being used. [4, 5]

$$\Delta P = \Delta P_{Friction} + \Delta P_{Momentum} + \Delta P_{Elevation} \tag{14}$$

1.4.7 Separated Flow Model

The Separated Flow Model is derived on the basis of the Lockhart and Martinelli correlations. The two-phase frictional pressure drop gradient for separated flow is given by equation (15):

$$\left(\Delta P/\Delta L\right)_{Friction,s} = \left(1-x\right)^{\left(2-C_{s3}\right)}\left(\Phi_L\right)^2\left(\Delta P/\Delta L\right)_{t,l} \tag{15}$$

The term Φ_L can be derived from equation (16):

$$\Phi_L = \left[1+\left(C_{S1}/X\right)+\left(1/X^2\right)\right]^{1/2} \tag{16}$$

X is the Martinelli parameter and is defined by equation (17):

$$X = \left[\frac{C_{S2,l}\left(\mathrm{Re}_{s,v}\right)^{C_{S3,v}}\rho_v}{C_{S2,v}\left(\mathrm{Re}_{s,l}\right)^{C_{S3,l}}\rho_l}\left(\frac{1-x}{x}\right)^2\right]^{1/2} \tag{17}$$

Table 4 defines C_{S1} for the Lockhart-Martinelli Correlator (Φ_L) in equation (16):

$\mathbf{Re_{s,l}}$	$\mathbf{Re_{s,v}}$	$\mathbf{C_{S1}}$
< 2300	< 2300	5
≥ 2300	< 2300	10
< 2300	≥ 2300	12
≥ 2300	≥ 2300	20

Table 4: C_{S1} in Lockart-Martinelli Correlator, Φ_L

Table 5 defines C_{S2} and C_{S3} in the Martinelli Parameter (*X*) in equation (17) for both the liquid and vapor portions of the flows based on the superficial Reynolds number.

	$Re_s < 2300$	$2300 \leq Re_s < 50{,}000$	$Re_s \geq 50{,}000$
C_{S2}	64	0.316	0.184
C_{S3}	1	0.25	0.2

Table 5: C_{S2} and C_{S3} in Martinelli Parameter, *X*

The pressure drop gradient if the entire flow were liquid that is used in equation (15) is given by equation (18):

$$\left(\frac{\Delta P}{\Delta L}\right)_{t,l} = \frac{f_{t,l} G^2}{2\rho_l d} \tag{18}$$

The friction factor, $f_{t,l}$, is defined by equation (19):

$$f_{t,l} = C_{f1}\left(Re_{t,l}\right)^{C_{f2}} \tag{19}$$

The terms C_{f1} and C_{f2} vary according to the Reynolds number as depicted in Table 6.

	$Re_{t,l} < 2300$	$3500 \leq Re_{t,l} < 20{,}000$	$Re_{t,l} \geq 20{,}000$
C_{f1}	64	0.316	0.184
C_{f2}	-1	-0.25	-0.2

Table 6: C_{f1} and C_{f2} in Friction Factor, $f_{t,l}$

For $2300 \leq Re_{t,l} < 3500$ the friction factor can be estimated by taking the average of the what is obtained by using equation (19) and applying the C_{f1} and C_{f2} for $Re_{t,l} < 2300$ and the C_{f1} and C_{f2} for $3500 \leq Re_{t,l} < 20{,}000$.

The two-phase separated flow momentum pressure drop is given by equation (20).

$$\Delta P_{Momentum,s} = \Phi_M \frac{G^2}{\rho_l} \tag{20}$$

The momentum pressure drop parameter, $\Phi_{M,}$ is calculated using equation (21)

$$\Phi_M = \frac{(1-x_{outlet})^2}{(1-\alpha_{outlet})} - \frac{(1-x_{inlet})^2}{(1-\alpha_{inlet})} + \rho_L \left[\frac{(x_{outlet})^2}{\alpha_{outlet}\rho_{v,outlet}} - \frac{(x_{inlet})^2}{\alpha_{inlet}\rho_{v,inlet}} \right] \tag{21}$$

The void fraction, α , is given by equation (22)

$$\alpha = 1 - \left[1 + (C_{s1}/X) + (1/X)^2 \right]^{-1/2} \tag{22}$$

The two-phase separated flow elevation pressure drop is given by equation (23)

$$\Delta P_{Elevation,s} = g\left(\rho_{ms,outlet} Z_{outlet} - \rho_{ms,inlet} Z_{inlet}\right) \tag{23}$$

The mean density for separated flow of the two-phase fluid can be related to the void fraction as shown in equation (24)

$$\rho_{ms} = \rho_v \alpha + \rho_l (1-\alpha) \tag{24}$$

Using equations (15), (20), and (23) in equation (14) it is possible to estimate the pressure drop using the separated flow model. [5]

1.4.8 Homogeneous Flow Model

Another technique for estimating the pressure drop is to use the homogeneous flow model. Appropriate mean flow properties are used with single-phase correlations for the homogeneous model. [5]

The frictional pressure drop gradient is given by equation (25)

$$\left(\frac{\Delta P}{\Delta L}\right)_{Friction,h} = \frac{f_h G^2}{2\rho_{mh} d} \tag{25}$$

The friction factor, f_h, is defined by equation (26)

$$f_h = C_{H1}\left(Re_h\right)^{C_{H2}} \tag{26}$$

The terms C_{H1} and C_{H2} vary according to the Reynolds number as depicted in Table 7.

	$Re_h < 2300$	$3500 \leq Re_h < 20{,}000$	$Re_h \geq 20{,}000$
C_{H1}	64	0.316	0.184
C_{H2}	-1	-0.25	-0.2

Table 7: C_{H1} and C_{H2} in Friction Factor, f_h

For $2300 \leq Re_h < 3500$ the friction factor can be estimated by taking the average of what is obtained by using equation (26) and applying the C_{h1} and C_{h2} for $Re_h < 2300$ and the C_{h1} and C_{h2} for $3500 \leq Re_h < 20{,}000$.

The mean density for homogeneous flow of the two-phase fluid is calculated using equation (27):

$$\rho_{\mathrm{mh}} = \frac{\rho_v \rho_l}{\rho_v (1-x) + \rho_l x} \tag{27}$$

The mean viscosity for homogeneous flow of the two-phase fluid is calculated using equation (28):

$$\mu_{\mathrm{mh}} = \frac{\mu_v \mu_l}{\mu_v (1-x) + \mu_l x} \tag{28}$$

The Reynolds number for homogeneous flow of the two-phase fluid is calculated using equation (29):

$$\mathrm{Re}_h = 4\dot{m} / (\pi d \mu_{mh}) \tag{29}$$

The two-phase homogeneous flow momentum pressure drop is given by equation (30):

$$\Delta P_{Momentum,h} = \frac{G^2 (x_{outlet} - x_{inlet})}{\rho_l} \left(\frac{\rho_l}{\rho_v} - 1 \right) \tag{30}$$

The two-phase homogeneous flow elevation pressure drop is given by equation (31)

$$\Delta P_{Elevation,h} = g (\rho_{mh,outlet} Z_{outlet} - \rho_{mh,inlet} Z_{inlet}) \tag{31}$$

Using equations (25), (30) and (31) in equation (14) it is possible to obtain the Pressure Drop Gradient for the homogeneous flow model. [5]

1.4.9 Background on Dryout Heat Flux

As described in section 1.4.2 it is possible that a dryout heat flux condition may be encountered in the pre-heater. Attempts have been made by Kutateladze and Collier to provide a correlation this phenomenon. [4, 5]

The dryout heat flux for a given quality is given by equation (32)

$$\dot{q}''_{dryout} = (1-x)\dot{q}''_{dryout,x=0} \tag{32}$$

The dryout heat flux at zero quality is given by equation (33):

$$\dot{q}''_{dryout,x=0} = \mathrm{C}_{\mathrm{Dryout}}\rho_v\lambda_{lv}\left[\frac{g\sigma_l(\rho_l-\rho_v)}{(\rho_v)^2}\right]^{1/4}\left[\frac{G}{\rho_{mh}}\left(\frac{\rho_l-\rho_v}{g\sigma_l}\right)^{1/4}\right]^{1/2} \tag{33}$$

In Kutateladze's correlation, $\mathrm{C}_{\mathrm{Dryout}} = 0.023$. [5]

1.5 Contributions of this Research

There has been very little work done on cryogenic flow boiling heat transfer. The major contribution of this dissertation was in reducing the lack of knowledge in two-phase up-flows parameters for helium I. The objective was to gain a better understanding of high Reynolds number helium internal flow boiling parameters by measuring the heat transfer coefficient and pressure drop for a range of flow qualities at high Reynolds numbers ($3.27e5 \leq \mathrm{Re}_{t,v} \leq 1.51e6$).

The study of these parameters will be very important for the design of two-phase cryogenic heat exchangers.

1.5.1 Research Contribution from Objective 1: Measure the High Reynolds Number Vertical Up-Flow Heat Transfer Coefficient for Two-Phase Helium

A few studies have been carried out for horizontal flow boiling at higher Reynolds numbers for argon and nitrogen. The correlation proposed by Liu-Winterton maps the available data the closest. Even fewer studies have been carried out for vertical flow boiling of helium. These have all been done at lower Reynolds numbers than what has been performed for this dissertation. Of the lower Reynolds number studies, only the correlation proposed by Ogato and Sato predicts the heat transfer coefficient for vertical helium up-flow spanning the entire quality range. However, this study was only done for $Re_{t,v} \leq 1.85e4$.

The series of experiments for this dissertation resulted in heat transfer coefficient data for $3.27e5 \leq Re_{t,v} \leq 1.51e6$ two-phase helium vertical up-flows that can be compared against the Ogato and Sato correlation. A new heat transfer correlation for this $Re_{t,v}$ range for the available flow quality range is proposed.

Figure 5 shows the predicted variation of the heat transfer coefficient with flow quality at $Re_{t,v} = 1.85e5$ using the Liu-Winterton horizontal correlation (correlation is data validated for argon and nitrogen for $Re_{t,v} \leq 2.22e6$) and the Ogato-Sato vertical correlation (correlation is data validated for helium for $Re_{t,v} \leq 1.85e5$). The heat transfer coefficients reported are several orders of magnitude larger for the Liu-Winterton correlation at the higher Reynolds number flows of argon and nitrogen than in the lower Reynolds number flows of helium in the vertical orientation. This experiment establishes a new correlation that for vertical up-flows of helium for $3.27e5 \leq Re_{t,v} \leq 1.51e6$.

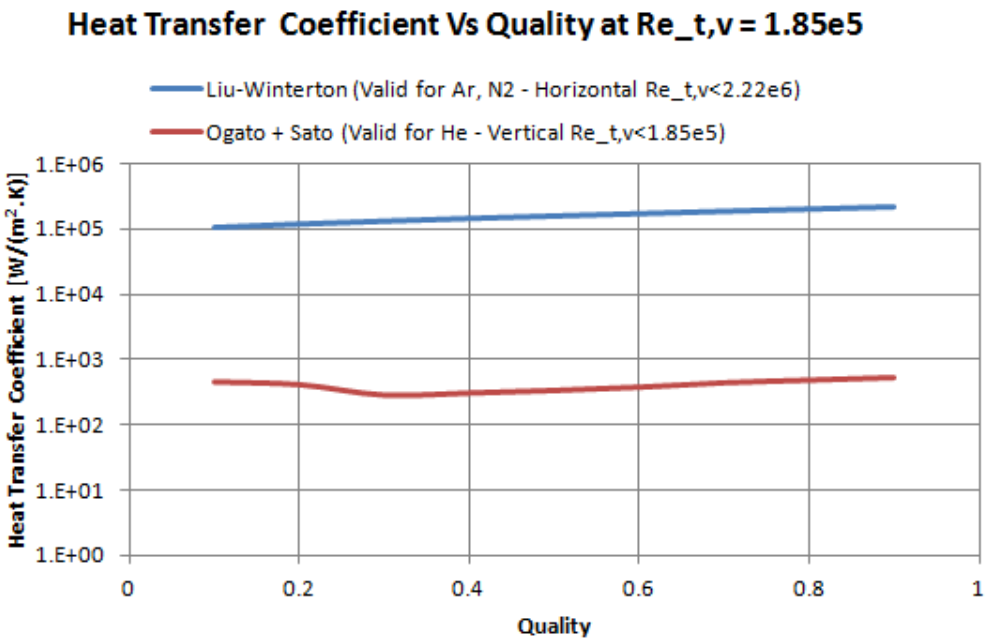

Figure 5: Predicted variation of Heat Transfer Coefficient with Quality for $Re_{t,v}$ =1.85e5

1.5.2 Research Contribution from Objective 2: Find the High Reynolds Number Vertical Up-Flow Pressure Drop for Two-Phase Helium

The current technique for predicting pressure drops in cryogenic flow boiling is to use either the separated or the homogeneous flow model or slight variations of these. Figure 6 shows the predicted variation of the pressure drop with the separated flow model and the homogeneous flow model for a 10 cm long vertical tube at $Re_{t,v}$=1.85e5. As can be seen the difference in the two pressure drop models is very large and seems to increase with increasing quality.

The series of experiments conducted for this research has resulted in pressure drop data for 3.27e5≤ $Re_{t,v}$≤1.51e6 two –phase helium vertical up-flows that can be compared against both the separated flow model correlation and the homogeneous flow model correlation. New pressure drop correlations for this $Re_{t,v}$ range are proposed.

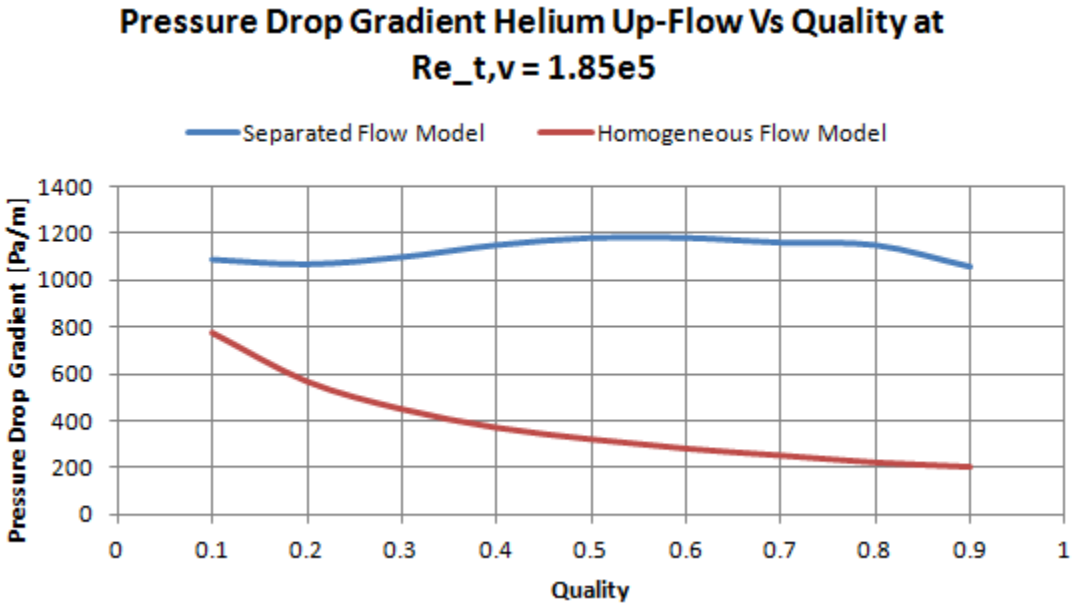

Figure 6: Predicted Variation of Pressure Drop with Flow Quality for $Re_{t,v}$=1.85e5

1.5.3 Research Contribution on Dryout Heat Flux

Figure 7 shows the variation of dryout heat flux with Reynolds number as predicted by Kutateladze and Collier for a dryout quality of 0.3. This series of experiments collected data for dryout heat flux in the pre-heater (section 2.1.5) for liquid helium for $3.27e5 \leq Re_{t,v} \leq 1.51e6$. This data will help to compare the generalized correlation for dryout heat fluxes as described in 1.4.9 with a specific dryout heat flux correlation for helium flowing in a copper tube with copper foam.

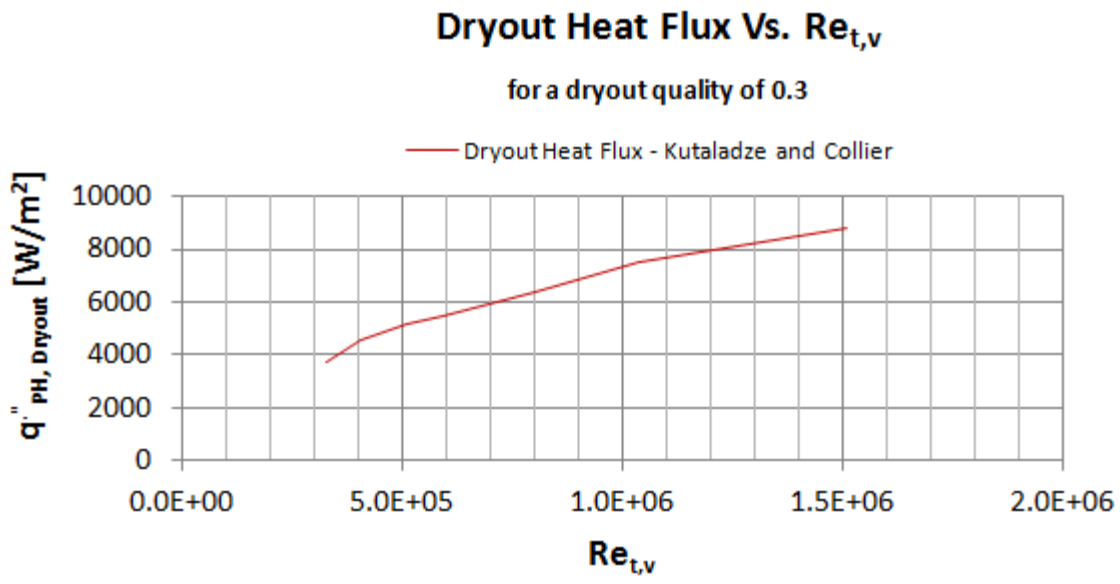

Figure 7: Variation of Dryout Heat Flux with Reynolds Number as predicted by Kutateladze and Collier

2 Experiment

2.1 *Experiment Hardware*

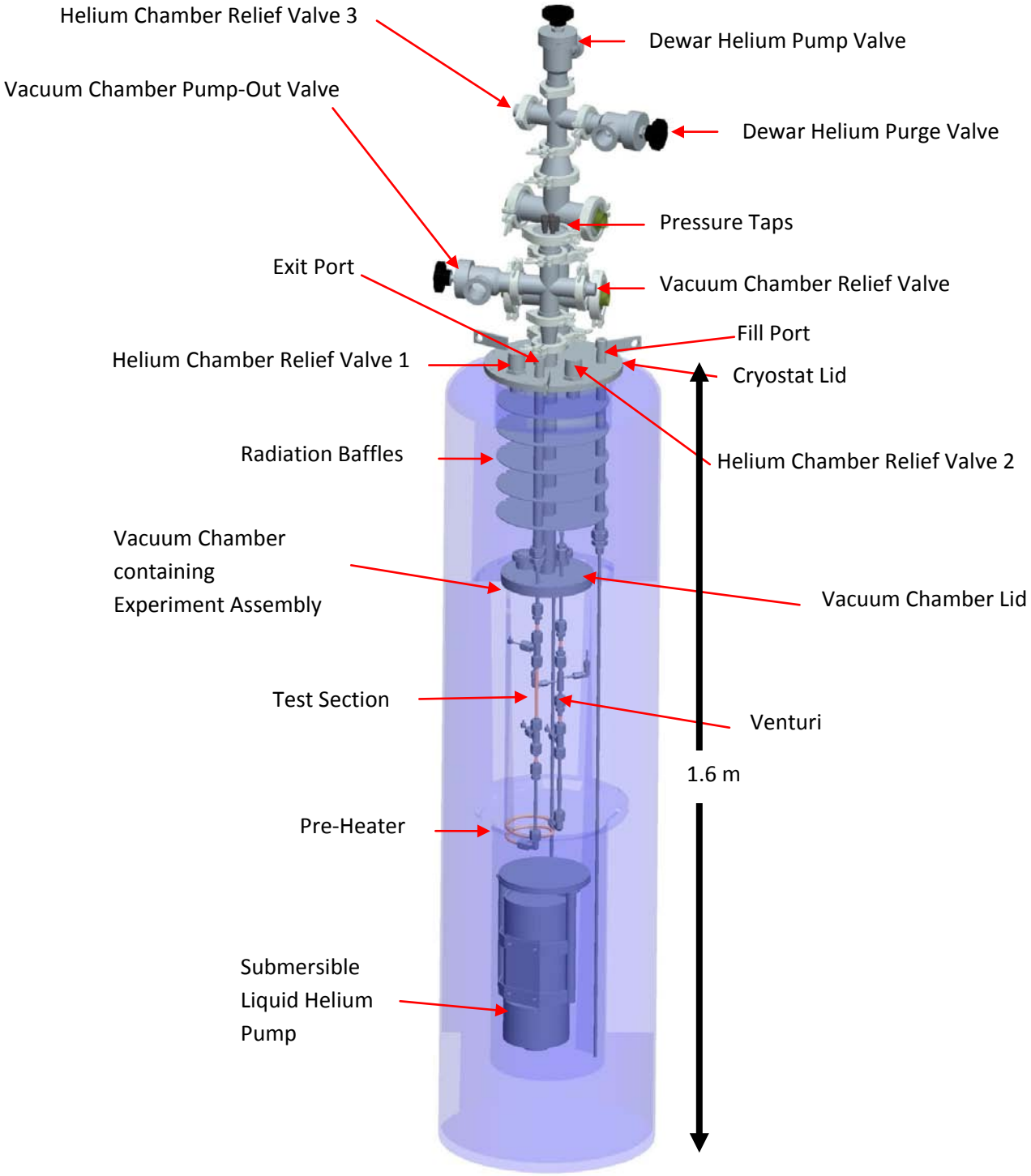

Figure 8: Experiment Hardware Assembly

Figure 8 shows a schematic of the hardware that was configured for the experiment. The dewar was filled with liquid helium through the fill port. A submersible liquid helium pump was used to pump liquid helium in a controlled fashion into the experiment components located in the vacuum chamber. The flow from the pump was routed through a venturi flow meter to measure the volumetric flow rate. The flow was then directed through a pre-heater section. The quality of the two-phase fluid was set in this section. The pump-venturi combination and the pre-heater section allowed for independent variation of the flow rate and the quality of the flow respectively. The heat transfer coefficient and pressure drop in the test section were measured for various flow rates and flow qualities. Temperature and pressure measurements were made to define the thermophysical properties of the fluid at various locations along the experiment. After passing through the test section the helium left through the exit port. The helium was vented to a fume hood.

2.1.1 Dewar

Figure 9: Precision Cryogenic System Dewar

The experiment was conducted in a Precision Cryogenic Systems dewar. The dewar consists of an inner vessel which holds the helium that is being used for this experiment and the experiment cryostat assembly. The cryostat was specially designed for the purpose of this

experiment. The penetrations and access points for the experiment are through this cryostat lid. These penetrations include plumbing lines, electrical connections, operation valves and relief valves. There are radiation baffles between the cryostat lid and the vacuum chamber to prevent direct thermal radiation from impinging on the vacuum chamber and the rest of the cryogen sitting in the dewar. The baffles also provide good staging points to thermally sink plumbing and electrical connections to reduce direct conduction into the cryogen and experiment. The inner vessel is surrounded by an outer vacuum jacketed vessel with multi-layer insulation (MLI) to reduce the convection and radiation heat loads. Figure 9 shows the Precision Cryogenic System dewar. Figure 10 shows the cryostat designed for this experiment and the vacuum chamber being assembled into the experiment dewar.

Figure 10: Cryostat and Vacuum Chamber for the Experiment

2.1.2 Vacuum Chamber

The vacuum chamber allowed the experiment to be conducted with a minimal amount of convective heat flux. In addition the vacuum chamber provided an ability to keep the experiment isothermal inside the helium bath while keeping a separation between the helium and the experiment. There are plumbing penetrations and hermetic electrical connectors through the

vacuum chamber lid. The vacuum chamber was specially designed for this experiment. Figure 10 shows this cryostat and vacuum chamber.

2.1.3 Pump

Figure 11 shows the pump that was used for this experiment. The pump is a liquefied natural gas pump that was specially modified for liquid helium operation for this experiment, making this the longest lead item and the most expensive component for this experiment. This Barber-Nichols BNLNG-01B-000 Submersible Centrifugal Transfer Pump has a 230 VAC 3-phase, 2-pole invert duty, induction motor that provides up to 224 W at 100 Hz. The motor is cooled by direct contact with the fluid. This implies that the pump operation itself warmed the helium in the dewar. This did result in some of the helium around the motor housing boiling off from the experiment while the helium near the pump inlet was pumped through the experiment. Since the pump is submerged it provides an adequate net positive suction head at the pump inlet. The motor speed of the pump is controlled by a Toshiba variable frequency drive (VFD). This allowed adjustment of the pump speed to produce any desired pressure head and flow within the available power range of the motor.

Figure 11: Barber-Nichols Pump

2.1.4 Temperature and Pressure Detection Stations

The local temperature of the fluid or the tube wall was detected using calibrated Lakeshore Cernox Thermometers that are attached by Stycast epoxy or with tape and vacuum grease to copper 101 alloy tubes. The Cernox thermometers are Zerconium Oxy-Nitride thin film resistance type temperature sensors that have accuracies of about 5mK The thermometers are small rectangular chips that are only 1.9 mm x 3.2 mm. The local pressure was detected using capillary pressure taps that were connected to the flow through Swagelok VCR connectors and that are run up to capacitance manometers (baratrons) operating at room temperature and pressure. Figure 12 shows some of the temperature and pressure detection stations in the experiment.

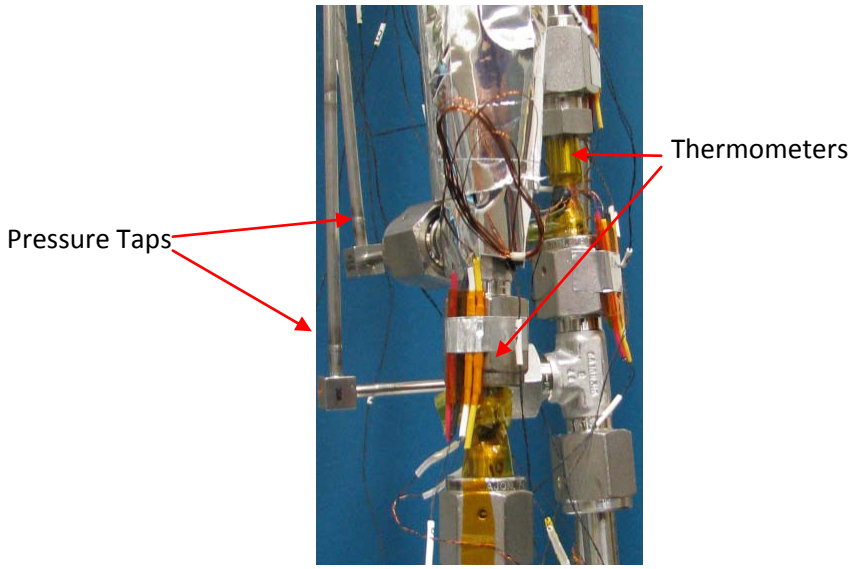

Figure 12: Temperature and Pressure Measurement Stations

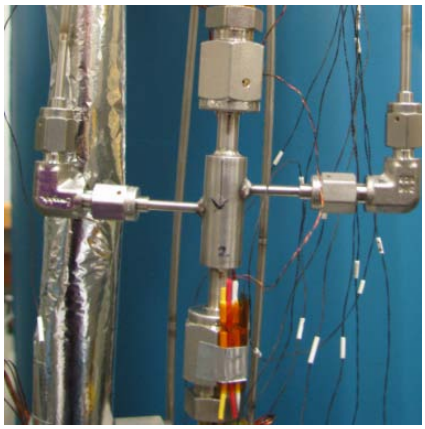

Figure 13: Venturi for this experiment

Venturi

Figure 13 shows the designed Venturi installed with the rest of the experiment hardware. The venturi is used to determine the mass flow rate through the experiment. Single phase liquid helium was pumped from the dewar into the venturi. The working correlation for the venturi is given by equation (34) [17]:

$$\dot{m} = C_D A_t \left\{ \frac{2\rho\Delta P}{\left(1-\beta^4\right)} \right\}^{1/2} \tag{34}$$

The density, ρ, is determined from the thermodynamic condition of the fluid at the venturi inlet. The differential pressure, ΔP, is measured using a differential pressure gauge. The design of the venturi was done in consultation with the Venturi manufacturer, Fox Venturi Products. The

throat area, A_t, and the throat to upstream diameter ratio, β, had to be a balanced between the machining capability of Fox Venturi and what the requirement for a measurable ΔP was for the lowest expected flow rates during the experiment. The inlet inner diameter of the venturi was set at 0.0046 m and the β was set at 0.63. The coefficient of discharge, C_D, is calculated using the equations (35)-(37) [17]:

$$\mathrm{Re}_{\mathrm{Venturi}} = \frac{d_i \beta^2 (2\rho\Delta P)^{1/2}}{\mu} \tag{35}$$

If $3000 \leq \mathrm{Re}_{\mathrm{Venturi}} \leq 2e5$

$$C_D = \frac{\log \mathrm{Re}_{\mathrm{Venturi}}}{0.60 + 0.90 \log \mathrm{Re}_{\mathrm{Venturi}}} \tag{36}$$

If $\mathrm{Re}_{\mathrm{Venturi}} \geq 2e5$

$$C_D = 0.988 \tag{37}$$

2.1.5 Pre-Heater

The Pre-Heater was designed to be able to set the quality of the flow into the test section. For high flow rates and high qualities this involved comparatively large amounts of heat being delivered into the cryostat. The pre-heater allowed for varying amounts of heat flux from small to large to be delivered to the flow, so that the heat transfer coefficient at the test section can be measured in controlled manner by inputting just a small amount of heat and measuring the resulting small temperature rise at the test section wall. The pre-heater consisted of a helical

coiled copper 101 tube (outer diameter = 6.35e-3 m, inner diameter = 4.63e-3 m, tube length = 0.463 m, helix height = 0.0254 m) with about 4 m of 28 gauge manganin wire that was directly attached to the copper tube surface using Stycast epoxy. This allowed up to 250 W of heat to be

Figure 14: Pre-Heater Configurations:
Left: Original Pre-Heater installed in experiment with MLI radiation shield;
Right: New Pre-Heater with Copper Foam Installed

imparted into the pre-heater section. To ensure that this large heat load is not radiating substantially to rest of the experiment components inside the vacuum chamber and to the cryogen bath around it, 10 layers of MLI were installed above the pre-heater section and 30 layers of MLI were installed on the bottom and the walls on the vacuum chamber up to the height of the pre-heater. Figure 14 shows the two different pre-heater configurations that were installed with the rest of the experiment hardware. A new pre-heater was fabricated with copper foam (Section 3.5) inserts to mitigate the dryout and superheating problem that was being observed.

2.1.6 Test Section

Figure 15 shows the experiment test section. The test section was designed so that a known amount of power could be delivered to the test section wall, as the corresponding temperature difference between the test section wall and the fluid in the test section was recorded over the desired range of Reynolds numbers and quality. By recording the temperature difference

Figure 15: Test Section Left: Without MLI Right: With MLI

between the flow and the wall for a given input power it was possible to calculate the heat transfer coefficient. The temperature of the wall of the test section is directly measured. The temperature of the fluid is measured by measuring the temperature at a measuring station (see Figure 12) just prior to the test section (see $T_{TS\text{-}F\text{-}In}$ in Figure 16).

The test section was a 0.1 m long copper 101 tube with an inner diameter of 4.6e-3 m and an outer diameter of 6.35e-3 m. The test section heater was about 1 m long stainless 304 wire that was directly attached to the surface of the copper tube using Stycast epoxy. This heater was capable of a 0.5 W input into the test section. This heat input was expected to allow at least a 0.5 K temperature difference between the test section wall and the flow, even for high heat transfer coefficients on the order of ~10^6 W/(m^2.K). The test section was also protected from radiative heat loads on it with 5 layers of MLI. The test section tube was chosen to be a commercially available copper 101 tube that would allow studies of the desired Reynolds number range given the liquid helium pumps capabilities. Performing the study using the non-dimensional Reynolds

number and the non-dimensional fluid quality as the independent variables allows the results to be applied to other tube dimensions.

2.2 Experiment Instrumentation

Figure 16 shows the location of the temperature and pressure sensors.

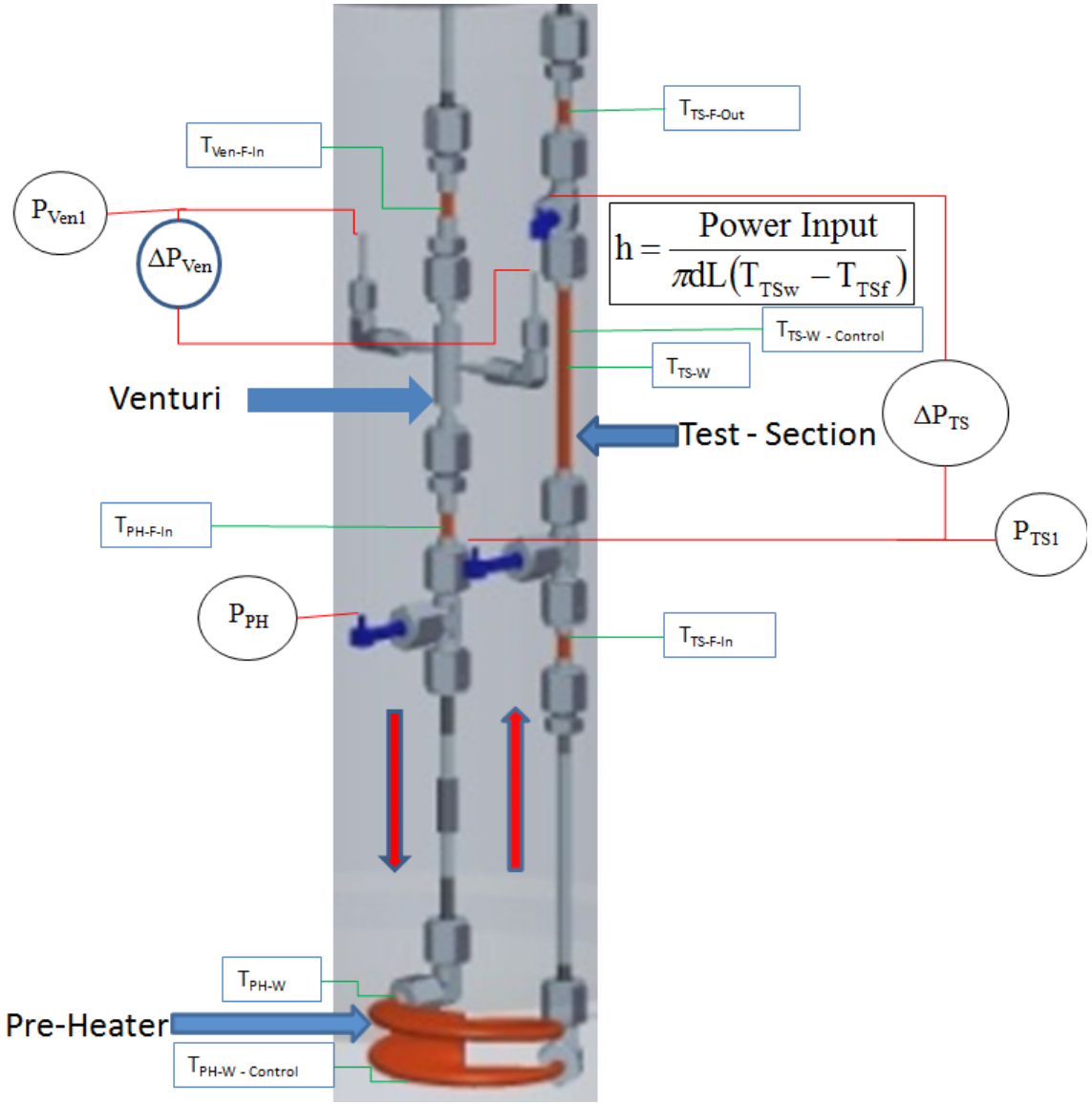

Figure 16: Temperature and Pressure Sensors for the experiment

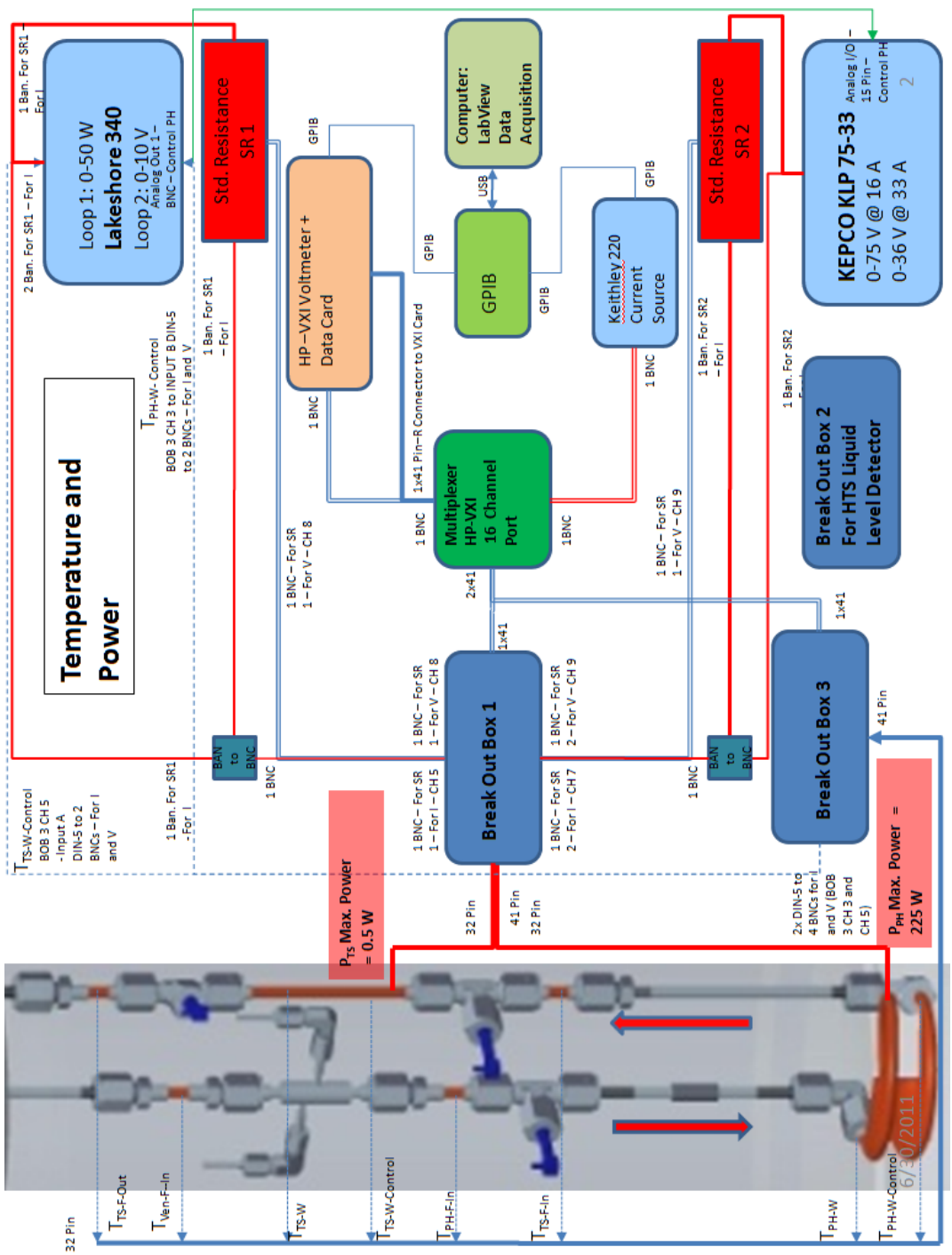

Figure 17: Temperature and Power Instrumentation Map

Figure 17 shows the Temperature and Power instrumentation map for the experiment.

2.2.1 Temperature

The temperature readings ("T") were done with calibrated Lakeshore Cernox resistance thermometers that were attached to the surfaces where the temperature was being measured using Stycast epoxy or using tape and grease. The thermometer measurements were four wire measurements. The voltage drop across the thermometers was measured directly to calculate the resistance in the Cernox thermometer when an excitation current is delivered to the thermometers. This resistance was compared against a temperature-resistance calibration to determine the temperature.

The fluid temperature was measured in four different locations ($T_{Ven\text{-}F\text{-}In}$, $T_{PH\text{-}F\text{-}In}$,$T_{TS\text{-}F\text{-}In,}$ $T_{TS\text{-}F\text{-}Out}$). The fluid temperature was measured by measuring the temperature of the wall of the Cu 101 alloy tube. The thermal conductivity of copper is above 800 W/(m.K) at helium temperatures (~4-5K). Without any significant heat load, the equilibrium temperature measured at the wall and the fluid temperature was the same. A small calculated Biot number on the order of 10^{-4} confirms that there are negligible thermal gradients in the copper wall and that the temperature at the tube inside wall and fluid interface is about the same (within 0.43 mK for a 0.56 W heat load) as the outside wall temperature of the copper tube that is measured (Section 4.1). A large calculated Peclet number on the order of 10^{6} also confirms that the heat transfer through the fluid bulk flow is substantially larger than heat transfer by conduction through the fluid (Section 4.2). The wall temperature response to heating was measured at four locations, two at the test section ($T_{TS\text{-}W,}$ $T_{TS\text{-}W\text{-}Control}$) and two at the pre-heater ($T_{PH\text{-}W,}$ $T_{PH\text{-}W\text{-}Control}$). Two thermometers ($T_{TS\text{-}W,}$ $T_{PH\text{-}W}$) were used to monitor the wall temperature for the experiment. The control thermometers ($T_{PH\text{-}W\text{-}Control,}$ $T_{TS\text{-}W\text{-}Control}$) could be used to monitor the heat input into the heat sections by the power supplies, and also monitor the temperatures of the pre-heater and the

test section independent of the data acquisition system. The control thermometers thus provided redundancy capability to ensure hardware safety. If the control thermometers registered a temperature above a safe limit, the heater power could be turned off restoring the experiment to a safe-mode. Apart from the control thermometers that were wired to the power supply, the other thermometers were monitored using a LabView data acquisition system.

2.2.2 Power

The power source for the pre-heater was a Kepco KLP 75-33 power supply that provided the high power (> 200 W for high qualities at high Reynolds numbers) that was required for setting the quality at high Reynolds numbers for this experiment. The power source for the test section was a HP 3616 A DC Power Supply that can be voltage controlled to deliver a desired power to the test section heater in order to set up a temperature difference between the test section wall and the fluid flow.

2.2.3 Pressure

Figure 18 shows the Pressure instrumentation map for the experiment. There are two types of pressure readings that were done for this experiment, two differential pressure measurements and three absolute pressure measurements. There were five capillary tubes (3.175e-3 m outer diameter and 1.753e-3 m inner diameter) that were connected to Swagelok VCR tees that provide direct access to the flow. These five capillaries provide a direct path out from the flow to 5 capacitance baratron pressure sensors. The differential pressure measurements are done with two 5000 Torr MKS 120 AD capacitance baratrons that were connected to a MKS 146 C - dual channel readout. The three absolute pressure measurements were done with 5000 Torr MKS 627 capacitance baratrons that were connected to two MKS PR 4000B dual channel readouts. Since there was a large temperature difference between the baratron location and the

measurement location thermal transpiration effects were accounted for in the measurements (Section 4.5). [18, 19]

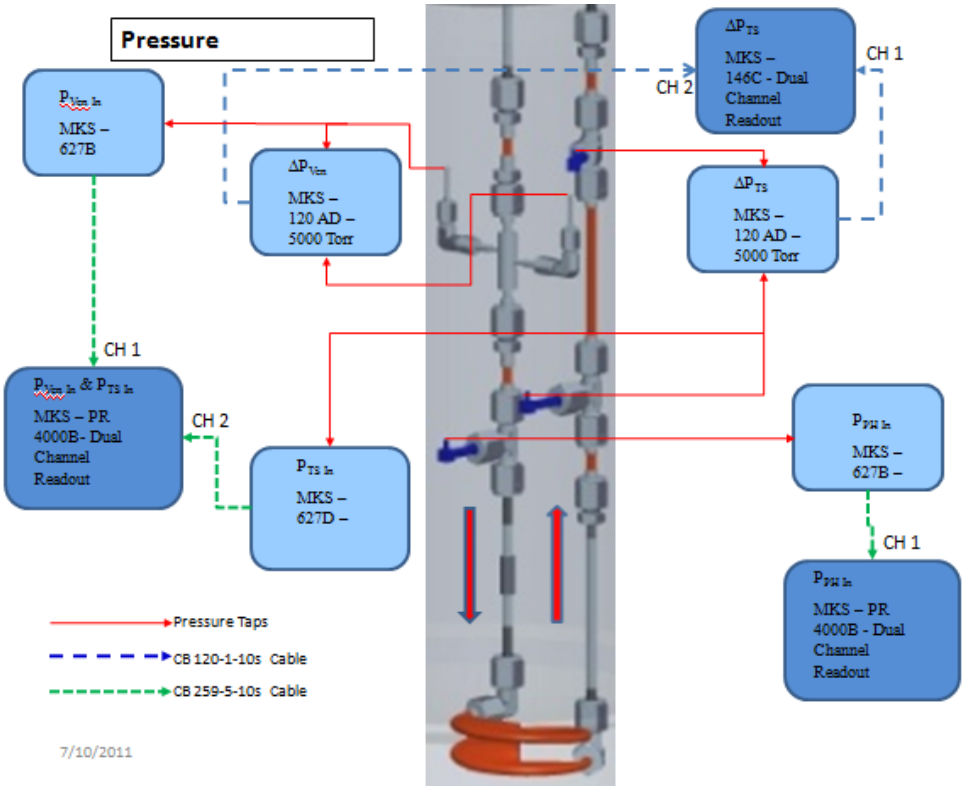

Figure 18: Pressure Instrumentation Map

Figure 19: Instrument rack for experiment

Figure 19 shows the instrument rack that was used to monitor and control the experiment.

2.3 Methodology

The detailed experiment procedure, including safety issues is discussed in the Appendix A (Section 12).The focus of this section is on the methodology for controlling the independent variables in the experiment (the Reynolds number, $Re_{t,v}$, and the flow quality, x) and measuring the dependent variables of the experiment (the heat transfer coefficient and the pressure drop).

2.3.1 Setting the Reynolds Number

The liquid helium in the dewar was pumped into the experiment assembly in the vacuum chamber. As the helium passed into the venturi its pressure (P_{Ven_In}) and temperature (T_{Ven_In}) was used to establish the thermodynamic properties of the liquid entering the venturi. With this information and by monitoring the pressure drop in the venturi (ΔP_{Ven}) it was possible to figure

out the mass flow rate using equation (34). The pump VFD was controlled to get the desired venturi pressure drop and hence the desired flow rate. This set the Reynolds number of the flow.

2.3.2 Setting the Quality of the Flow

The thermodynamic condition of the flow after the venturi and at the inlet of the pre-heater was evaluated by measuring the pressure (P_{PH_In}) and temperature (T_{PH_In}) of the flow. The power required in the pre-heater was given by the difference between the enthalpy at the desired quality, $x_{Desired}$, at P_{PH_In}, $E(x_{Desired},P_{PH\_In})$, and the enthalpy at pre-heater inlet condition $E(T_{PH\_In},P_{PH\_In})$. The required Pre-Heater Power is given by equation (38):

$$\text{Power}_{\text{Pre-Heater}} = \dot{m}\left[E\left(x_{\text{Desired}}, P_{\text{PH\_In}}\right) - E\left(T_{\text{PH\_In}}, P_{\text{PH\_In}}\right)\right] \tag{38}$$

When the $\text{Power}_{\text{Pre-Heater}}$ was input into the Pre-Heater controls, and $T_{PH\text{-}W}$ reached steady state, the flow had reached its desired quality. This set the quality of the flow. The flow rate is maintained using the pump VFD to compensate for any impedance changes in the pre-heater as the fluid was heated to the desired quality.

2.3.3 Measuring the Heat Transfer Coefficient in the Test Section

The heat transfer coefficient was measured by delivering an applied power ($\text{Power}_{\text{TS-Applied}}$) to the test section wall and measuring the resulting temperature difference ($\Delta T_{TS}=T_{TS\text{-}W} - T_{TS\text{-}F\text{-}In}$). The temperature of the Test Section Wall ($T_{TS\text{-}W}$) and the temperature of the flow ($T_{TS\text{-}F\text{-}In}$) were measured by the LabView data acquisition system. The heat transfer coefficient of the applied power was then calculated using equation (39).

$$h_{\text{TS - Applied}} = \frac{\text{Power}_{\text{TS - Applied}}}{\pi dL\left(T_{TS-W} - T_{TS-F-In}\right)} = \frac{V^2_{\text{TS - Applied}}}{\pi dLR_{TS}\left(T_{TS-W} - T_{TS-F-In}\right)} \tag{39}$$

2.1.6 Measuring the Pressure Drop in the Test Section

The pressure drop in the test section was measured directly using a differential pressure gauge. A 5000 torr MKS 120AD capacitance baratron was connected to a MKS 146C readout and the LabView Data Acquisition system showed the pressure drop in the 10 cm long test section for a given Reynolds number and flow quality. The baratron operated at room temperature and was located external to the dewar. Two capillary tubes on each end of the test section were used to probe the pressure at the cryogenic conditions and connect to the room temperature baratron. Since there was a large temperature difference between the baratron location and the measurement location thermal transpiration effects were accounted for in the measurements. Figure 20 shows the differential and absolute baratrons that were used for this experiment.

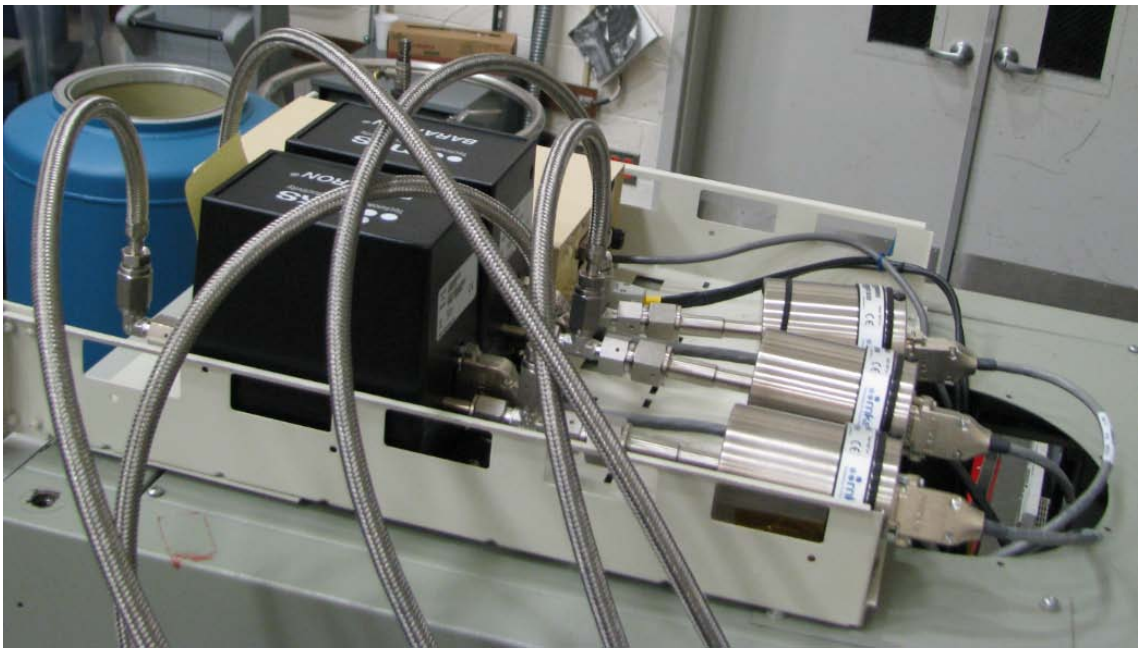

Figure 20: Absolute and Differential Baratrons

3 Cryogenic Challenges

` As with most cryogenic experiments, many challenges were surmounted dealing with fabrication and warm leaks to even operate the experiment. This section will however describe the challenges that were surmounted in order to collect the relevant data.

3.1 Thermal Acoustic Oscillations

When the pump was initially operated and liquid helium was flowing through the experiment, unusual variations in pressure were observed on the pressure gauges. After ensuring that all the connections were made properly it was determined that the most likely candidate for these strange phenomena was thermal acoustic oscillations (TAOs).

Cryogenic TAOs are not very well understood. However, it has been noticed that under certain conditions columns of gas that are subject to steep temperature gradients, particularly in tubes connecting liquid helium to the ambient room temperature exhibit pressure oscillations in an undamped manner [21 - 23]. In this experimental setup it was recognized that the pressure taps that connect the experiment locations to the external baratrons could possibly be forming this oscillating gas column.

It is theorized that this type of TAOs might be the result of a cyclical film boiling pattern set up at the liquid cryogen low temperature end. Initially, as the vapor thickness of the film

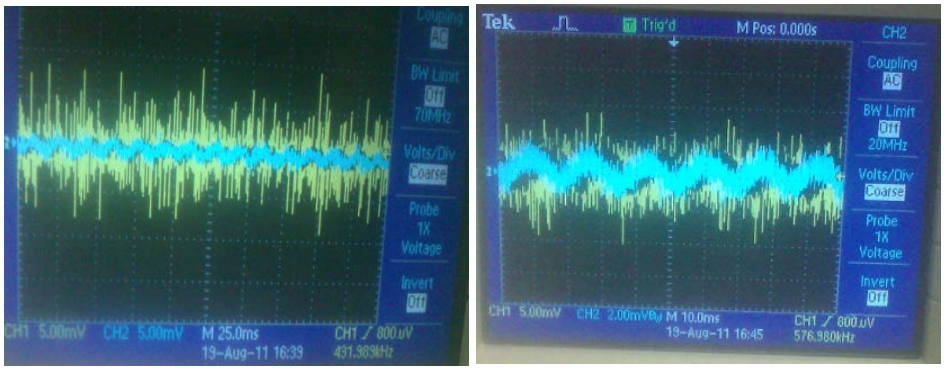

Figure 21: Evidence of Thermal Acoustic Oscillations (TAOs) in experiment

grows at the cold end of the tube there is less boiling and less vapor is generated in the tube. Eventually more liquid accumulates at the bottom of the tube generating more boiling and more vapor generation. The cyclical nature of this vapor generation at the cold end of the tube may cause the TAOs.

To investigate a potential TAO scenario, an oscilloscope was used to check the pressure reading resulting from the flow. Figure 21 shows the oscillatory pressure behavior as observed from the venturi pressure taps. The screenshot on the right is just a higher resolution output of the TAO signal that was originally seen on the left.

A literature survey for TAO damping strategies revealed only a few options. Suggestions include changing the tube radii, varying the temperature profile in the tube, or adjusting the length ratio of the warm section of the tube to the cold section [22]. It would have been difficult to change the hardware to accommodate these suggestions, however it was theorized that changing the warm to cold length ratio was effectively changing the warm volume to cold volume ratio. An attempt was made to change the warm volume to cold volume ratio by adding extra volume at each of the five baratrons and this approach worked well. Figure 22 shows how the addition of extra volumes to the baratron helped damp out the TAOs in the experiment.

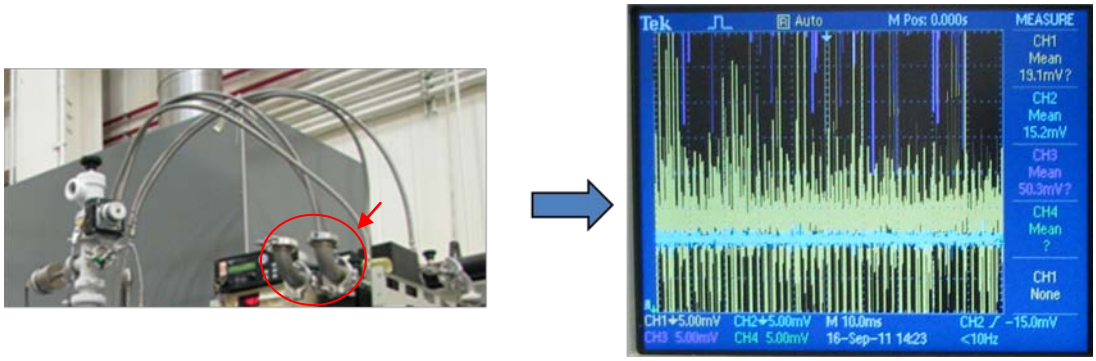

Figure 22: Adding extra volumes to the baratrons (Left) helped eliminate the Thermal Acoustic Oscillations (Right: no variation on the light blue channel).

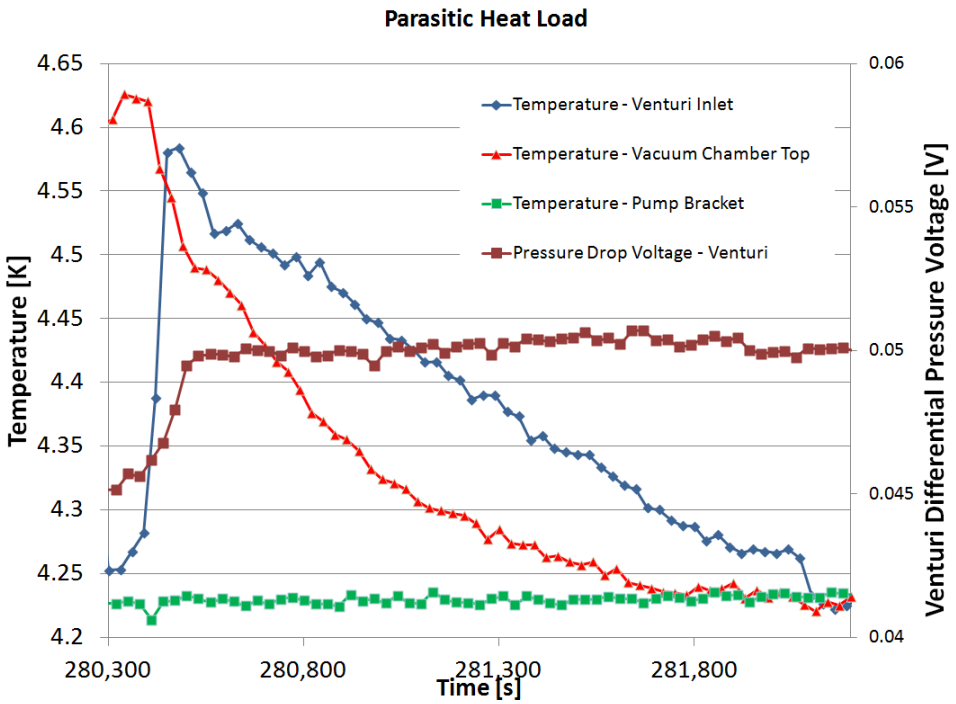

Figure 23: Parasitic Heat Load

3.2 Parasitic Heat Load

One of the consequences of the low boiling point and low heat of vaporization of helium is that helium experiments are extremely sensitive to parasitic heat that can fairly easily change the phase of the fluid flow from liquid to gas. Very careful thermal isolation is necessary to maintain the fluid in its desired condition.

Figure 23 demonstrates the effect of parasitic heat load on the experiment. The "Vacuum Chamber Top" temperature stayed warmer than the saturation temperature (~ 4.23 K, depicted by the "Pump Bracket" temperature) because of the parasitic heat load on the top of the vacuum chamber top. This heat load was incident on the top due to radiation and conduction, even though the cryostat was designed to minimize these parasitic heat sources. The vacuum chamber top being at a higher temperature also resulted in the flow that is passing through the vacuum chamber top being at a temperature higher than the saturated temperature as can be seen in the

Venturi In reading. The Venturi In temperature was above saturation implying that the flow into the venturi was two-phase, which resulted in an inaccurate estimate of the mass flow rate. The Venturi In temperature could be forced down to saturated temperature by using the helium as a coolant for the Vacuum Chamber Top. As the flow rate is ramped up (depicted by the Venturi Differential (Pressure Voltage)) the Venturi In fluid temperature initially rose as it picked up heat from the vacuum chamber top. However, over time the Vacuum chamber top temperature fell, and as this occurred the Venturi In fluid temperature also fell to single phase liquid temperatures. Under these conditions it was possible to get an accurate measurement of the flow rate using the venturi, and conducting the experiment became possible. However this meant that although the higher Reynolds number conditions could be tested, the lower Reynolds number conditions ($Re_{t,v}$ < 4.95e5) could not be tested with the current hardware unless the parasitic heat load on the vacuum chamber top was somehow removed.

In order to mitigate this problem, some steps were taken to reduce and remove the parasitic heat from the vacuum chamber top. Conductive heavy gauge copper straps were used to thermally sink the top of the vacuum chamber top and the inlet tube (connecting the pump to the experiment) to the helium bath at the bottom of the dewar. Figure 24 shows these straps.

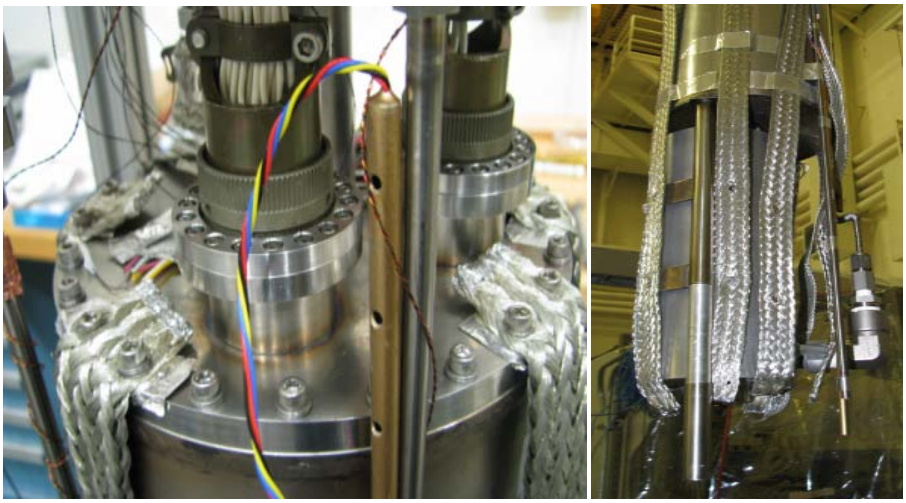

Figure 24: Conductive heavy gauge copper straps to divert parasitic heat loads from the vacuum chamber top and the vacuum chamber inlet tube to the helium bath at the bottom of the dewar.

In addition steps were taken to provide additional radiative isolation for the experiment inside the vacuum chamber. Copper wool and multi layer insulation (MLI) blankets were used to minimize the direct 300 K radiation shining in on the cryostat through the vacuum tube leading to the vacuum chamber. Figure 25 shows the copper wool and the MLI blankets.

Figure 25: Radiative isolation from 300 K radiation shining through vacuum chamber tube provided by copper wool and MLI blankets.

3.3 Solid Air Plug

In a system like this where the cryostat is open to the air it is sometimes possible for the air to back-stream into the cryostat if there is little or no flow leaving the cryostat. This air can then solidify and plug the plumbing in the hardware. It is seldom possible to visually observe the interior of a cryogenic system and a condensed solid air plug can accumulate over time. Unfortunately after a few runs such a solid air plug did form in the plumbing. When this happened the only resolution for this experiment was to let the cryostat warm up to about 100 K from 4.2 K to ensure that the air had re-vaporized. To expedite this process the liquid helium had to be transferred back out of the experiment dewar to the supply dewar. Subsequent to this solid air plug formation care was taken to put a relief valve on the exit line of the cryostat when helium was not being flown out during the experiment operation.

3.4 Cold Leak

After a few cool down and warm up cycles (room temperature to 4.2 K and back up to room temperature) of the experiment hardware it was discovered that the contents of the vacuum chamber were cooling down unusually fast. It was also discovered that turning the pre-heater on was resulting in the unusually quick heating of other components in the vacuum chamber. These were indications that somehow the vacuum chamber had some helium vapor inside it which was convectively cooling down the hardware during the cool down and warming up the experiment hardware when the pre-heater was turned on. Helium could be the only possible source of convection inside the vacuum chamber at the low temperatures of 4.2 K because all other gases would have cryo-pumped (condensed) onto the vacuum chamber wall. Since the vacuum chamber is submerged in a bath of liquid helium this leak would have to be small. The vacuum chamber had been checked with mass spectrometer helium leak detector at room temperatures and no leaks were observed before the cool down. When the vacuum chamber was brought back

up to room temperatures and leak checked no leak was observed. This indicated that the leak that had developed was a cold leak. A cold leak is a leak that can be detected only at cryogenic temperatures. It is often the result of differential contraction of materials at cryogenic temperatures and it is exacerbated by multiple thermal cycles as had been sustained by the vacuum chamber. Cold leaks are very challenging to diagnose, as unless the leaking interface is cold it is not possible to find the leak. However, if the leaking cryostat interface is inside the dewar it is not possible to isolate the potential leaking surfaces to figure out the source of the leak. To get around this challenge the entire cryostat was lowered into an open insulated bucket and the vacuum chamber was then connected to the leak detector. Although, it is not possible to contain liquid helium in an open insulated bucket in the ambient atmosphere, it is possible to contain liquid nitrogen in an open insulated bucket. The bucket with the cryostat was filled with liquid nitrogen at 77 K. The interfaces were individually isolated and precisely exposed to gaseous helium using a syringe. Precautions were taken to not allow the boiling nitrogen to displace the helium gas. As the vacuum chamber cooled down, the source of the leak was located at the flange for an electrical connector that was improperly fabricated. This flange was replaced and the leak was plugged. Figure 24 shows the location of the electrical connector flange on the cryostat. Figure 26 shows the hardware used to perform the cold leak check on the cryostat.

Figure 26: Cold leak check of vacuum chamber being performed in an open bucket with liquid nitrogen.

3.5 Dryout Heat Flux

Another problem that was faced while conducting this experiment was that whenever large quantities of heat were being used to set the quality of the flow in the pre-heater, a situation was created where the flow was becoming superheated. The onset of this superheating appeared to happen when the dryout heat flux for the pre-heater was attained. The dryout heat flux was measured by finding the applied pre-heater voltage for which the test section inlet temperature (i.e the inlet fluid temperature) becomes superheated. Equation (40) can be used to find the pre-heater dryout heat flux.

$$\dot{q}''_{PH,Dryout} = \frac{V^2_{PH,Dryout}}{\pi d_{PH} L_{PH} R_{PH}} \tag{40}$$

Figure 27 shows the superheating effect of imparting a large amount of heat on the pre-heater. In this situation the quality of the flow was increased from 0.1 to 0.8 at a $Re_{t,v}$ = 1.95e5 with 62 W of heat (~36.75 V at the pre-heater). As the pre-heater power is increased to this level, the Pre-Heater In flow temperature stays the same and the Pre-Heater Wall temperature rises as expected. However, the Test Section In flow temperature that was just downstream of the pre-heater rose dramatically, indicating that at least portions of the flow was getting superheated.

The pre-heater has a uniform distribution of heat at the wall because it consisted of a spiral resistance wire wrapped around the outer wall of the pre-heater. The vapor that was in contact with the dry portion of the tube was superheating. It was theorized that a more mixed distribution of the flow inside the pre-heater might reduce this superheating of the vapor.

Two potential strategies were investigated to attempt to distribute the heat more evenly

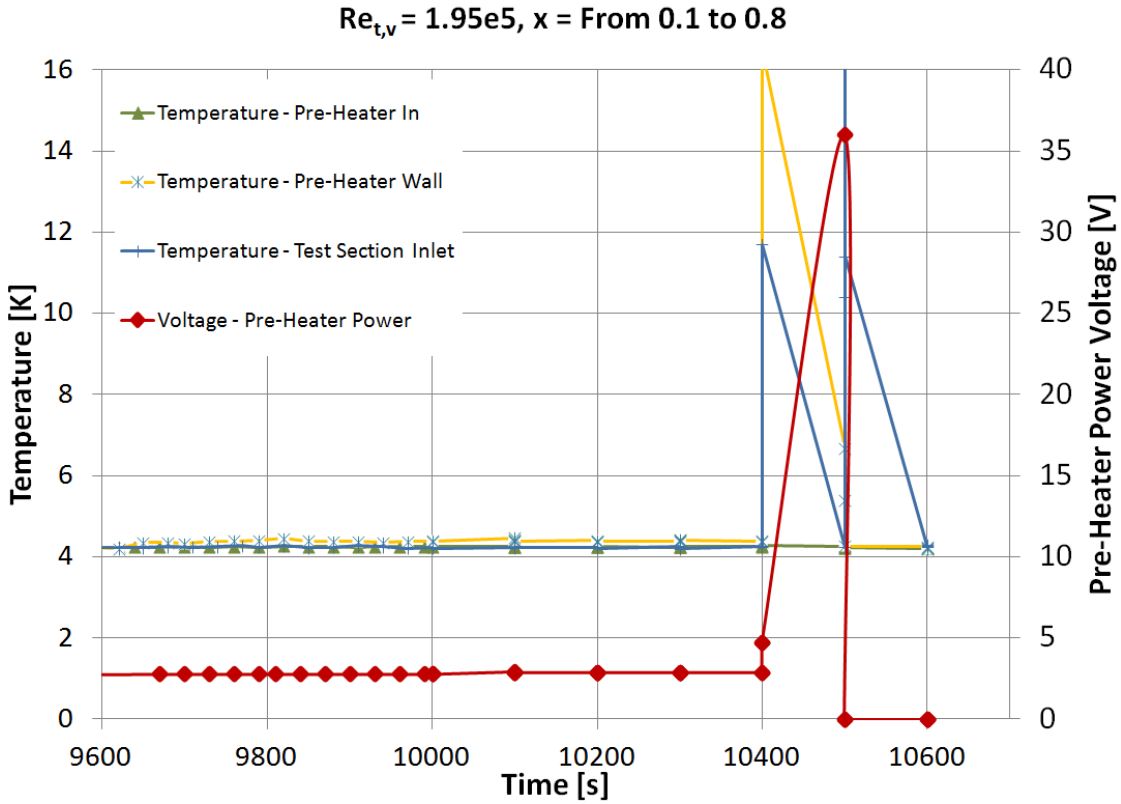

Figure 27: Superheating of flow in pre-heater at Re_t,v = 1.95e5 going from x=0.1 to 0.8.

between the liquid and the vapor in the pre-heater. The simpler strategy of using a twisted tape insert (Figure 28 Left) to try to fling the liquid to the walls of the pre-heater was attempted. This twisted tube insert strategy did not sufficiently rectify the superheating situation. For the second strategy, copper foam cylinders, 11 mm in diameter (Figure 28 Center) were swaged into a re-fabricated pre-heater section (Figure 28 Right). The Duocel copper foam was a 10 pores per inch Copper 101 alloy manufactured by ERG Materials and Aerospace Corporation. This second approach helped prevent the dryout condition from happening until higher heat fluxes were achieved at the pre-heater. This allowed for data collections for qualities up to about 0.3 even at these very high Reynolds numbers.

Although Ogato and Sato acknowledge that even at the lower Reynolds numbers that they were operating in they experienced dryout conditions they do not identify what the temperature of the bulk flow at their test section inlet was. Instead they present their data as a function of the wall superheat at the test section. While it is certainly possible to measure heat transfer coefficient of a fluid with superheated vapor with entrained liquid droplets, it is not an accurate measurement of the heat transfer coefficient of a higher quality unless the flow is homogeneous to the extent that the vapor and the liquid are isothermal. It is unclear from both Kielen and

Figure 28: Pre-heater superheating mitigation strategies –
(Left to Right) Twisted Tape Insert, Copper Foam, Aluminum New Pre-Heater with Copper Foam

Ogato and Sato's published studies that they ensured that the fluid entering their test sections did not consist of superheated vapor. [15, 16]

4 Potential Extraneous Influences on the Experiment

4.1 Biot Number

The Biot number is given by equation (41):

$$Bi = h_{lv} L_c / k \tag{41}$$

If the Biot number is less than 0.1 the resistance to conduction within the copper tube can be considered to be significantly less than the resistance to convection out of the tube. The Biot number for this experiment is on the order of 10^{-4} implying that there are negligible thermal gradients in the copper tube wall. The temperatures measured at discrete locations on the copper tubes are therefore good representations of the overall copper tube temperature.

4.2 Peclet Number

The Peclet number is given by equation (42):

$$Pe = \mathrm{Re}\,\mathrm{Pr} \tag{42}$$

A large Peclet number ensures that the rate of thermal advection dominates the rate of thermal conduction. For this experiment the Peclet numbers are on the order of 10^{6}. This large magnitude of Peclet number confirms that the heat transfer through the fluid bulk flow is substantially larger than heat transfer by conduction through the fluid.

4.3 Swirl Number

It is necessary to evaluate if the swirl in the flow created by the helical pre-heater affected the parameters being tested in the test section. The swirl number is a measure of the swirl that has been created. At the exit of the pre-heater the swirl number correlation can be reduced to equation (43):

$$S_{PH,exit} = Z_{PH} / L_{PH} \tag{43}$$

where Z_{PH} is the overall linear height of the pre-heater and L_{PH} is the total curved length of the helical pre-heater.[23]

The swirl that is generated then decays exponentially along the stainless steel tube that connects the pre-heater to the test section and the swirl number at the inlet of the test section is given by equation (44):

$$S_{TS,inlet} = S_{PH,exit} \exp\left(\frac{-\kappa f_{PH\ to\ TS} L_{PH\ to\ TS}}{4 d_{PH\ to\ TS}} \right) \tag{44}$$

where κ is attenuation factor that is tabulated against Reynolds number, $f_{PH\ to\ TS}$ is the friction factor, $L_{PH\ to\ TS}$ is the length, and $d_{PH\ to\ TS}$ is the diameter of the stainless steel tube connecting the pre-heater section to the test section. [24] The largest swirl number estimates obtained at the inlet of the test section are about 0.03. Swirl numbers below 0.5 are considered to be very small and hence the swirl generated in the pre-heater is unlikely to affect the parameters being measured in the test section.

4.4 Flow Instabilities

It is important to have a good understanding of the potential oscillatory behavior of two-phase flows since there are several mechanisms by which oscillations can happen. Having a good understanding of the causes and potential mitigating solutions will allow for the design of more reliable heat exchangers. There are three types of flow instabilities that are commonly observed in two phase cryogenic flows: thermal acoustic oscillations, Ledinegg Instabilities, and density wave oscillations. Thermal acoustic oscillations were addressed in Section 3.1, since this form of instability was experienced and rectified in order to run this experiment. The other two instabilities were also considered for this experiment and are described in more detail in this section. [25]

4.4.1 Ledinegg Instability

Ledinegg instability could potentially occur if the pressure drop decreases for an increase in mass flow rate. This situation may arise when the fluid at the inlet is subcooled and the fluid at the outlet is two phase. This is the situation that is experienced at the pre-heater when the experiment is operated and hence it is of interest to investigate the possibility of Ledinegg instabilities for this experiment. Figure 29 shows the possible configuration where Ledinegg

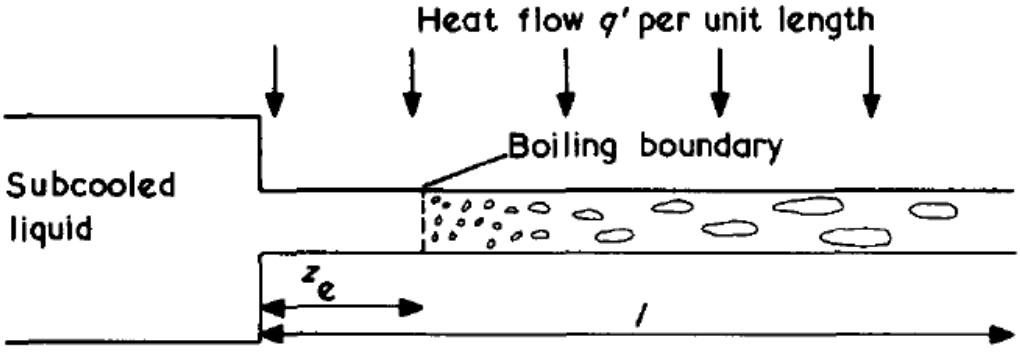

Figure 29: Experiment scenario potentially leading to Ledinegg instability. [24]

instability might be generated. Under this condition as the mass flow rate is decreased the boiling boundary would move towards the inlet. This would result in the total pressure drop increasing if the mean pressure gradient in the two-phase fluid is greater than that in the subcooled liquid. This is an unstable scenario since the higher pressure drop would promote a higher mass flow, forcing the boiling boundary to again move towards the outlet. Then, if the pressure drop in the subcooled liquid is less than the mean pressure gradient in the two phase fluid this reduced overall pressure drop would tend to decrease this mass flow rate setting up an unstable flow oscillation.

Bald and Hands has described a model that helps to predict the circumstances under which Ledinegg Instabilities can happen. [25] Thermodynamic equilibrium is assumed at all points along the tube thus effects of subcooled boiling are ignored. The Jacob number for the system is used to predict conditions of stability. Jacob number is given by equation (45):

$$\mathrm{Ja} = \frac{\Delta \mathrm{E}_{\text{Subcool To x=0, inlet}} \left(\rho_{l,inlet} - \rho_{v,nlet} \right)}{\lambda_{lv} \rho_{v,nlet}} \tag{45}$$

The condition for unconditional stability is:

For Ja< 2

$$4\mathrm{f}_{t,l,inlet} \frac{\mathrm{L}}{\mathrm{d_i}} \rangle \mathrm{Ja} \tag{46}$$

For 2< Ja <4+ $2(3)^{0.5}$

$$\left[1+\frac{1}{2}\left\{\frac{d_i}{Lf_{t,l,inlet}}-\left(3\left[1+\frac{d_i}{Lf_{t,l,inlet}}\right]\right)^{0.5}\right\}\right]^{-1} \rangle Ja \qquad (47)$$

If $Ja>4+ 2(3)^{0.5}$ the system will always be potentially unstable.

The maximum Jacob number that was calculated for all the experimental runs was less than 0.05. The minimum required length to diameter ratio (L/d_i) of the pre-heater to ensure unconditional stability is less than 0.7. However, the length to diameter ratio of the pre-heater is about 41.8; hence the pre-heater in this experiment did not experience any Ledinegg instabilities.

4.4.2 Density Wave Oscillations

Figure 30 shows the possible configuration where density wave oscillations might arise. Density wave oscillations occur when liquid entering a heated tube is completely vaporized by the time it reaches the outlet. This condition was not experienced in this experiment, since a quality of 1 was never attained in the pre-heater. However, it is worth considering this form of oscillation for future two-phase heat exchangers that are built on the basis of this research. If the

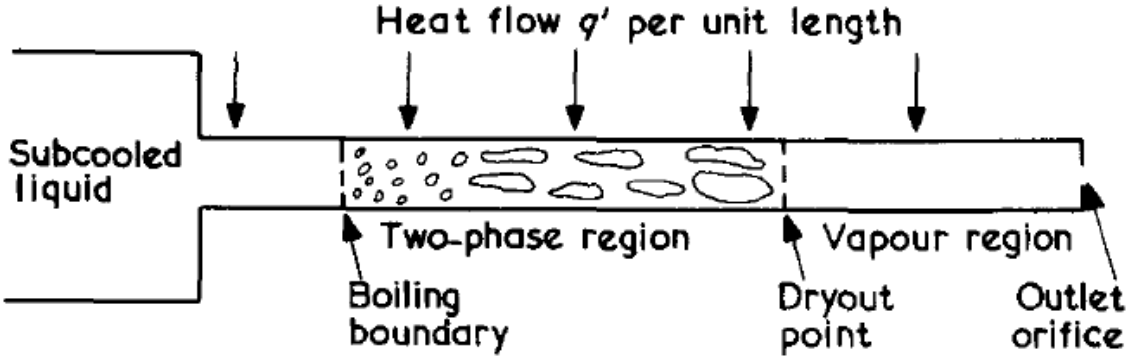

Figure 30: Experiment scenario potentially leading to density wave oscillations. [24]

flow rate in the tube increases above its equilibrium value, the vapor at the outlet becomes cooler than before and may even become two-phase if the dryout point moves towards the outlet. The resulting change in density of the flow may result in the pressure drop in the vapor section of the tube increasing. If the mass flow rate initially stays constant the pressure drop in the rest of the tube decreases which after a time delay causes a lower flow rate. The lower flow rate now results in warmer vapor that results in a decreased pressure drop. This time delay in the effects of the mass flow rate and the resulting pressure drop between the liquid, two phase, and vapor portions of the tube can set up flow rate and pressure drop oscillations.[25]

The lack of accurate data on pressure drops in cryogenic fluids has inhibited the construction of models that explain density wave oscillations. Observations of density wave oscillations in other fluids such as water and freon have revealed a few general clues to their behavior. The period of the oscillations is on the order of the residence time of a fluid particle in the heated tube. Stability is increased by increasing the inlet pressure drop or by decreasing the outlet pressure drop. Thus the presence of an inlet orifice stabilizes the flow and the presence of an outlet orifice tends to reduce the stability of the flow. If the overall system pressure is increased the vapor density increases and reduces the effect of density on the two-phase and vapor pressure drops leading to increased flow stability. The level of subcooling at the inlet also affects the stability of the system depending on the degree of subcooling. [25] Density wave oscillations were not a factor for the pre-heater in this experiment since the flow was not fully vaporized before it left the pre-heater.

4.5 Thermal Transpiration

Thermal transpiration can occur in a capillary tube when a temperature gradient between the ends of the tube results in a pressure gradient that causes a flow from the cold end to the warm end of the tube. This effect may be observed if the mean free path of the gas molecules is comparable to the tube diameter. A situation like this could arise in the capillary tubes that connect the pressure taps at the vacuum chamber at 4.2 K to the baratrons which operate at room temperature. If thermal transpiration occurs, this effect needs to be accounted for in the pressure measurements [18, 19].

Liang proposed the thermal transpiration correction factor shown in equation (48):

$$TT = \frac{P_{T,Low}}{P_{T,High}} = \frac{\tau_{He}\left(\upsilon_g U\right)^2 + \omega_{He}\left(\upsilon_g U\right) + W}{\tau_{He}\left(\upsilon_g U\right)^2 + \omega_{He}\left(\upsilon_g U\right) + 1} \tag{48}$$

where, $P_{T,Low}$ and $P_{T,High}$ are the pressures (in mm of Hg) at the low temperature (T_{Low}) end and the high temperature (T_{High}) end of the capillary tube respectively. τ_{He} is a constant with the value 2.52. υ_g is a pressure shifting factor which depends on the gas and is defined such that υ_{He} is 1. W is defined by equation (49):

$$W = \left(T_{Low} / T_{High}\right)^{0.5} \tag{49}$$

ω_{He} is defined by equation (50):

$$\omega_{He} = 7.68\left(1 - W\right) \tag{50}$$

U is defined by equation (51):

$$U = P_{T,High} d_{i,mm} \tag{51}$$

where, $d_{i,mm}$ is the inner diameter of the capillary tube in mm.

Calculating the thermal transpiration effect in this experiment reveals that TT≈1. Therefore thermal transpirations effects did not make a significant difference to the pressure readings in this experiment.

5 Uncertainty Analysis

The uncertainty in the measurements and calculations for the test section are discussed in this section. The uncertainty analysis is performed using the Kline McClintock technique for uncertainty analysis for single sample experiments. [26] Neither Keilin nor Ogato and Sato provide a comprehensive uncertainty analysis with the data that they presented.

5.1 Temperature, Pressure, Differential Pressure, Lengths, Voltages

Uncertainty in Measurement	Device	Symbol	Accuracy or Relative Accuracy
Temperature - Cernox Thermometer - Rated	Cernox Thermometer	δT_{Cernox}	± 5e-3 K
Current - Excitation - Cernox Thermometer	Keithley 220	δI_E	± (0.1e-3% + 1e-9A)
Voltage - Excitation - Cernox Thermometer	HP E1410 A	δV_E	± (4e-3 % + 3.9e-6 V)
Resistance - Test Section Heater	HP E1410 A	δR_{TS}	± (4.5e-3% + 4.5e-3Ω)
Voltage - Test Section Heater	HP E1410 A	δV_{TS}	± (3.5e-3 % + 200e-6 V)
Current - Test Section Heater	HP/Agilent E3616A	δI_{TS}	± 0.5 % + 2 Counts
Voltage - Pre-Heater	HP E1410 A	δV_{PH}	For 3 V<V_{PH}≤30 V: δV_{PH} = ± (3.5e-3% + 200e-6 V) For 30 V<V_{PH}≤300 V: δV_{PH} = ± (6.3e-3% + 700e-6 V)
Resistance - Pre-Heater	HP E1410 A	δR_{PH}	± (6.5e-3% + 60e-3Ω)
Diameter	Calipers	δd	± 1.27e-5 m
Length	Ruler	δL	± 5e-4 m
Absolute Pressure - Rated	MKS 627	δP/P	± 0.12 %
Differential Pressure - Rated	MKS 120AD	δΔP/ΔP	± 0.12 %
Voltage - Test Section - Differential Pressure	HP E1410 A	$\delta V_{TS\Delta P}$	± (1.7e-3 % + 9e-6 V)
Discharge Coefficient - Venturi	Fox Valve Venturi	$\delta C_D/C_D$	± 2 %
Venturi - Diameter Inlet	Fox Valve Venturi	δd_{VenIn}	± 1.27e-4 m
Venturi - Diameter Throat	Fox Valve Venturi	$\delta d_{VenThroat}$	± 2.54e-5 m

Table 8: Accuracy or relative accuracy of instrument used to make relevant measurements.

Table 8 summarizes the accuracies or relative accuracies of the various direct measurements that were made. Each measurement device was calibrated to ensure the accuracy specified by the device manufacturer.

5.2 Heat Transfer Coefficient

The heat transfer coefficient is an explicit function of measured values, so the uncertainty in the heat transfer can be calculated by taking the differential on both sides of equation (39). [26] The heat transfer coefficient uncertainty and relative uncertainties are given by equation (52) :

$$\delta h_{TS} = \left[\left(\frac{\partial h_{TS}}{\partial V} \delta V \right)^2 + \left(\frac{\partial h_{TS}}{\partial I} \delta I \right)^2 + \left(\frac{\partial h_{TS}}{\partial d} \delta d \right)^2 + \left(\frac{\partial h_{TS}}{\partial L} \delta L \right)^2 + \left(\frac{\partial h_{TS}}{\partial \Delta T} \delta \Delta T \right)^2 \right]^{0.5} \qquad (52)$$

Equation (52) can be reduced to equation (53) to determine the relative uncertainty of the measured and calculated test section heat transfer coefficient.

$$\frac{\delta h_{TS}}{h_{TS}} = \left[\left(\frac{\delta V}{V} \right)^2 + \left(\frac{\delta I}{I} \right)^2 + \left(\frac{\delta d}{d} \right)^2 + \left(\frac{\delta L}{L} \right)^2 + \left(\frac{\delta T_w}{(T_w - T_f)} \right)^2 + \left(\frac{\delta T_f}{(T_w - T_f)} \right)^2 + \frac{2 \delta T_w \delta T_f}{(T_w - T_f)^2} \right]^{0.5} \qquad (53)$$

The temperature measurements are made using a four wire resistance measurement across the Cernox thermometers. An excitation current (I_E) is delivered and the resulting excitation voltage drop (V_E) across the Cernox thermometer is measured. The resistance of the cernox thermometer, given by the ratio of V_E to I_E, is compared to the specific calibration provided by the manufacturer of the Cernox thermometer, Lake Shore Cryotronics, Inc. The uncertainty in the temperature measurements can be calculated using equation (54)

$$\delta T = \left[\left(\frac{\partial T}{\partial I_E} \delta I_E \right)^2 + \left(\frac{\partial T}{\partial I_E} \delta V_E \right) + \delta T_{Cernox}^2 \right]^{0.5} \tag{54}$$

Equation (54) can be reduced to equation (55) to directly calculate the uncertainty in the Cernox thermometer measurements.

$$\delta T = \left[\left(R \frac{dT}{dR} \frac{\delta I_E}{I_E} \right)^2 + \left(\frac{1}{I_E} \frac{dT}{dR} \delta V_E \right) + \delta T_{Cernox}^2 \right]^{0.5} \tag{55}$$

The term δT_{Cernox} is the thermometer accuracy provided by Lake Shore. The thermometer resistance, R and the thermometer sensitivity dR/dT=1/(dT/dR), can be found from the calibration certificate of the individual thermometer for a specified temperature. The thermometer excitation current, I_E, controlled by the LabView Data Acquisition System and delivered by a Keithley 220 current source is calculated as a function of the temperature and the corresponding thermometer resistance and is given by equation (56).

$$I_E = \left[1e-9 \frac{T^2}{R} \right]^{0.5} \tag{56}$$

Many steps were taken in the planning of this experiment to minimize the heat leak from the test section to the surroundings, such as the use of low thermal conductivity support structures, a vacuum chamber for convective isolation and the use of MLI for radiative isolation. This heat leak may be a source of systematic error for this experiment and needed to be quantified to calculate the correct heat transfer coefficient. In order to quantify the heat leak from the test section the following analysis was performed. Figure 31 shows the test section and the relevant heat sources and temperatures.

A steady-state energy balance of the test section is given by equation (57):

$$\dot{q}_{TS} - \dot{q}_{TS,\,Leak} = h_{TS} A_{TS} \left(T_{TS-W} - T_{TS-F-In} \right) \tag{57}$$

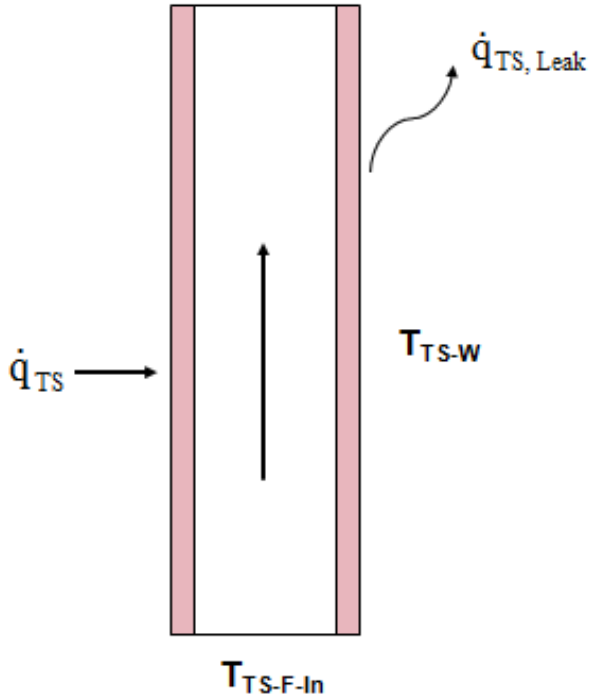

Figure 31: Heat leak, power applied, wall and flow temperatures in test section.

This heat leak is added to the numerator on the right hand side of equation (39) to get the systematic error corrected heat transfer coefficient in equation (58)

$$h_{TS} = \frac{\dot{q}_{TS} - \dot{q}_{TS\text{-}Leak}}{\pi dL\left(T_{TS-W} - T_{TS-F-In}\right)} \tag{58}$$

Careful measurement and accounting of all the sources of heat leak from the test section to the surroundings accounting for all the conductive and radiative losses (there are no convective losses since the test section is in vacuum), reveals the maximum overall heat leak is very small; $\dot{q}_{TS\text{-}Leak,Max}$ = 0.267e-3 W. The applied heat for performing the heat transfer coefficient is comparatively very large; $\dot{q}_{TS}$ = 0.5 W. Since the heat leak is extremely small compared to the applied heat, the heat leak is not a significant source of systematic error and equation (58) can be simplified to equation (59):

$$h_{TS} = \frac{\dot{q}_{TS}}{\pi dL\left(T_{TS-W} - T_{TS-F-In}\right)} \tag{59}$$

Equation (59) is the same as equation (39) and the uncertainty in the heat transfer coefficient can be calculated using equation (53). The maximum uncertainty in the heat transfer coefficient measurement is less than 2.5% for all the heat transfer coefficient data that has been collected for this experiment.

5.3 Pressure Drop Gradient

The pressure drop gradient in the test section is given by equation (60)

$$\Delta P'_{TS} = \frac{\Delta P}{L_{TS}} \tag{60}$$

The pressure drop gradient is an explicit function of measured values, so the uncertainty in the heat transfer can be calculated by taking the differential on both sides of equation (60). The pressure drop gradient uncertainty is given by equation (61):

$$\delta\Delta P'_{TS} = \left[\left(\frac{\partial \Delta P'_{TS}}{\partial \Delta P_{TS}} \delta\Delta P_{TS} \right)^2 + \left(\frac{\partial \Delta P'_{TS}}{\partial L_{TS}} \delta L_{TS} \right)^2 \right]^{0.5} \tag{61}$$

Equation (61) can be reduced to equation (62) to determine the relative uncertainty of the measured and calculated pressure drop gradient.

$$\frac{\delta\Delta P'_{TS}}{\Delta P'_{TS}} = \left[\left(\frac{\delta\Delta P_{TS}}{\Delta P_{TS}} \right)^2 + \left(\frac{\delta L_{TS}}{L_{TS}} \right)^2 \right]^{0.5} \tag{62}$$

The maximum uncertainty in the pressure drop gradient measurement is less than 0.52%.

5.4 Dryout Heat Flux

The dryout heat flux is an explicit function of measured values, so the uncertainty in the heat transfer can be calculated by taking the differential on both sides of equation (40). The heat transfer coefficient uncertainty can be given by equation (63):

$$\delta \dot{q}''_{PH} = \left[\left(\frac{\partial \dot{q}''_{PH}}{\partial V_{PH}} \delta V_{PH} \right)^2 + \left(\frac{\partial \dot{q}''_{PH}}{\partial R_{PH}} \delta R_{PH} \right)^2 + \left(\frac{\partial \dot{q}''_{PH}}{\partial d_{PH}} \delta d_{PH} \right)^2 + \left(\frac{\partial \dot{q}''_{PH}}{\partial L_{PH}} \delta L_{PH} \right)^2 \right]^{0.5} \quad (63)$$

Equation (63) can be reduced to equation (64) to determine the relative uncertainty of the measured and calculated pre-heater dryout heat flux.

$$\frac{\delta \dot{q}''_{PH}}{\dot{q}''_{PH}} = \left[\left(\frac{2\delta V_{PH}}{V_{PH}} \right)^2 + \left(\frac{\delta R_{PH}}{R_{PH}} \right)^2 + \left(\frac{\delta d_{PH}}{d_{PH}} \right)^2 + \left(\frac{\delta L_{PH}}{L_{PH}} \right)^2 \right]^{0.5} \quad (64)$$

The maximum uncertainty in the dryout heat flux measurement is less than 0.33%.

5.5 Reynolds Number and Quality

The Reynolds number and quality were set in this experiment based on measurements of the mass flow rate and the inlet thermodynamic condition, as shown in equations (35) and (38) respectively. The mass flow rate was calculated by measuring the pressure drop in the venturi which was read as a voltage. The turbulent flow fluctuated so the voltage reading fluctuates. The voltage reading is compared to a calibration of the differential baratron to determine the pressure drop. This pressure drop is then used to calculate the mass flow rate as shown in equation (34). The mass flow rate can then be used to calculate the Reynolds number if the entire flow was vapor ($Re_{t,v}$). In addition, given this mass flow rate, and the inlet thermodynamic conditions a known amount of power is applied at the pre-heater to increase the enthalpy of the fluid to the required enthalpy level for the desired quality. The highly turbulent two-phase flow fluctuated about a nominal observed value. To calculate the observed uncertainty in the Reynolds number and quality measurements, the highest observed value and the lowest observed value for the venturi pressure drop voltage are recorded along with the nominal pressure drop voltage. For each of these extreme values of uncertainty in the pressure drop the mass flow rate is calculated. The maximum and minimum mass flow rate numbers are used to calculate the maximum and

minimum Reynolds numbers for each run. This provides the uncertainty in the observed Reynolds number ($\delta Re_{t,v,Observe}$) due to flow fluctuation. Similarly the maximum and minimum mass flow rates are used to calculate the maximum and minimum qualities obtained using equations (34) and (38). This provides the uncertainty in the observed quality ($\delta x_{Observe}$) due to flow fluctuation.

The observed uncertainty in the Reynolds number is combined with the uncertainty in the measurement of the terms associated with calculation of the Reynolds number, to get the total uncertainty in the Reynolds number, as shown in equation (65).

$$\frac{\delta \mathrm{Re}}{\mathrm{Re}} = \left[\left(\frac{\delta \dot{m}}{\dot{m}} \right)^2 + \left(\frac{\delta d_{TS}}{d_{TS}} \right)^2 + \left(\frac{\delta \mu}{\mu} \right)^2 + \left(\frac{\delta \mathrm{Re}_{\mathrm{Observe}}}{\mathrm{Re}_{\mathrm{Observe}}} \right)^2 \right]^{0.5} \tag{65}$$

The observed uncertainty in the quality is combined with the uncertainty in the measurement of the terms associated with calculation of the quality, to get the total uncertainty in the quality, as shown in equation (66).

$$\frac{\delta x}{x} = \left[\left(\frac{\delta E_{PHIn}}{E_{PHIn}} \right)^2 + \left(\frac{\delta \dot{m}}{\dot{m}} \right)^2 + \left(\frac{\delta V_{PH}}{V_{PH}} \right)^2 + \left(\frac{\delta R_{PH}}{R_{PH}} \right)^2 + \left(\frac{\delta P_{TSIn}}{P_{TSIn}} \right)^2 + \left(\frac{\delta \Delta P_{TS}}{\Delta P_{TS}} \right)^2 + \left(\frac{\delta x_{Observe}}{x_{Observe}} \right)^2 \right]^{0.5} \tag{66}$$

The uncertainty in the mass flow rate is given by equation (67).

$$\frac{\delta \dot{m}}{\dot{m}} = \left[\left(\frac{\delta C_D}{C_D} \right)^2 + \left(\frac{\delta \rho}{\rho} \right)^2 + \left(\frac{\delta \Delta P_{Ven}}{\Delta P_{Ven}} \right)^2 + \left(\frac{\delta d_{VenIn}}{d_{VenIn}} \right)^2 + \left(\frac{\delta d_{VenThroat}}{d_{VenThroat}} \right)^2 \right]^{0.5} \tag{67}$$

For the Reynolds number the dominant source of measurement uncertainty is in the available data for viscosity of helium (10%) [26].For the quality the dominant sources of measurement uncertainty are in the available data for density and enthalpy (1%) [27] and the

venturi discharge coefficient (2%) [28]. The total uncertainty in the Reynolds number is less than 12% for all the experimental data points and the total uncertainty in the quality is less than 7% for all the experimental data points. [26]

6 Data and Results

The experimental data obtained in this research will be presented in this section and depicts the high Reynolds number vertical up-flow parameters for cryogenic two-phase helium I for Reynolds numbers between 3.27e5 and 1.51e6 and for qualities between 0 and 0.3. Figure 32 compares the range of previously published data on high Reynolds number vertical up-flow parameters for two-phase helium with the data points obtained in this study. [15,16]

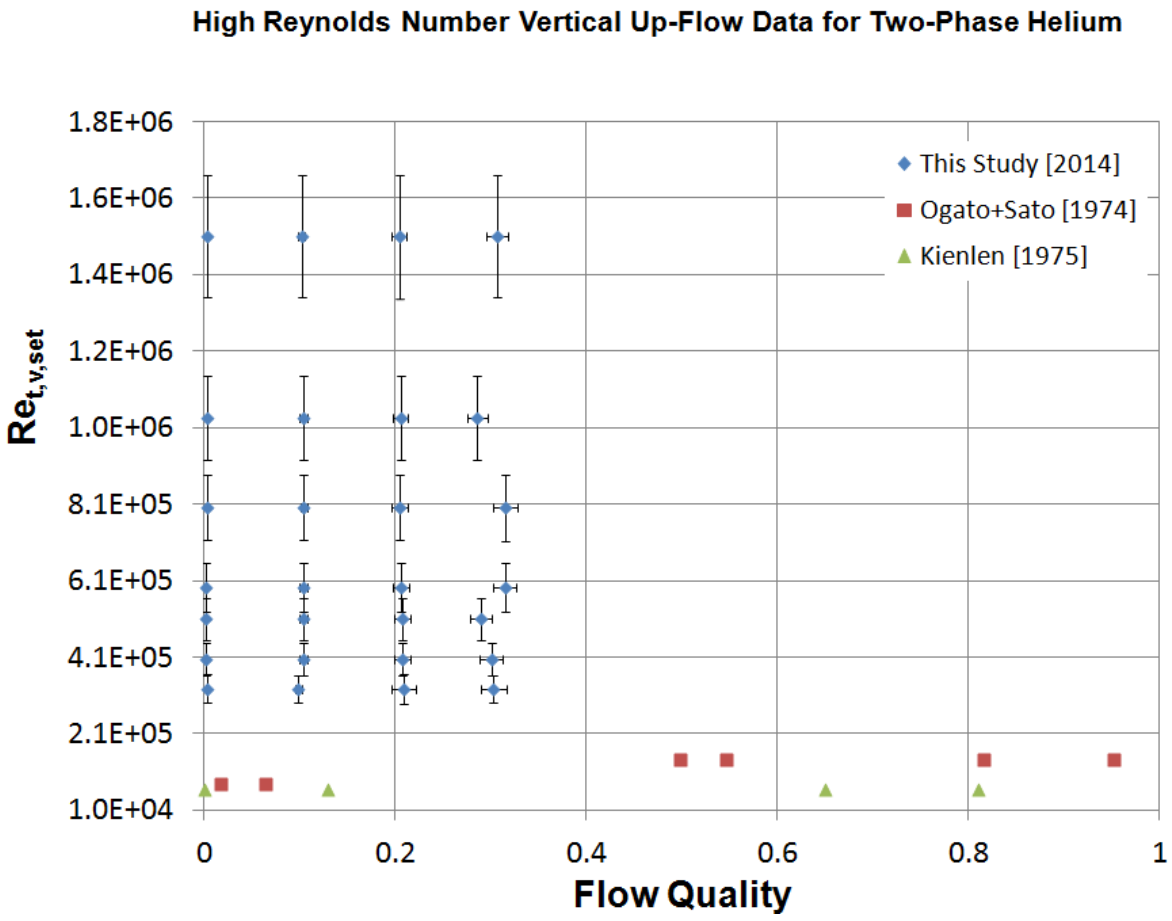

Figure 32: Comparison of Reynolds Number and Quality obtained in this study with prior Higher Reynolds Number studies

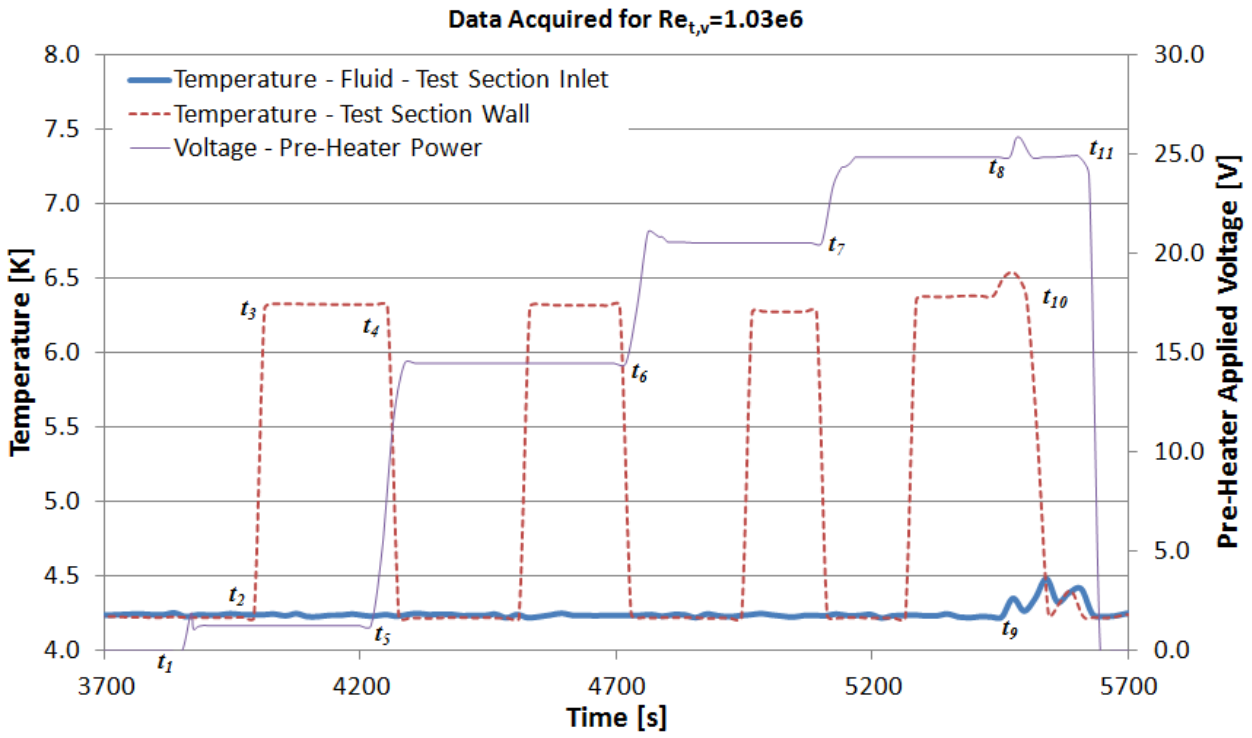

Figure 33: Unprocessed data acquired for a typical experiment run at Re$_{t,v}$=1.03e6

Figure 33 shows the unprocessed data acquired for a typical experiment run at Re$_{t,v}$=1.03e6. At time, t_1, the pre-heater was turned on to change the quality of the flow from a subcooled condition to 0.003. At t_2 the test section heater was turned on and a measured amount of power is applied to the test section wall. As a result of this heater power application the test section wall temperature started rising. At t_3 the test section wall temperature reached a steady state condition and the temperature of the test section wall along with the test section inlet temperature were recorded to calculate the heat transfer coefficient using equation (39). After the data was recorded, the test section heater was turned off at t_4. At t_5 the pre-heater power was increased to increase the quality of the flow to 0.104 and the process from t_1 to t_4 was repeated to get the heat transfer coefficient at a quality of 0.104. The process from t_1 to t_4 was again repeated at t_6 to obtain the heat transfer coefficient at a quality of 0.206 and then again at t_7 to obtain the heat transfer coefficient at a quality of 0.286. During the process from t_1 to t_7 the Test Section Inlet

temperature remained the same at around the saturation temperature of the liquid helium. However at t_8 as the pre-heater voltage was increased to try and obtain a flow quality of 0.4, the test section inlet temperature rose above the saturation temperature at t_9 indicating that a dryout condition had been reached and that at least portions of the flow had becoming superheated. When the superheating was observed the test section heater was turned off at t_{10} and the pre-heater was turned off at t_{11}. With the data acquisition for $Re_{t,v}$=1.03e6 completed, the data set for the next $Re_{t,v}$ is similarly obtained.

Table 9 summarizes the entire data set that was obtained. The data collection technique involved setting the Reynolds number and then varying the quality. Since the nature of the flow was turbulent the Reynolds number would vary slightly during the collection of the data. For each desired Reynolds number and desired quality the Reynolds number ($Re_{t,v,set}$) and quality (x_{set}) that is eventually set is recorded. The uncertainty in the set Reynolds number ($Re_{t,v,set}$ Uncertainty[%]) and the set quality (x_{set} Uncertainty[%]) are also presented in Table 9, and account for the variations in flow due to the turbulent nature of the flow. The parameters of interest are the variation of heat transfer coefficient (h_{TS}), and the the pressure drop gradient ($\Delta P'_{TS}$) with the Reynolds number and the quality at the test section. The dryout heat flux ($q''_{PH,Dryout}$) for each Reynolds number was also measured. Table 9 also shows the uncertainties in the heat transfer coefficient (h_{TS} Uncertainty [%]), pressure drop gradient ($\Delta P'_{TS}$ Uncertainty [%]) and dryout heat flux ($q''_{PH,Dryout}$ Uncertainty [%]) measurements.

Run Number	$Re_{l,v,set}$ Average	$Re_{l,v,set}$ Uncertainty [%]	x_{set}	x_{set} Uncertainty [%]	h_{TS} [W/(m^2.K)]	h_{TS} Uncertainty [%]	$\Delta P'_{TS}$ [Pa/m]	$\Delta P'_{TS}$ Uncertainty [%]	$q''_{PH,\ Dryout}$ [W/m^2]	$q''_{PH,\ Dryout}$ Uncertainty [%]
1a	3.27E+05	11.66	0.003	4.77	165	2.37	20700	0.51	719	0.32
1b			0.099	4.13	164	2.40	8687	0.51		
1c			0.209	6.19	166	2.38	6017	0.51		
1d			0.303	4.41	150	2.41	4101	0.51		
2a	4.04E+05	10.72	0.003	3.89	166	2.35	19923	0.51	737	0.32
2b			0.105	3.89	166	2.35	9050	0.51		
2c			0.208	3.96	166	2.35	5943	0.51		
2d			0.301	4.16	151	2.37	3782	0.51		
3a	5.09E+05	10.68	0.003	3.87	164	2.37	18956	0.51	911	0.32
3b			0.104	3.92	165	2.36	9673	0.51		
3c			0.208	3.99	166	2.35	6847	0.51		
3d			0.290	3.95	152	2.37	5905	0.51		
4a	5.93E+05	10.71	0.003	4.01	164	2.37	19618	0.51	1130	0.32
4b			0.104	3.97	165	2.36	10204	0.51		
4c			0.207	3.92	168	2.35	7851	0.51		
4d			0.315	3.93	153	2.37	7716	0.51		
5a	8.01E+05	10.77	0.003	3.85	166	2.35	21589	0.51	1495	0.32
5b			0.105	3.92	168	2.34	12323	0.51		
5c			0.205	3.90	170	2.34	10577	0.51		
5d			0.315	4.18	159	2.36	11617	0.51		
6a	1.03E+06	10.65	0.003	3.85	168	2.34	21883	0.51	1752	0.32
6b			0.104	3.86	168	2.34	14454	0.51		
6c			0.206	3.88	172	2.34	12563	0.51		
6d			0.286	3.86	163	2.34	16615	0.51		
7a	1.51E+06	10.68	0.004	3.85	168	2.34	25309	0.51	2804	0.32
7b			0.102	3.86	169	2.34	23286	0.51		
7c			0.205	3.95	174	2.34	24904	0.51		
7d			0.307	3.85	166	2.35	32052	0.51		

Table 9: Data Collected for High Reynolds Number Vertical Up-flow for Two Phase Helium.

6.1 *Heat Transfer Coefficient*

Figure 34 shows the variation of heat transfer coefficient with flow quality for various Reynolds number vertical up-flows of two phase helium. There is an increase in heat transfer coefficient with Reynolds number at a given quality. This is easily distinguishable for large increments in Reynolds number. It appears that fairly large increases in Reynolds number are necessary to see substantial increases in heat transfer coefficient. It was not possible to obtain qualities above 0.3 with the current hardware because of the dryout at the pre-heater. However it is observed that there is a fairly dramatic drop in heat transfer coefficient as the flow changes from a single phase type nature at lower qualities to a different flow pattern at the intermediate

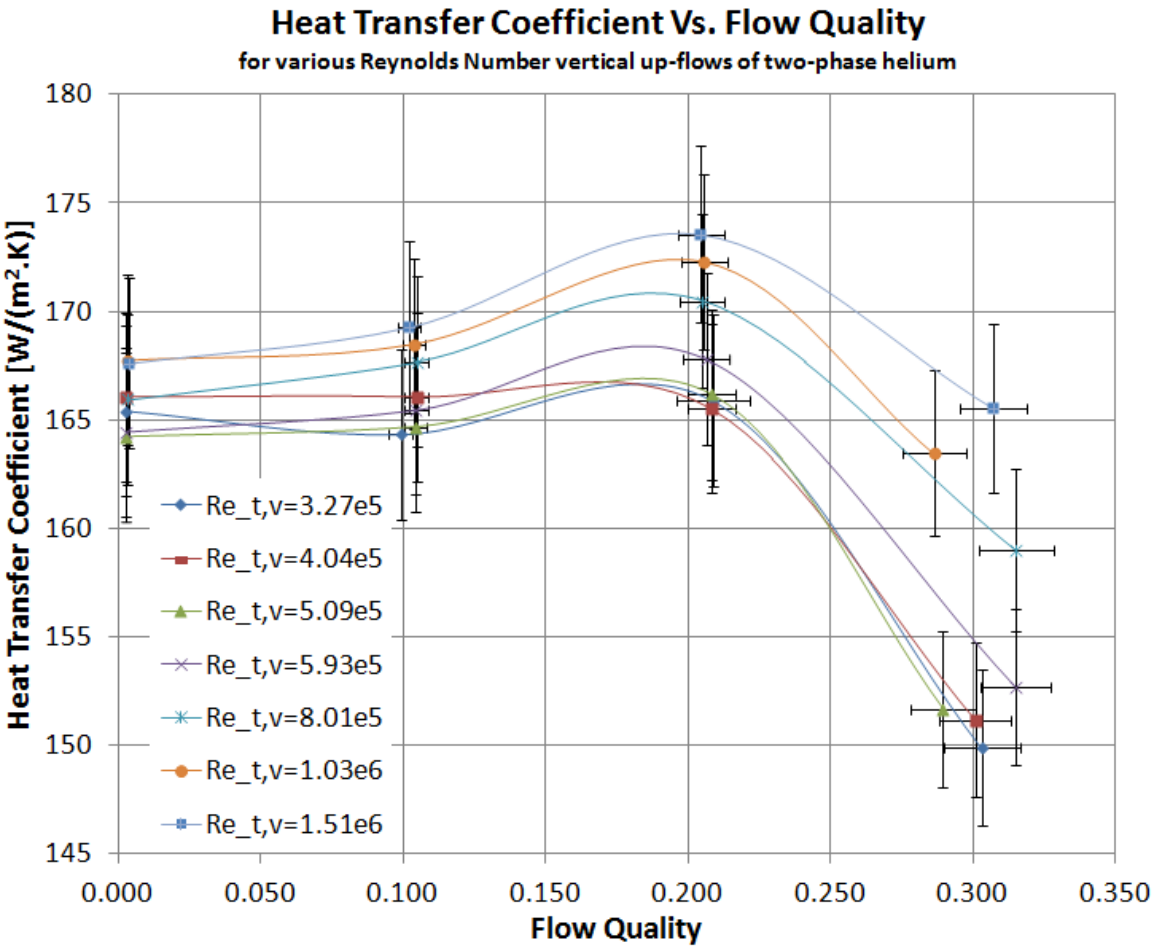

Figure 34: Heat transfer coefficient variation with flow quality for various Reynolds Number vertical up-flows of two -phase helium.

quality above 0.2. The increase in heat transfer coefficient with Reynolds number becomes more pronounced at the intermediate qualities above 0.2.

6.2 Pressure Drop

Figure 35 shows the variation of pressure drop gradient with flow quality for various Reynolds number vertical up-flows of two phase helium. As may be expected there is an increase in pressure drop gradient with Reynolds number which is easily distinguishable for large increments in Reynolds number. It was not possible to obtain qualities above 0.3 for the existing hardware because of the dryout at the pre-heater. At the lower Reynolds numbers, of up to 5e5 the pressure drop gradient keeps falling at the intermediate quality of 0.3. At Reynolds numbers

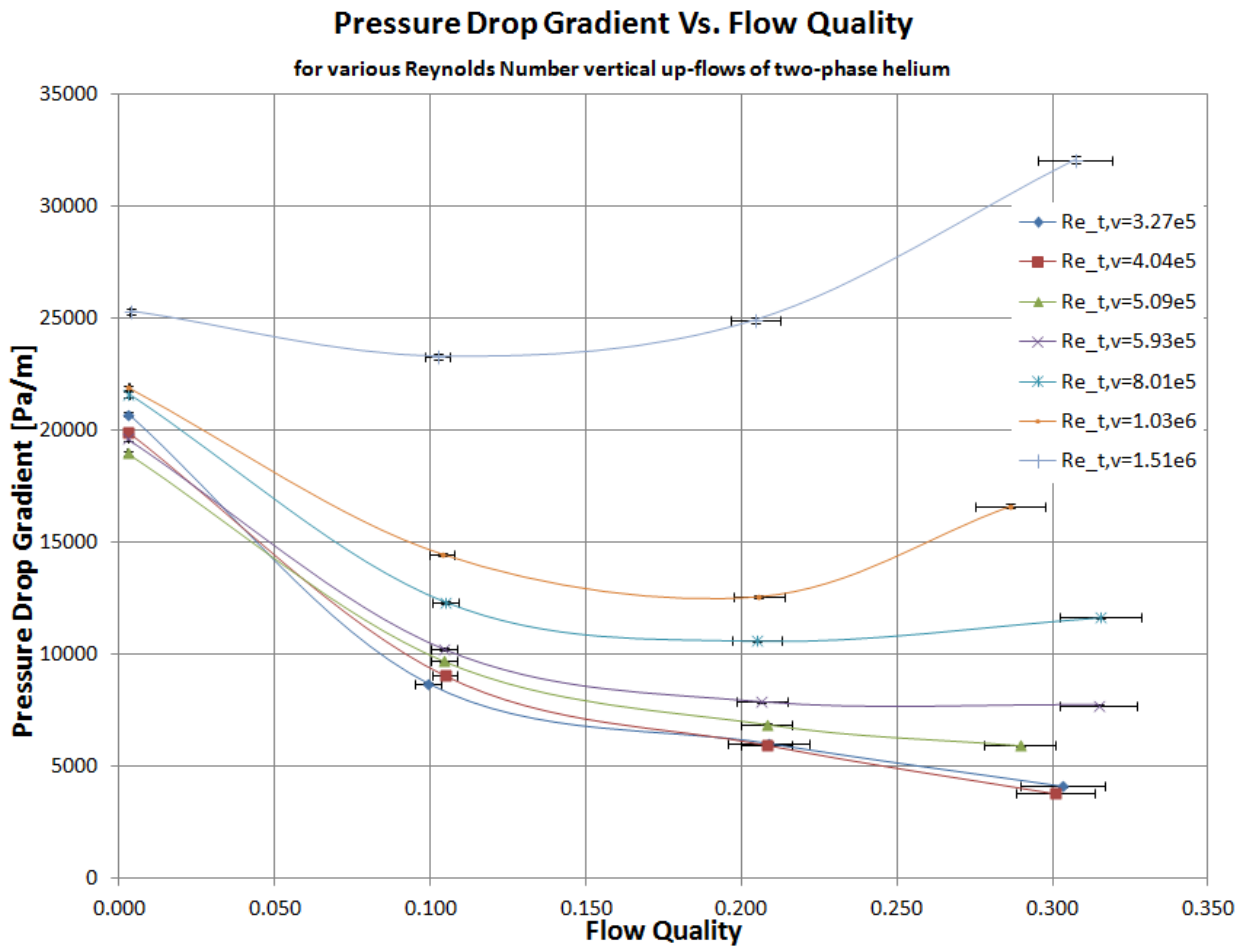

Figure 35: Pressure Drop Gradient variation with flow quality for various Reynolds Number vertical up-flows of two -phase helium.

around 5.93e5 it is observed that the pressure drop gradient starts rising again at increasing qualities.

6.3 Dryout Heat Flux

Figure 36 shows the variation in the dryout heat flux with Reynolds number. As might be expected the dryout heat flux increases with Reynolds number.

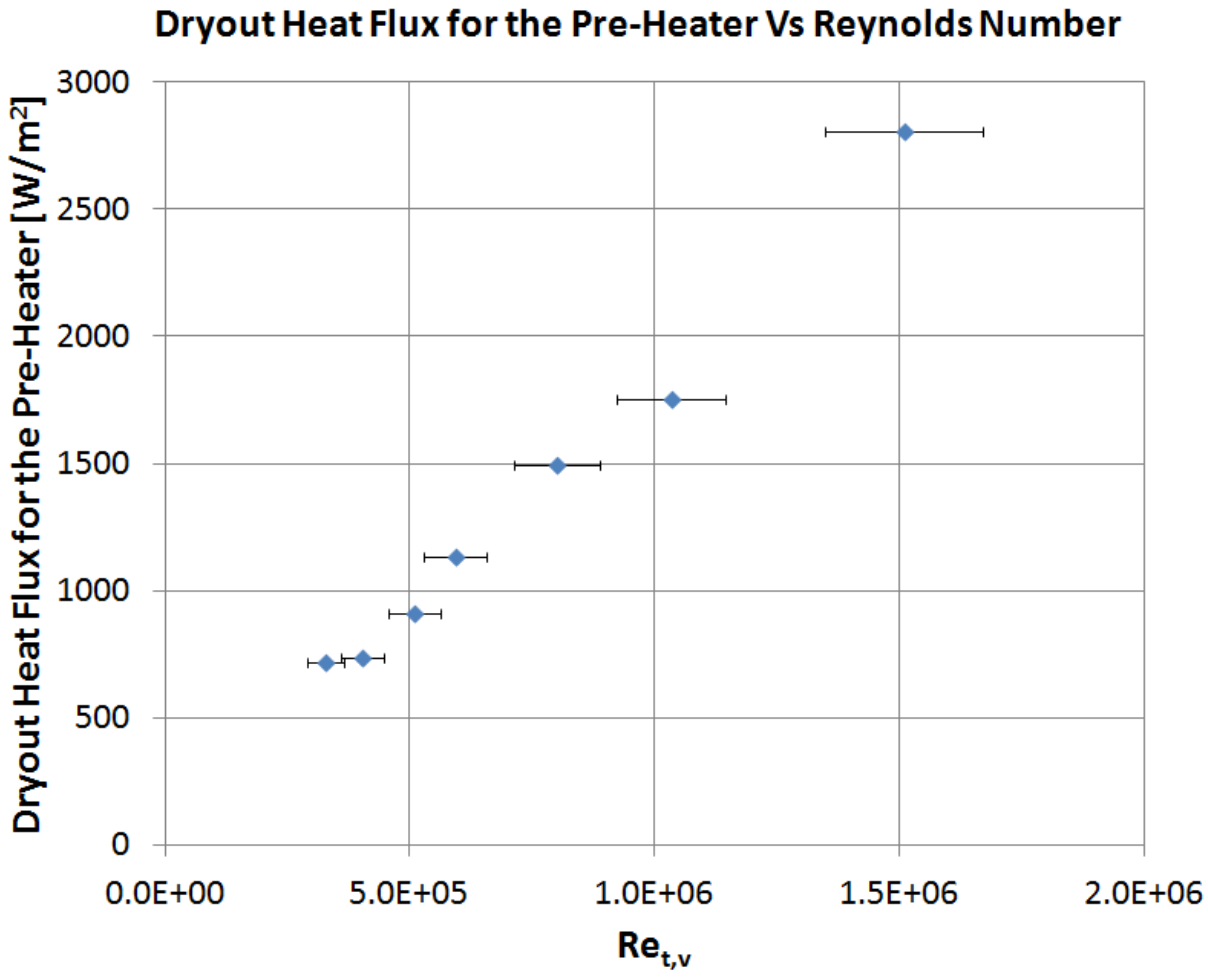

Figure 36: Dryout Heat Flux in Pre-Heater with variation with Reynolds Number.

7 New Correlation Development

In this section new correlations are developed for the heat transfer coefficient, pressure drop and dryout heat flux for vertical two phase helium up-flows for Reynolds numbers between 3.27e5 and 1.51e6 and for qualities between 0 and 0.3. These new correlations have a significantly improved agreement with the data collected for this experiment when compared with previous correlations.

7.1 Heat Transfer Coefficient – New Correlation

The Ogato and Sato model described in 1.4.5 for lower qualities and intermediate qualities serves as an appropriate model for the heat transfer coefficient [16]. This model uses a reduced form of the conventional single phase convection correlation shown in equation (68):

$$h_{lv} = \mathrm{C_L}\ \mathrm{Re}^{0.8}\ \mathrm{Pr}^{0.4}\ k / d_i \tag{68}$$

Ogato and Sato define Re = $\mathrm{Re_{s,l}}$, k =$\mathrm{k_l}$ and Pr = $\mathrm{Pr_l}$ and assumed $\mathrm{C_L}$ = 0.015 for x<0.25.

For the intermediate qualities, 0.25≤x≤0.75, Ogato and Sato proposed the correlation depicted by equation (69):

$$h_{lv} = \left(\mathrm{C_1} X_{tt}^{\ \mathrm{n_1}} + \mathrm{C_2} Bo^{\mathrm{n_2}}\right)\mathrm{h_{t,l}} \tag{69}$$

Here, $\mathrm{h_{t,l}}$ is derived from equation (68) assuming the entire flow is liquid. Ogato and Sato assumed $\mathrm{C_1}$ = 1, $\mathrm{C_2}$ = 1.5e3, $\mathrm{n_1}$ = -0.66, and $\mathrm{n_2}$ = 0.8 for 0.25≤x≤0.75. Figure 37 compares the experimental heat transfer coefficient data for $\mathrm{Re_{t,v}}$ = 3.27e5 with the Ogato and Sato correlation. There is a large disparity between the Ogato and Sato correlation and what was

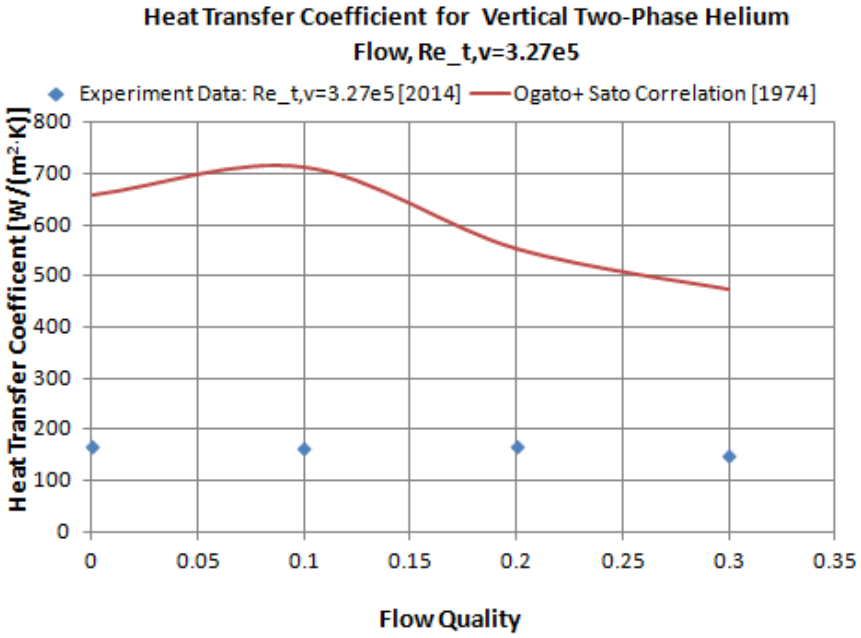

Figure 37: Heat Transfer Coefficient experimental data compared with Ogato and Sato Correlation

experimentally observed. This is true for all the Reynolds numbers that were studied experimentally.

To build a new correlation the effect of varying the constants (C_L, C_1, C_2, n_1, and n_2) was studied and a least squares optimization was carried out with each constant to minimize the disparity between the experimental data and the correlation. For $Re_{t,v}$=3.27e5, the value of the constants obtained in this way was C_L = 0.0036, C_1 = -0.11, C_2 = 6.61e5, n_1 = -0.67, and n_2 = 0.8. Figure 38 shows the new $Re_{t,v}$=3.27e5 correlation super imposed on the comparison shown on Figure 37 and shows a significantly improved agreement between the data and the new correlation for this Reynolds number.

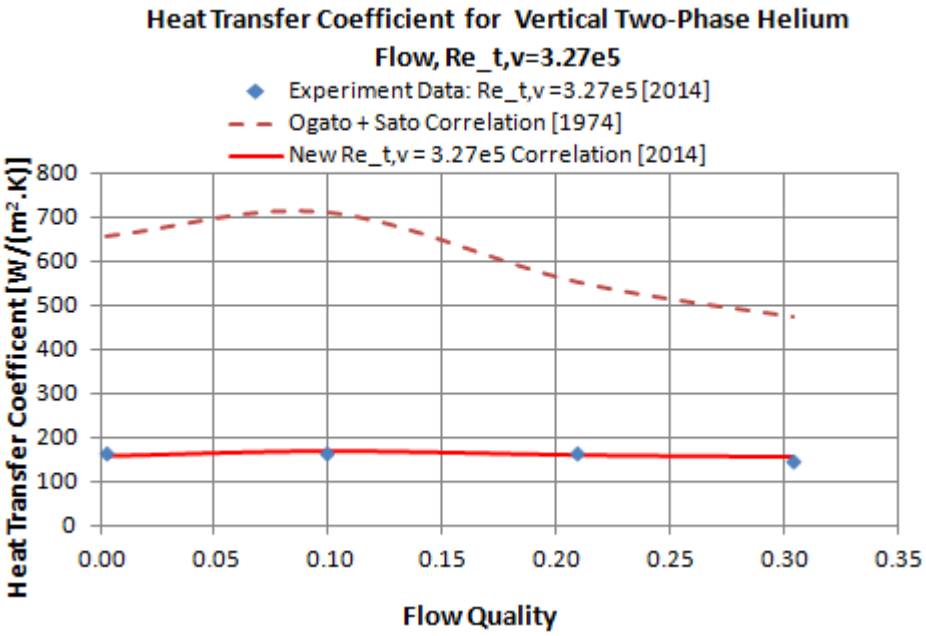

Figure 38: Heat Transfer Coefficient experimental data compared with Ogato and Sato Correlation and the new Re_t,v = 3.27e5 correlation.

A similar analysis is done for all the Reynolds number heat transfer coefficients that were being investigated. Table 10 summarizes the optimized constant values for each Reynolds number being investigated and compares it to the Ogato and Sato constant values.

$Re_{t,v}$	C_L	C_1	n_1	C_2	n_2
Ogato+Sato	0.015	1	-0.66	1.50E+03	0.8
3.27E+05	0.0040	-0.11	-0.67	6.61E+05	0.8
4.04E+05	0.0035	1.38	-0.67	1.24E+05	0.8
5.09E+05	0.0029	1.50	-0.67	4.50E+04	0.8
5.93E+05	0.0025	1.55	-0.67	2.30E+04	0.8
8.01E+05	0.0020	1.57	-0.66	1.33E+03	0.8
1.03E+06	0.0017	1.57	-0.66	1.82E+04	0.8
1.51E+06	0.0012	1.61	-0.66	1.53E+04	0.8

Table 10: Optimized Constants for Equations (68) and (69) for various Reynolds Numbers

In order to obtain a generalized correlation for the heat transfer coefficient it is necessary to correlate the constants that have the strongest variation with $Re_{t,v}$ (C_L, C_1, and C_2) as functions of $Re_{t,v}$. Since the values of C_1, and C_2 for $Re_{t,v}$=3.27e5 are substantially different for the values of C_1, and C_2 for the other $Re_{t,v}$, the curve fits are done on the basis of the other $Re_{t,v}$ in order to get the closest fit between the generalized correlation and the experimental data.

Figure 39 plots C_L as a function of $Re_{t,v}$. A power law curve fit yields the correlation depicted in equation (70):

$$C_L = 58.67 Re_{t,v}^{-0.765} \tag{70}$$

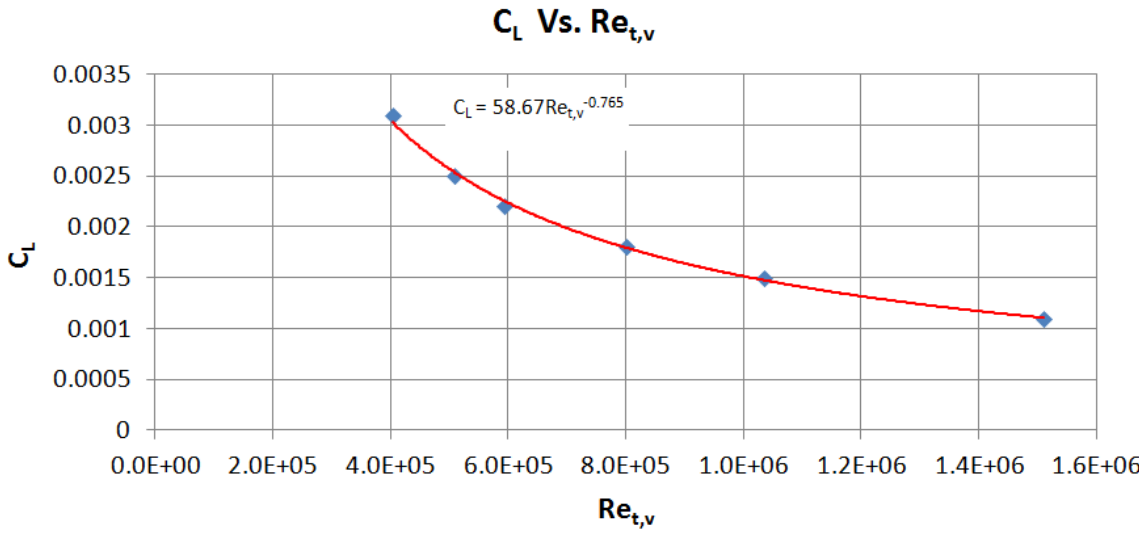

Figure 39: Power law curve fit of C_L for varying Reynolds Numbers.

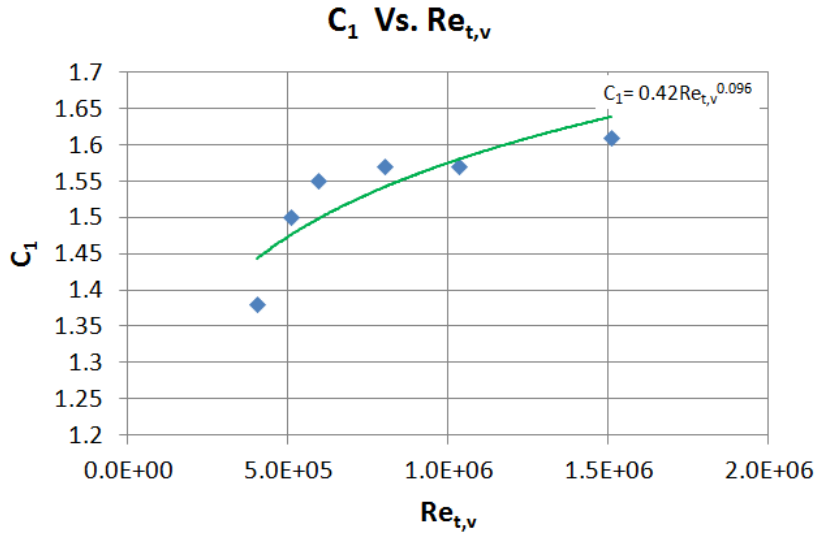

Figure 40: Power law curve fit of C_1 for varying Reynolds Numbers.

Figure 40 plots C_1 as a function of $Re_{t,v}$. A power law curve fit yields the correlation shown in equation (71):

$$C_1 = 0.42Re_{t,v}^{0.096} \tag{71}$$

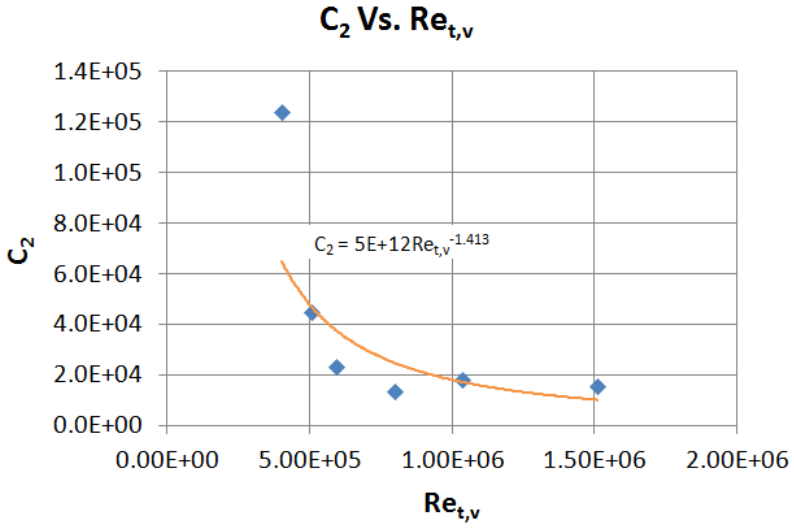

Figure 41: Power law curve fit of C_2 for varying Reynolds Numbers.

Figure 41 plots C_2 as a function of $Re_{t,v}$. A power law curve fit yields the correlation shown in equation (72):

$$C_2 = 5E+12Re_{t,v}^{-1.413} \tag{72}$$

The new generalized model for heat transfer coefficient for vertical up-flows in two-phase helium for Reynolds numbers between 3.27e5 and 1.51e6 for x<0.2 is thus given by equation (73):

$$h_{lv} = C_L \, Re^{0.8} \, Pr^{0.4} \, k / d_i \tag{73}$$

where, $Re = Re_{s,l}$, $k = k_l$ and $Pr = Pr_l$ and C_L is defined by equation (70).

For the intermediate qualities, $0.20 \leq x \leq 0.35$, equation (74) can be used:

$$h_{lv} = \left(C_1 X_{tt}^{-0.67} + C_2 Bo^{0.8} \right) h_{t,l} \tag{74}$$

Here, $h_{t,l}$ is derived from equation (73) assuming the entire flow is liquid. C_1 and C_2 are defined by equations (71) and (72) respectively.

Figure 42 to Figure 48 compares the experimental data and the new correlation for heat transfer coefficient for vertical up-flows in two-phase helium for Reynolds numbers between 3.27e5 and 1.51e6 with the existing Ogato + Sato correlation. It might be challenging to see the uncertainty bars on the data points since the uncertainty bars are about the same size as the markers. A better indication of the uncertainty bars for the heat transfer coefficient is available in Figure 34.

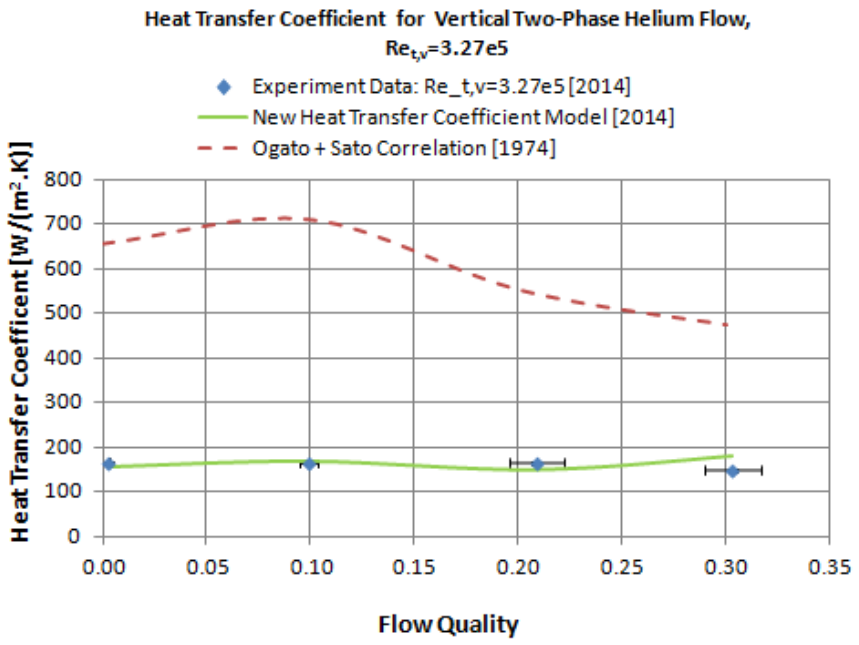

Figure 42: Heat Transfer Coefficient experimental data compared with the New Model and the Ogato and Sato Correlation for $Re_{t,v}$=3.27e5

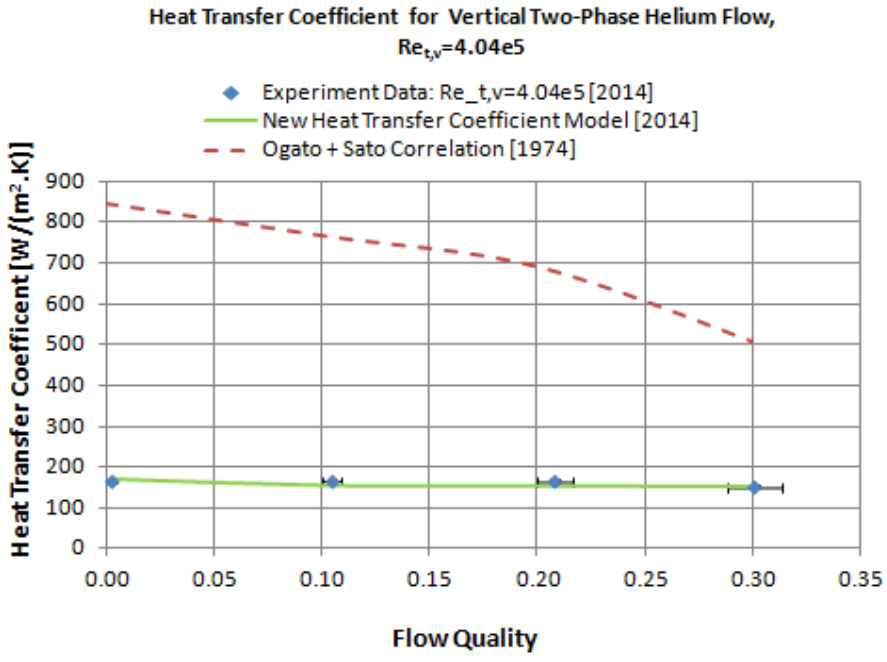

Figure 43: Heat Transfer Coefficient experimental data compared with the New Model and the Ogato and Sato Correlation for $Re_{t,v}$=4.04e5

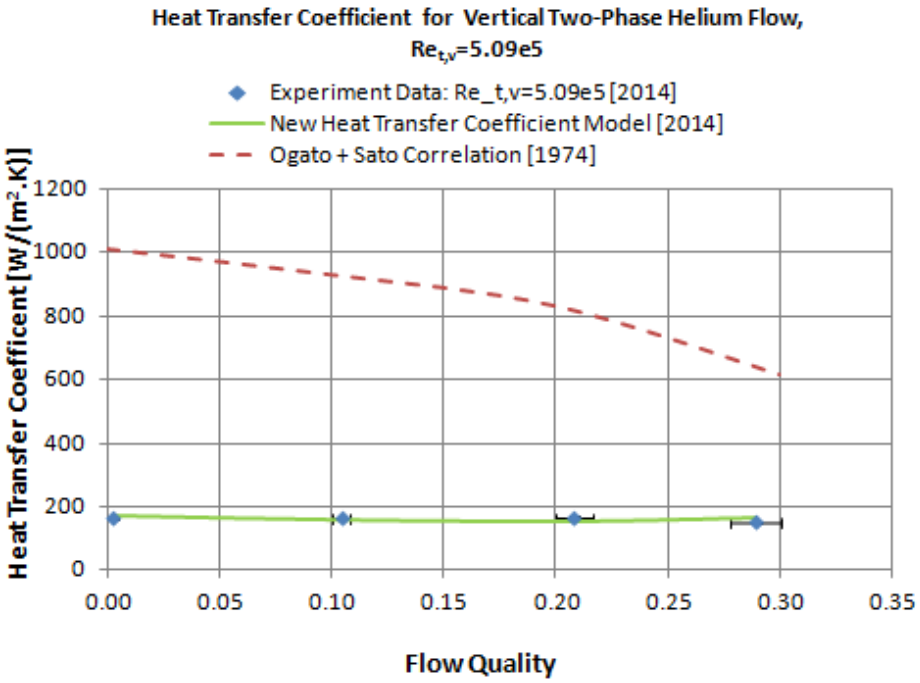

Figure 44: Heat Transfer Coefficient experimental data compared with the New Model and the Ogato and Sato Correlation for $Re_{t,v}$=5.09e5

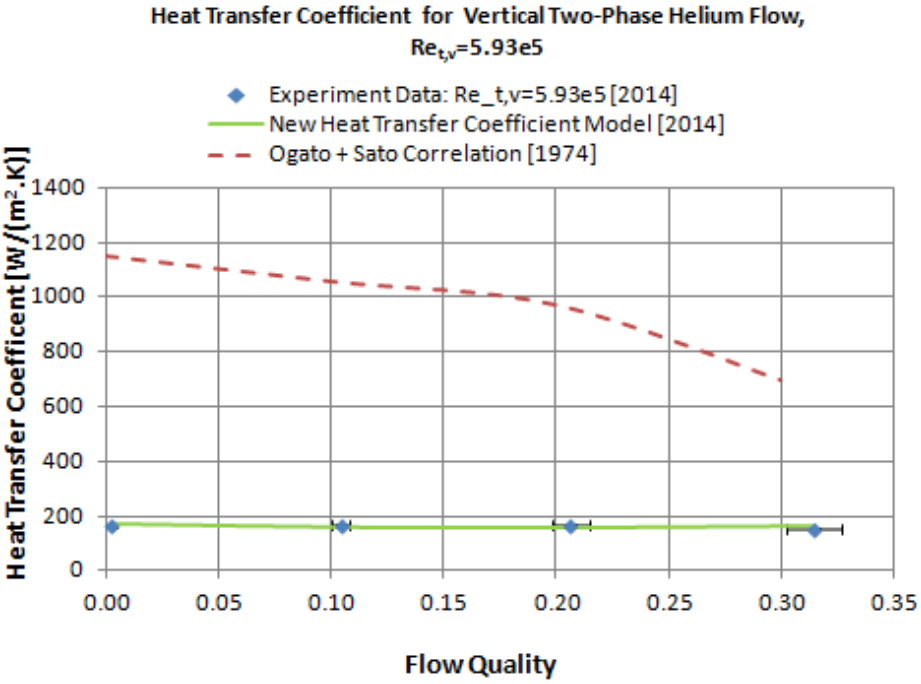

Figure 45: Heat Transfer Coefficient experimental data compared with the New Model and the Ogato and Sato Correlation for $Re_{t,v}$=5.93e5

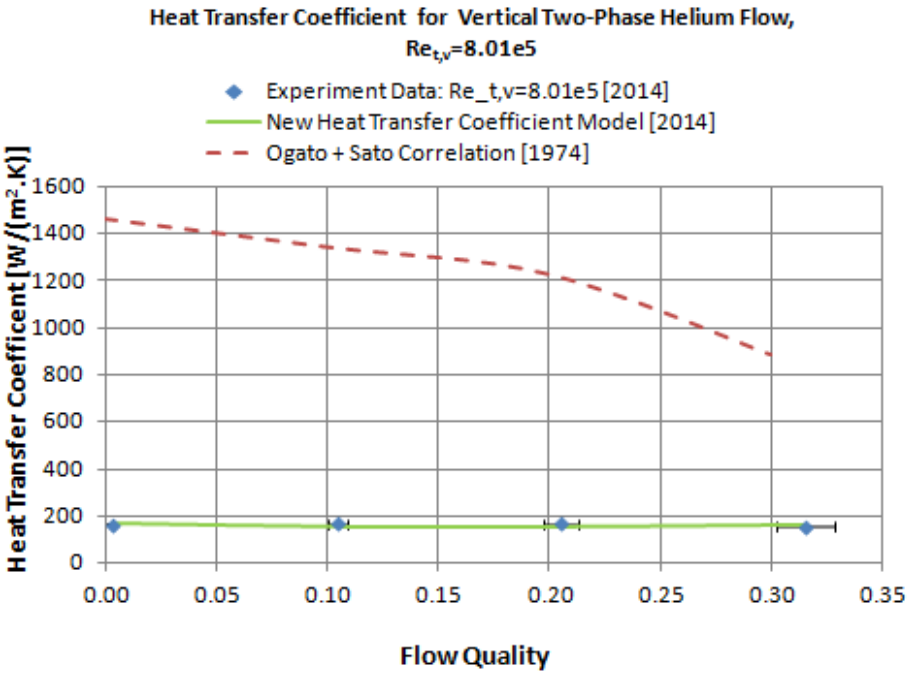

Figure 46: Heat Transfer Coefficient experimental data compared with the New Model and the Ogato and Sato Correlation for $Re_{t,v}$=8.01e5

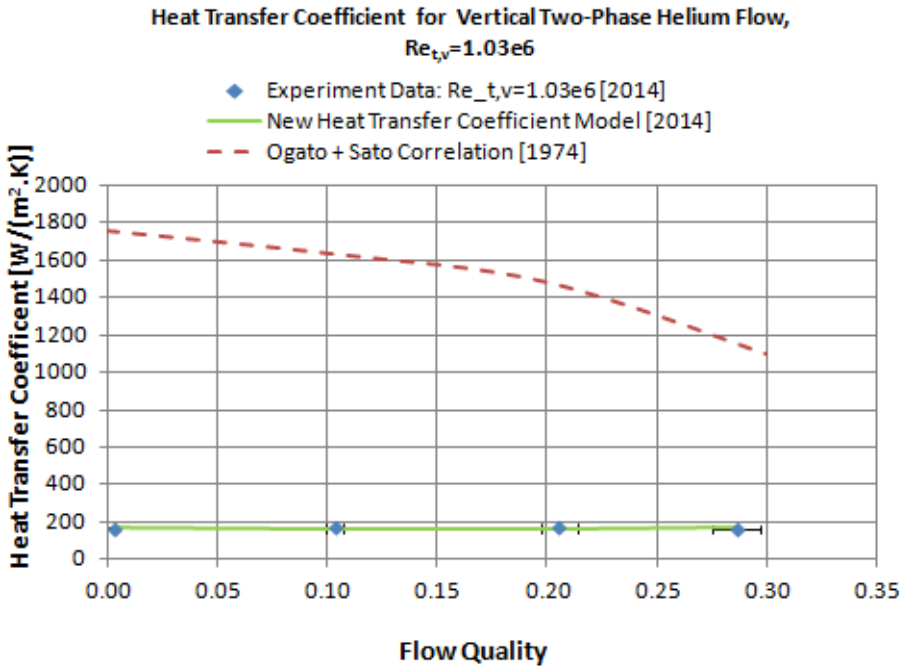

Figure 47: Heat Transfer Coefficient experimental data compared with the New Model and the Ogato and Sato Correlation for $Re_{t,v}$=1.03e6

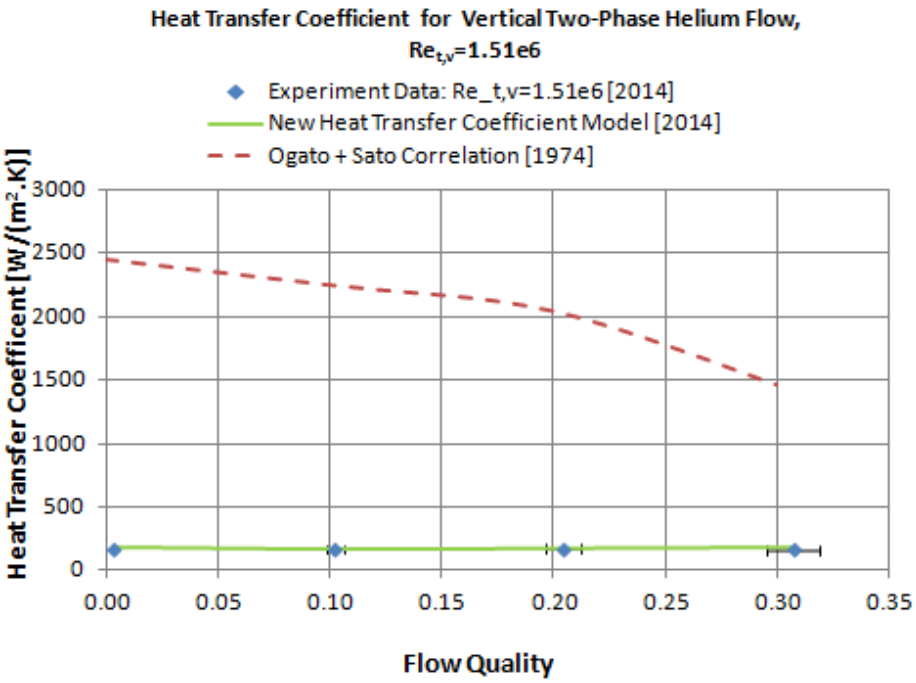

Figure 48: Heat Transfer Coefficient experimental data compared with the New Model and the Ogato and Sato Correlation for $Re_{t,v}$=1.51e6

7.2 Pressure Drop Gradient – New Correlations

The pressure drop gradient can be modeled using the separated model (Section 1.4.7) or the homogeneous model (Section 1.4.8). Figure 49 compares each of these correlations with the experimental data that is obtained and shows that there is fairly poor agreement between these correlations and the experimental data. To improve the agreement between the experimental data and the new correlations the assumed constants in each pressure drop correlation was studied and expressed as a function of the Reynolds number.

7.2.1 Separated Flow – New Correlation

The proposed new separated flow correlation is a variation of the separated flow correlation that is described in section 1.4.7. The old separated flow model is derived on the basis of the Lockhart and Martinelli correlations.

The two-phase frictional pressure drop gradient for separated flow is given by equation (75):

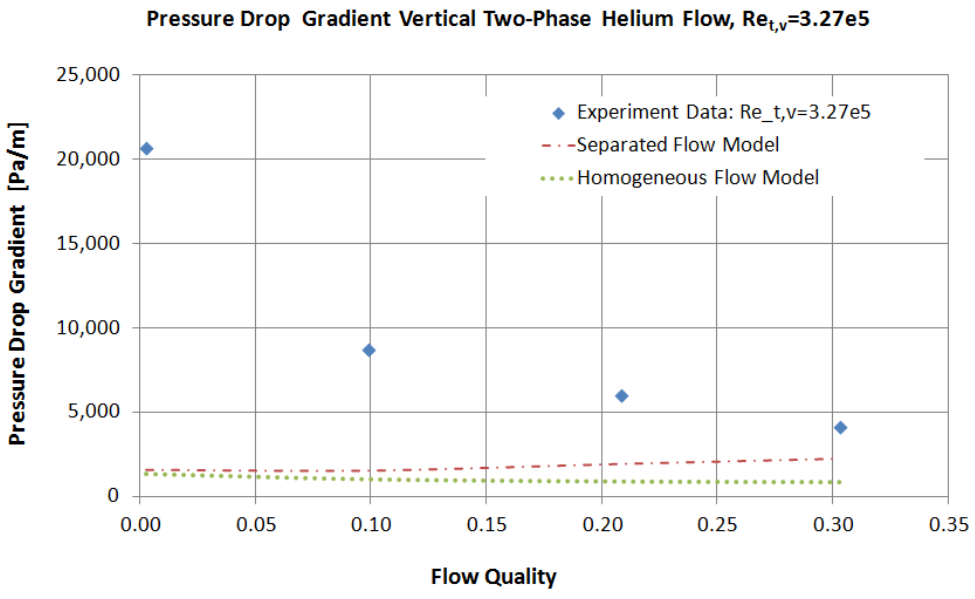

Figure 49: Pressure Drop Gradient Experimental Data compared with predictions from Separated Flow Model and Homogeneous Flow Model for Ret,v=3.27e5

$$\left(\Delta P/\Delta L\right)_{Friction,s} = \left(1-x\right)^{\left(2-C_{s3}\right)}\left(\Phi_L\right)^2\left(\Delta P/\Delta L\right)_{t,l} \tag{75}$$

The term Φ_L can be derived from equation (76):

$$\Phi_L = \left[1+\left(C_{S1}/X\right)+\left(1/X^2\right)\right]^{1/2} \tag{76}$$

X is the Martinelli parameter and is defined by equation (77):

$$X = \left[\frac{C_{S2,l}\left(\mathrm{Re}_{s,v}\right)^{C_{S3,v}}\rho_v}{C_{S2,v}\left(\mathrm{Re}_{s,l}\right)^{C_{S3,l}}\rho_l}\left(\frac{1-x}{x}\right)^2\right]^{1/2} \tag{77}$$

The effect of varying the constants (C_{S1}, $C_{S2,}$ and C_{S3}) was studied and a least squares

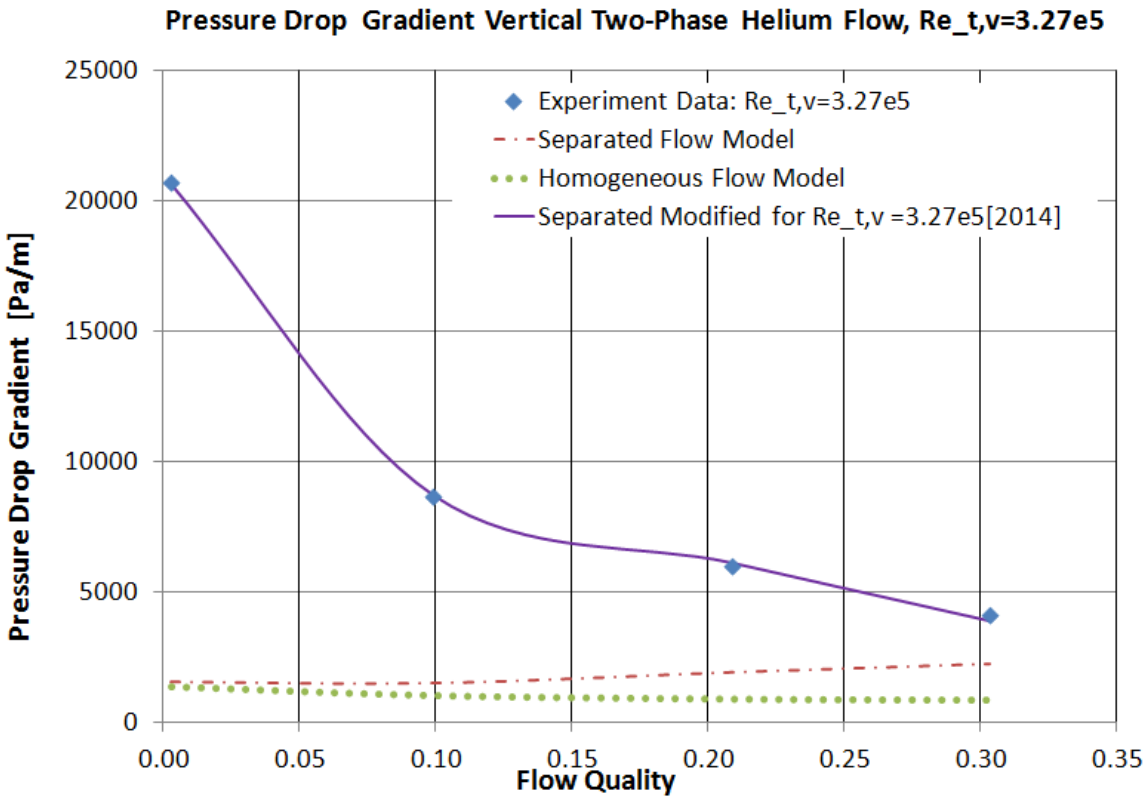

Figure 50: Pressure Drop Gradient Experimental Data compared with predictions from the previous Separated Flow Model and Homogeneous Flow Model and the Modified Separated Flow Model for Ret,v=3.27e5

optimization was carried out with each constant to minimize the disparity between the experimental data and the correlation. It was observed that the pressure drop trend seemed to change between x=0.1 and x=0.2, so two different correlations were obtained for $x \leq 0.15$ and $x>0.15$. This is probably associated with changes in the flow regime from saturated nucleate boiling to film evaporation as described in Figure 4. For $Re_{t,v}$=3.27e5, the value of the constants obtained in this way was C_{S1} = 208, C_{S2} = 0.138, C_{S3} = 0.61, for $x \leq 0.15$ and C_{S1} = 9, C_{S2} = 0.102, C_{S3} = 6.40 for $x > 0.15$. Figure 50 shows the new $Re_{t,v}$=3.27e5 correlation super imposed on the comparison shown on Figure 49 and shows a significantly improved agreement between the data and the new separated flow correlation for this Reynolds number.

A similar analysis is done for all the Reynolds numbers that were being investigated. Table 11 summarizes the optimized constant values for each Reynolds number being investigated and compares them to the previous separated flow correlation constant values.

$Re_{t,v}$	$x \leq 0.15$			$x > 0.15$		
	C_{S1}	C_{S2}	C_{S3}	C_{S1}	C_{S2}	C_{S3}
Separated Model (Previous)	20	0.184	0.2	20	0.184	0.2
3.27E+05	208	0.138	0.61	9	0.102	6.40
4.04E+05	131	0.151	0.61	5	0.099	6.42
5.09E+05	79	0.176	0.60	30	0.075	3.04
5.93E+05	64	0.176	0.59	28	0.100	2.27
8.01E+05	49	0.164	0.55	23	0.139	1.37
1.03E+06	34	0.178	0.51	20	0.288	-0.70
1.51E+06	26	0.199	0.44	20	0.184	0.48

Table 11: Optimized Constants for Equations (75)**,** (76)**, and** (77) **for various Reynolds Numbers**

In order to obtain a generalized correlation for the separated flow model pressure drop gradient it is necessary to correlate the constants C_{S1}, $C_{S2,}$ and C_{S3} with $Re_{t,v}$.

Figure 51 plots C_{S1} as a function of $Re_{t,v}$ for $x \leq 0.15$. A power law curve fit yields the correlation shown in equation (78) for $x \leq 0.15$:

$$C_{S1} = 3.67E9Re_{t,v}^{-1.331} \tag{78}$$

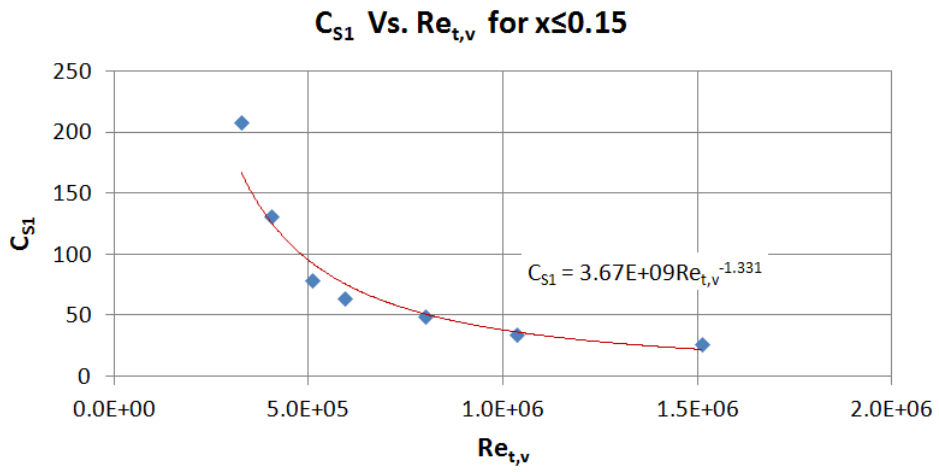

Figure 51: Power law curve fit of C_{s1} for $x \leq 0.15$ varying Reynolds Numbers.

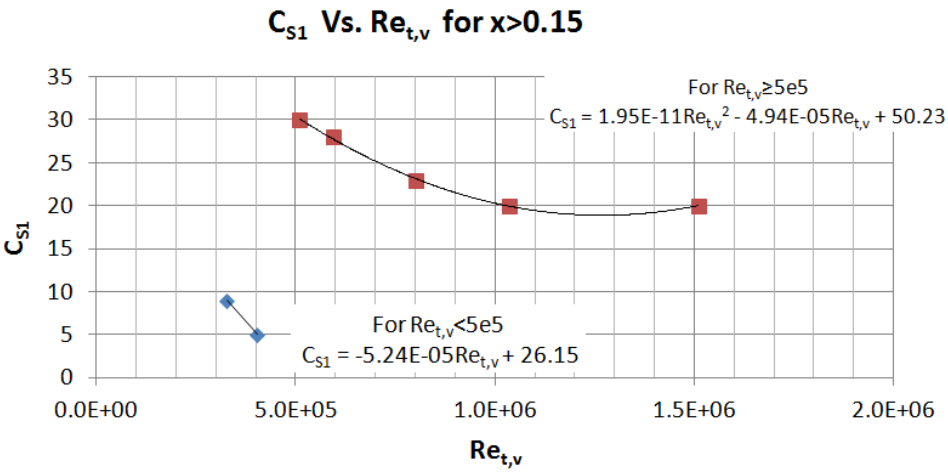

Figure 52: Curve fits of C_{s1} for x>0.15 for Ret,v <5e5 and Ret,v ≥5e5

Figure 52 plots C_{S1} as functions of $Re_{t,v}$ for x>0.15. Two correlations are obtained. For $Re_{t,v}$ < 5e5 and x>0.15, C_{S1} is given by equation (79):

$$C_{S1} = -5.24E\text{-}05Re_{t,v} + 26.15 \quad (79)$$

For $Re_{t,v} \geq$ 5e5 and x>0.15, C_{S1} is given by equation (80):

$$C_{S1} = 1.95E\text{-}11Re_{t,v}^{2} - 4.94E\text{-}05Re_{t,v} + 50.23 \quad (80)$$

Figure 53 plots C_{S2} as a function of $Re_{t,v}$ for x≤0.15. A fourth order polynomial curve fit yields the correlation shown in equation (81) for x≤ 0.15:

$$C_{S2} = -8.08E\text{-}25Re_{t,v}^{4} + 3.00E\text{-}18Re_{t,v}^{3} - 3.90E\text{-}12Re_{t,v}^{2} + 2.12E\text{-}06Re_{t,v} - 0.24 \quad (81)$$

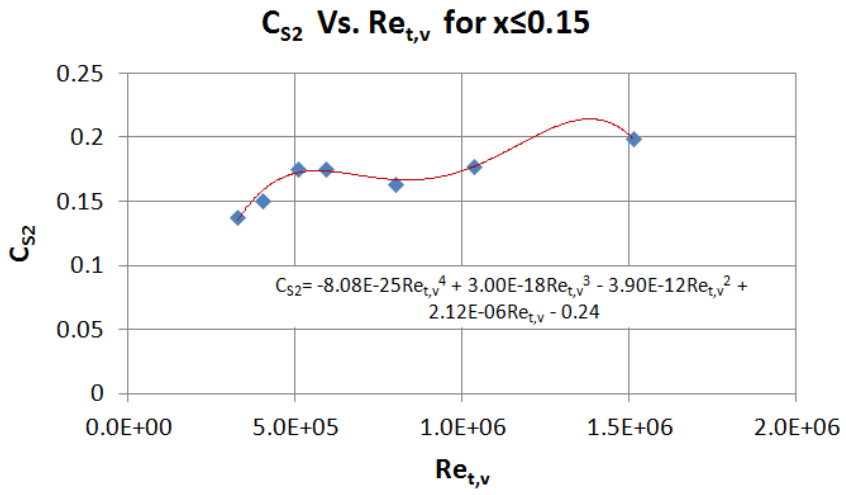

Figure 53: Polynomial Curve fits of C_{S2} for x≤0.15 for various Reynolds Numbers

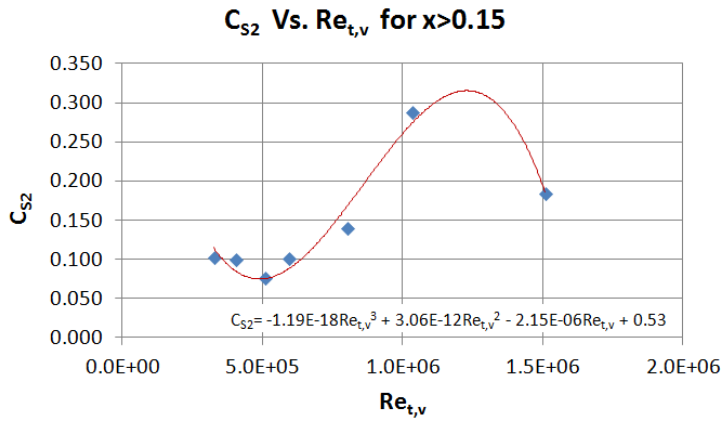

Figure 54: Polynomial Curve fits of CS2 for x>0.15 for various Reynolds Numbers

Figure 54 plots C_{S2} as a function of $Re_{t,v}$ for x>0.15. A third order polynomial curve fit yields the correlation shown in equation (82) for x>0.15:

$$C_{S2}= -1.19E\text{-}18Re_{t,v}^{3} + 3.06E\text{-}12Re_{t,v}^{2} - 2.15E\text{-}06Re_{t,\,v} + 0.53 \quad (82)$$

Figure 55 plots C_{S3} as a function of $Re_{t,v}$ for x≤0.15. A second order polynomial curve fit yields the correlation shown in equation (83) for x≤ 0.15:

$$C_{S3} = -1.8748E\text{-}14Re_{t,v}^{2} - 1.1823E\text{-}07Re_{t,v} + 0.6591 \quad (83)$$

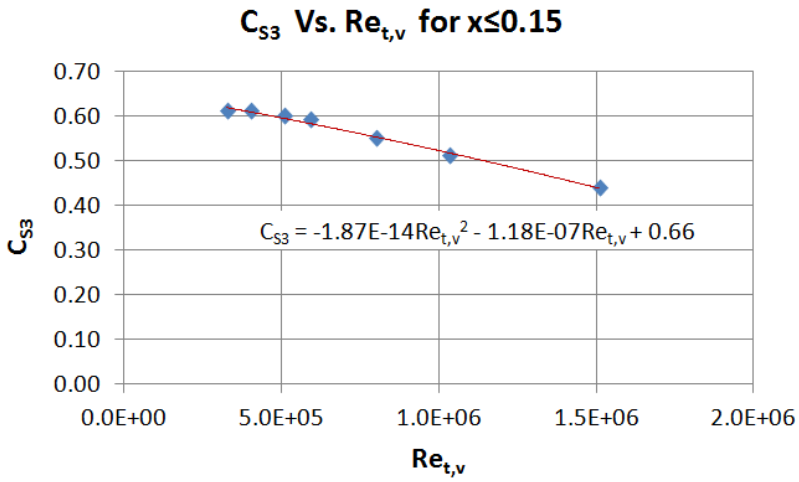

Figure 55: Polynomial Curve fits of CS3 for x≤0.15 for various Reynolds Numbers

Figure 56 plots C_{S3} as a function of $Re_{t,v}$ for x>0.15. A second order polynomial curve fit yields the correlation shown in equation (84) for x>0.15:

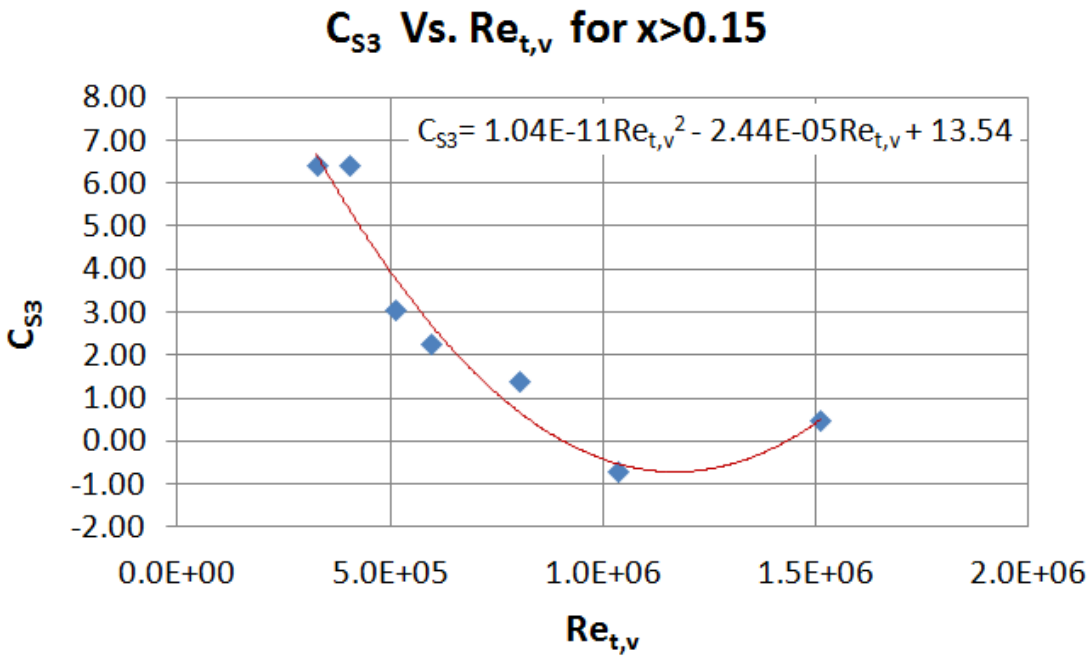

Figure 56: Polynomial Curve fits of CS3 for x>0.15 for various Reynolds Numbers

$$C_{S3}= 1.04E\text{-}11Re_{t,v}^{2} - 2.44E\text{-}05Re_{t,v} + 13.54 \quad (84)$$

Table 12 redefines C_{S1} (in contrast to Table 4) for equation (76)

$Re_{s,l}$	$Re_{s,v}$	C_{S1}
< 2300	< 2300	5
≥ 2300	< 2300	10
< 2300	≥ 2300	12
≥ 2300	≥ 2300	*For x≤0.15:* Equation (78) *For x>0.15:* $Re_{t,v}$ <5e5: Equation (79) $Re_{t,v}$≥5e5: Equation (80)

Table 12: C_{S1} in Lockart-Martinelli Correlator, Φ_L, for new correlation

Table 13 redefines C_{S2} and C_{S3} (in contrast to Table 5) for equation (75) and equation (77) for both the liquid and vapor portions of the flow based on the superficial Reynolds number.

	$Re_s < 2300$	$2300 \leq Re_s < 35{,}000$	$Re_s \geq 35{,}000$
C_{S2}	64	0.316	*For x≤0.15:* Equation (81) *For x>0.15:* Equation (82)
C_{S3}	1	0.25	*For x≤0.15:* Equation (83) *For x>0.15:* Equation (84)

Table 13: C_{S2} and C_{S3} in Martinelli Parameter, *X*

The pressure drop gradient if the entire flow were liquid that is used in equation (75) is given by equation (85):

$$\left(\frac{\Delta P}{\Delta L}\right)_{t,l} = \frac{f_{t,l} G^2}{2\rho_l d} \tag{85}$$

The friction factor, $f_{t,l}$, is defined by equation (86):

$$f_{t,l} = C_{f1}\left(Re_{t,l}\right)^{C_{f2}} \tag{86}$$

The terms C_{f1} and C_{f2} vary according to the Reynolds number as depicted in Table 14.

	$Re_{t,l} < 2300$	$3500 \leq Re_{t,l} < 20{,}000$	$Re_{t,l} \geq 20{,}000$
C_{f1}	64	0.316	0.184
C_{f2}	-1	-0.25	-0.2

Table 14: C_{f1} and C_{f2} in Friction Factor, $f_{t,l}$

For $2300 \leq Re_{t,l} < 3500$ the friction factor can be estimated by taking the average of the what is obtained by using equation (70) and applying the C_{f1} and C_{f2} for $Re_{t,l} < 2300$ and the C_{f1} and C_{f2} for $3500 \leq Re_{t,l} < 20{,}000$.

The two-phase separated flow momentum pressure drop is given by equation (87):

$$\Delta P_{Momentum,s} = \Phi_M \frac{G^2}{\rho_l} \tag{87}$$

The momentum pressure drop parameter, Φ_M, is calculated using equation (88)

$$\Phi_M = \frac{(1-x_{outlet})^2}{(1-\alpha_{outlet})} - \frac{(1-x_{inlet})^2}{(1-\alpha_{inlet})} + \rho_L \left[\frac{(x_{outlet})^2}{\alpha_{outlet}\rho_{v,outlet}} - \frac{(x_{inlet})^2}{\alpha_{inlet}\rho_{v,inlet}} \right] \tag{88}$$

The void fraction, α, is given by equation (89):

$$\alpha = 1 - \left[1 + (C_{s1}/X) + (1/X)^2 \right]^{-1/2} \tag{89}$$

The two-phase separated flow elevation pressure drop is given by equation (90):

$$\Delta P_{Elevation,s} = g\left(\rho_{ms,outlet} Z_{outlet} - \rho_{ms,inlet} Z_{inlet}\right) \tag{90}$$

The mean density for separated flow of the two-phase fluid can be related to the void fraction as shown in equation (91):

$$\rho_{ms} = \rho_v \alpha + \rho_l (1-\alpha) \tag{91}$$

Using equations (75), (87), and (90) in equation (14) it is possible to estimate the pressure drop using the new separated flow correlation.

7.2.2 Homogeneous Flow – New Correlation

The proposed new homogeneous flow correlation is a variation of the homogeneous flow correlation that is described in section 1.4.8. Appropriate mean flow properties are used with single-phase correlations for the homogeneous model.

The frictional pressure drop gradient is given by equation (92):

$$\left(\frac{\Delta P}{\Delta L}\right)_{Friction,h} = \frac{\mathrm{f_h} G^2}{2\rho_{mh} d} \tag{92}$$

The friction factor, $\mathrm{f_h}$, is defined by equation (93):

$$\mathrm{f_h} = C_{\mathrm{H1}} \left(\mathrm{Re}_h\right)^{C_{\mathrm{H2}}} \tag{93}$$

The effect of varying the constant C_{H1} was studied and a least squares optimization was carried out with this constant to minimize the disparity between the experimental data and the correlation. It was observed that the pressure drop trend seemed to change between x=0.1 and x=0.2, so two different correlations were obtained for $x \leq 0.15$ and x>0.15. This is probably associated with changes in the flow regime from saturated nucleate boiling to film evaporation as described in Figure 4. For $Re_{t,v}$=3.27e5, the value of the constants obtained in this way was C_{H1} = 13.075, for $x \leq 0.15$ and C_{H1} = 2.59 for x>0.15. Figure 57 shows the new $Re_{t,v}$=3.27e5 correlation super imposed on the comparison shown on Figure 49 and shows a significantly improved agreement between the data and the new homogeneous flow correlation for this Reynolds number.

A similar analysis is done for all the Reynolds number homogeneous flow model pressure drop gradients that were being investigated. Table 15 summarizes the optimized C_{H1} for each Reynolds number being investigated and compares it to the previous homogeneous flow

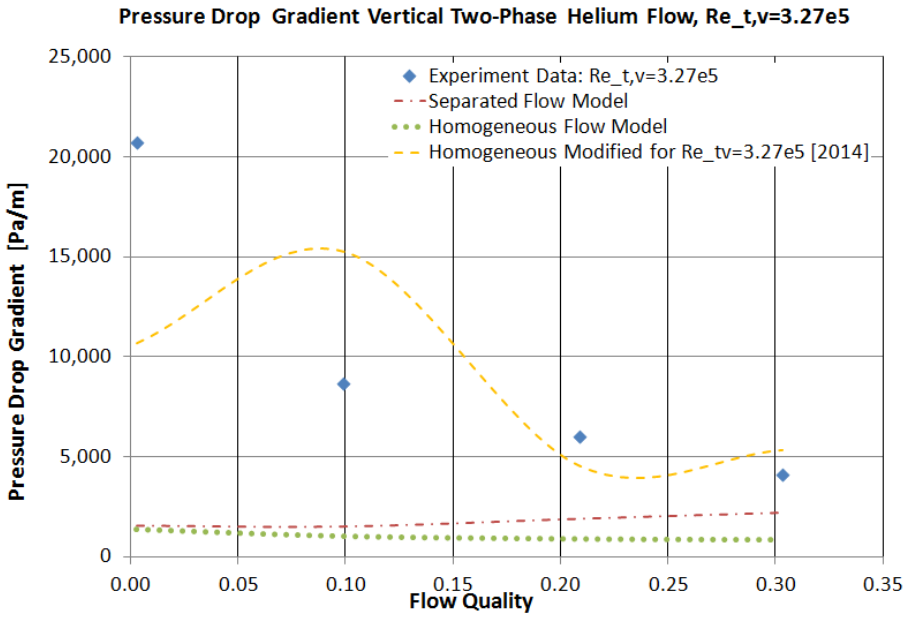

Figure 57: Pressure Drop Gradient Experimental Data compared with predictions from the previous Separated Flow Model and Homogeneous Flow Model and the Modified Homogeneous Flow Model for Ret,v=3.27e5

model constant values.

$Re_{t,v}$	C_{H1} For $x \leq 0.15$	C_{H1} For $x > 0.15$
Homogeneous Model (Previous)	0.184	0.184
3.27E+05	13.075	2.59
4.04E+05	8.761	1.692
5.09E+05	5.776	1.548
5.93E+05	4.619	1.433
8.01E+05	3.099	1.218
1.03E+06	2.137	1.064
1.51E+06	1.523	1.048

Table 15: Optimized Constants for Equation (93) for various Reynolds Numbers

In order to obtain a generalized correlation for the homogeneous flow model pressure drop gradient it is necessary to correlate the constants C_{H1} with $Re_{t,v}$.

Figure 58 plots C_{H1} as a function of $Re_{t,v}$ for $x \leq 0.15$. A power law curve fit yields the correlation shown in equation (94) for $x \leq 0.15$:

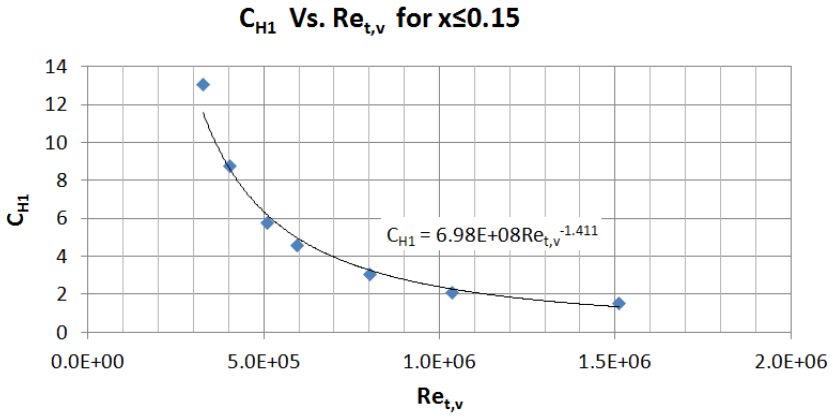

Figure 58: Power law curve fit of C_{H1} for $x \leq 0.15$ varying Reynolds Numbers.

$$C_{H1} = 6.98E{+}08Re_{t,v}^{-1.411} \quad (94)$$

Figure 59 plots C_{H1} as a function of $Re_{t,v}$ for x>0.15. A third order polynomial curve fit yields

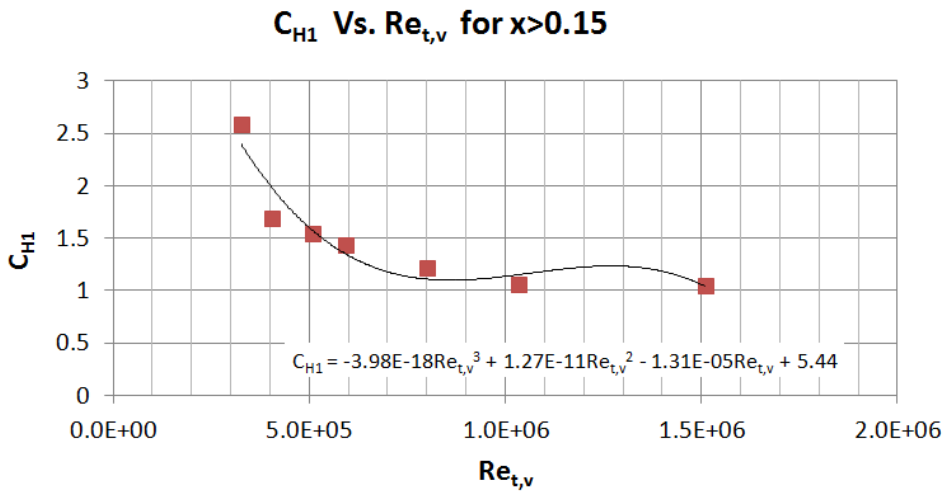

Figure 59: Polynomial Curve fit of CH1 for x>0.15 for various Reynolds Numbers

the correlation shown in equation (95) for x>0.15:

$$C_{H1} = -3.98E{-}18Re_{t,v}^{3} + 1.27E{-}11Re_{t,v}^{2} - 1.31E{-}05Re_{t,v} + 5.44 \quad (95)$$

Table 16 redefines C_{H1} (in contrast to Table 7)

	$Re_h < 2300$	$3500 \leq Re_h < 20{,}000$	$Re_h \geq 20{,}000$
C_{H1}	64	0.316	*For x≤0.15: Equation (94)* *For x>0.15: Equation (95)*
C_{H2}	-1	-0.25	-0.2

Table 16: C_{H1} and C_{H2} in Friction Factor, f_h, for new correlation

For $2300 \leq Re_h < 3500$ the friction factor can be estimated by taking the average of what is obtained by using equation (93) and applying the C_{H1} and C_{H2} for $Re_h < 2300$ and the C_{H1} and C_{H2} for $3500 \leq Re_h < 20{,}000$.

The mean density for homogeneous flow of the two-phase fluid is calculated using equation (96):

$$\rho_{\text{mh}} = \frac{\rho_v \rho_l}{\rho_v (1-x) + \rho_l x} \tag{96}$$

The mean viscosity for homogeneous flow of the two-phase fluid is calculated using equation (97):

$$\mu_{\text{mh}} = \frac{\mu_v \mu_l}{\mu_v (1-x) + \mu_l x} \tag{97}$$

The Reynolds number for homogeneous flow of the two-phase fluid is calculated using equation (98):

$$\text{Re}_h = 4\dot{m}/(\pi d \mu_{mh}) \tag{98}$$

The two-phase homogeneous flow momentum pressure drop is given by equation (99):

$$\Delta P_{Momentum,h} = \frac{G^2 (x_{outlet} - x_{inlet})}{\rho_l} \left(\frac{\rho_l}{\rho_v} - 1 \right) \tag{99}$$

The two-phase homogeneous flow elevation pressure drop is given by equation (100):

$$\Delta P_{Elevation,h} = g\left(\rho_{mh,outlet} z_{outlet} - \rho_{mh,inlet} z_{inlet}\right) \tag{100}$$

Using equations (92), (99)and (100) in equation (14) it is possible to obtain the pressure drop gradient for the new homogeneous flow correlation.

7.3 New Pressure Drop Correlations compared with Data

Figure 60 to Figure 66 compare the experimental data and the new separated flow and homogeneous flow correlations for pressure drop for vertical up-flows in two-phase helium for Reynolds numbers between 3.27e5 and 1.51e6 with the previous separated flow and homogeneous flow models. It might be challenging to see the uncertainty bars on the data points since the uncertainty bars are about the same size as the markers. A better indication of the uncertainty bars for the pressure drop is available in Figure 35.

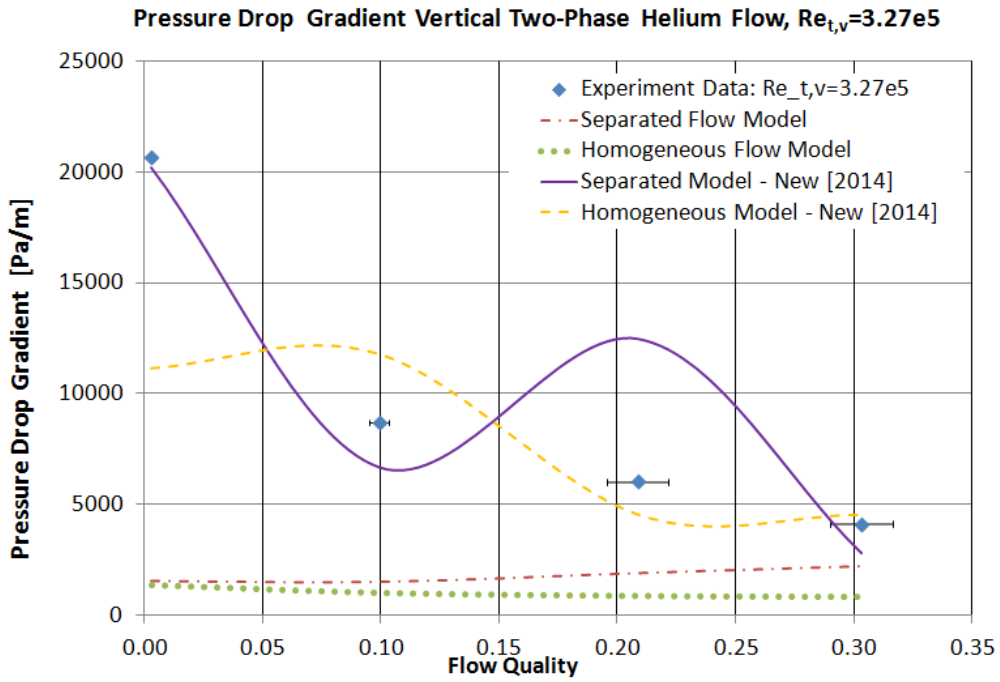

Figure 60: Pressure Drop Gradient experimental data compared with the new models and previous models for $Re_{t,v}$=3.27e5

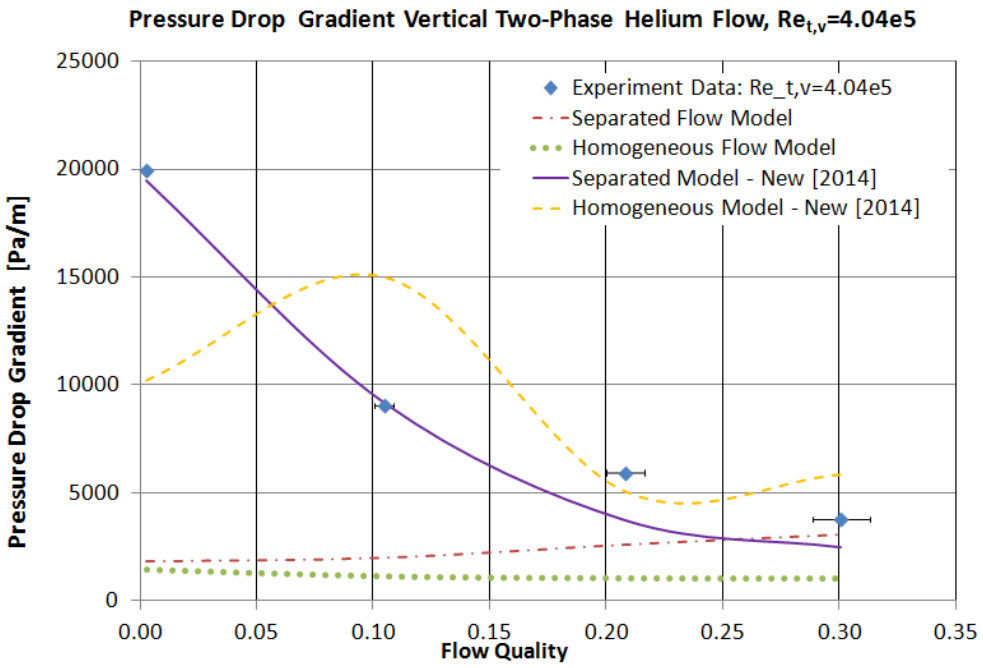

Figure 61: Pressure Drop Gradient experimental data compared with the new models and previous models for $Re_{t,v}$=4.04e5

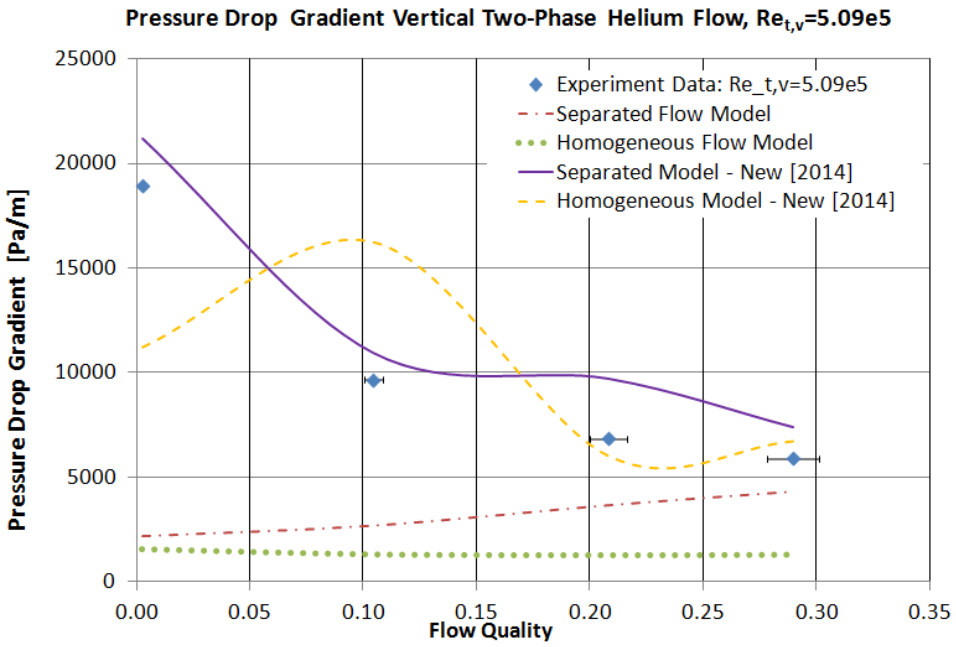

Figure 62: Pressure Drop Gradient experimental data compared with the new models and previous models for $Re_{t,v}$=5.09e5

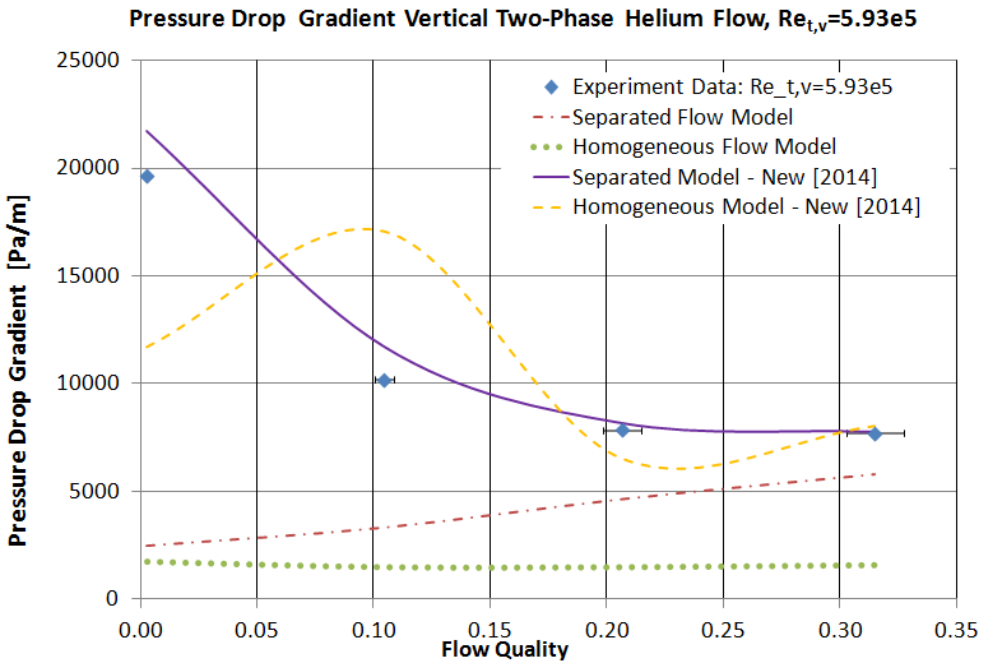

Figure 63: Pressure Drop Gradient experimental data compared with the new models and previous models for $Re_{t,v}$=5.93e5

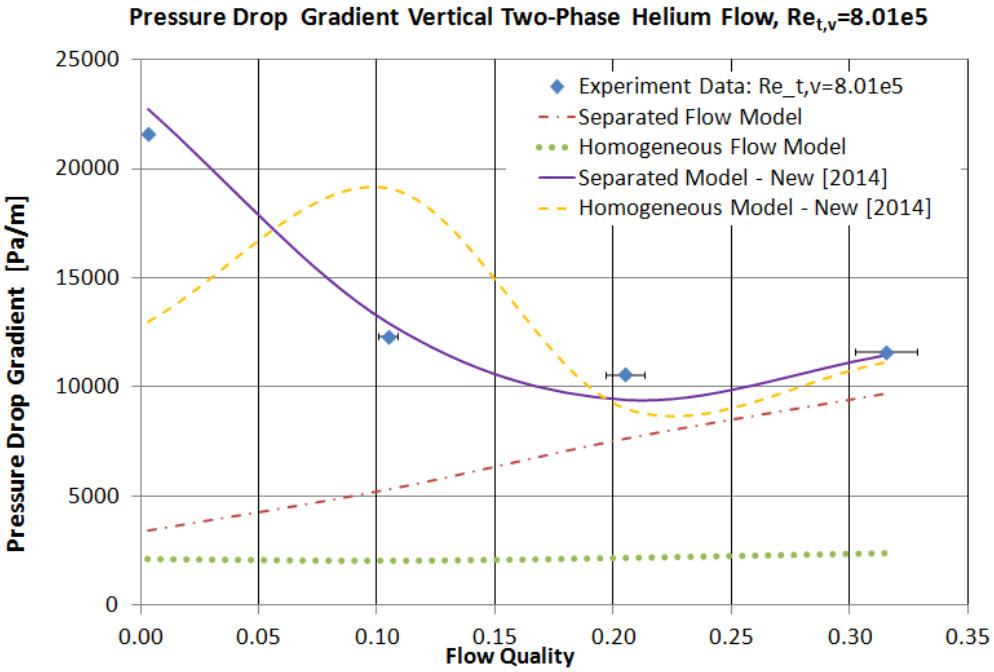

Figure 64: Pressure Drop Gradient experimental data compared with the new models and previous models for $Re_{t,v}$=8.01e5

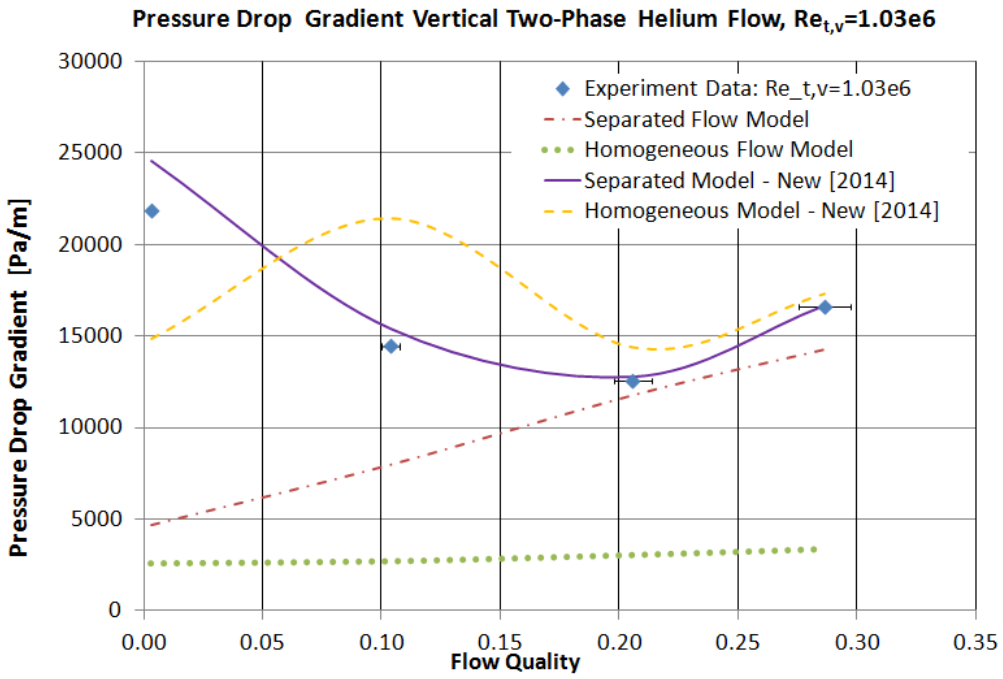

Figure 65: Pressure Drop Gradient experimental data compared with the new models and previous models for $Re_{t,v}$=1.03e6

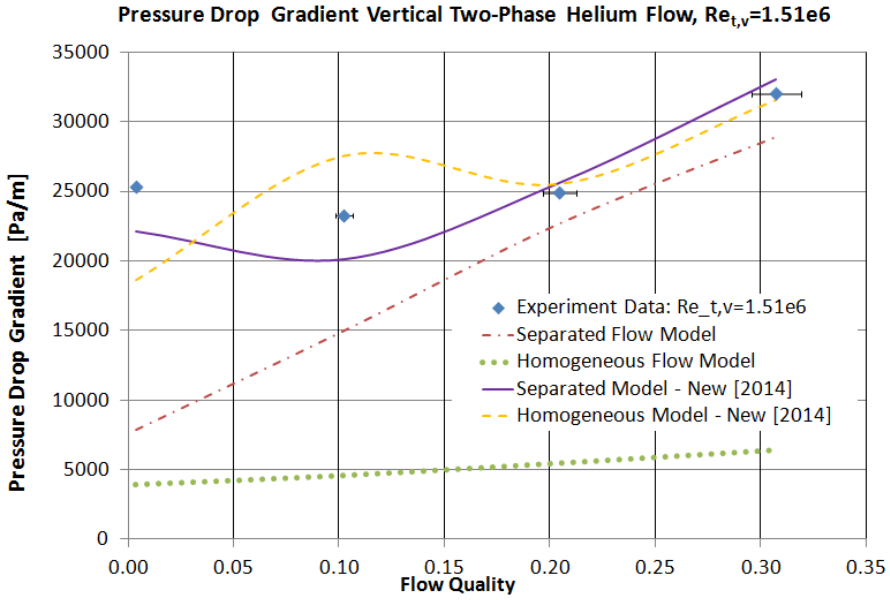

Figure 66: Pressure Drop Gradient experimental data compared with the new models and previous models for $Re_{t,v}$=1.51e6

7.4 *Dryout Heat Flux*

Attempts have been made by Kutateladze and Collier to explain the dryout heat flux phenomenon. [4, 5] The dryout heat flux for a given quality is given by equation (101).

$$\dot{q}''_{dryout} = (1-x)\dot{q}''_{dryout,x=0} \tag{101}$$

The dryout heat flux at zero quality is given by equation (102)

$$\dot{q}''_{dryout,x=0} = C_{Dryout}\rho_v\lambda_{lv}\left[\frac{g\sigma_l(\rho_l-\rho_v)}{(\rho_v)^2}\right]^{1/4}\left[\frac{G}{\rho_{mh}}\left(\frac{\rho_l-\rho_v}{g\sigma_l}\right)^{1/4}\right]^{1/2} \tag{102}$$

In Kutateladze's correlation, $C_{Dryout} = 0.023$.

Figure 67 shows the wide divergence between the experimental data obtained for the dryout heat flux and the previous dryout heat flux correlation. In order to match the experiment

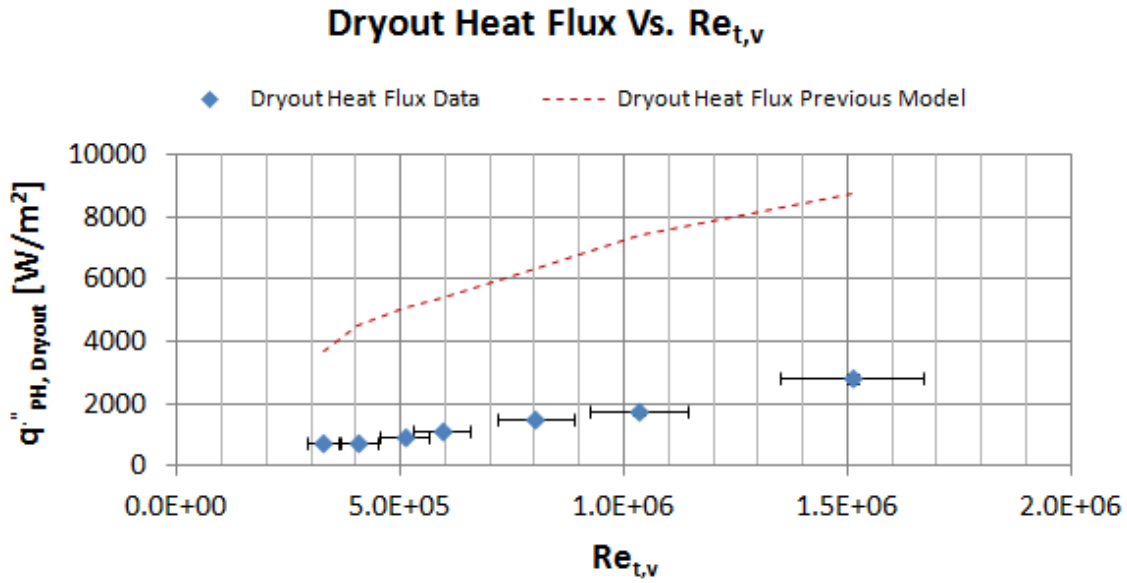

Figure 67: Dryout Heat Flux experiment data and prediction from previous model

data with the correlation predictions, new values of C_{Dryout} were calculated for each Reynolds number. Table 17 summarizes the new C_{Dryout} values for various Reynolds numbers and compares these to the constant value used in the previous correlation.

$Re_{t,v}$	C_{Dryout}
Previous	0.023
3.27E+05	0.004473
4.04E+05	0.003746
5.09E+05	0.004101
5.93E+05	0.004797
8.01E+05	0.005410
1.03E+06	0.005417
1.51E+06	0.007388

Table 17: C_{Dryout} for Equation (102) various $Re_{t,v}$ compared to the previous correlation

Figure 68 plots C_{Dryout} as a function of $Re_{t,v}$ to obtain a correlation between the Reynolds number and C_{Dryout}. A linear curve fit yields the correlation between C_{Dryout} and $Re_{t,v}$ as shown in equation (103):

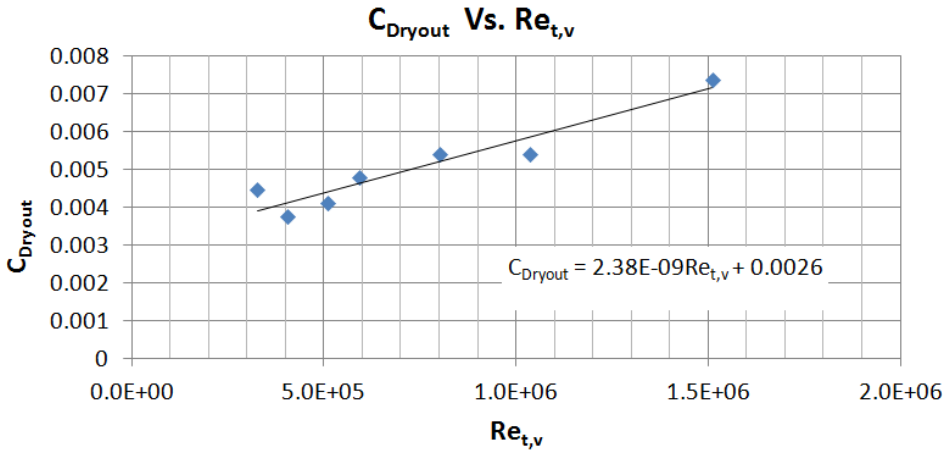

Figure 68: Linear Curve fit of C_{Dryout} for various Reynolds Numbers

$$C_{Dryout} = 2.38E\text{-}09Re_{t,v} + 0.0026 \quad (103)$$

Using equations (103) and (102) in equation (101) it is possible to obtain the dryout heat flux from this new dryout heat flux correlation.

Figure 69 compares the experimental data with the new dryout heat flux correlation and the previous dryout heat flux correlation. The new correlation provides a significant improvement over the old correlation in estimating the dryout heat flux for two-phase helium in the copper foam filled pre-heater.

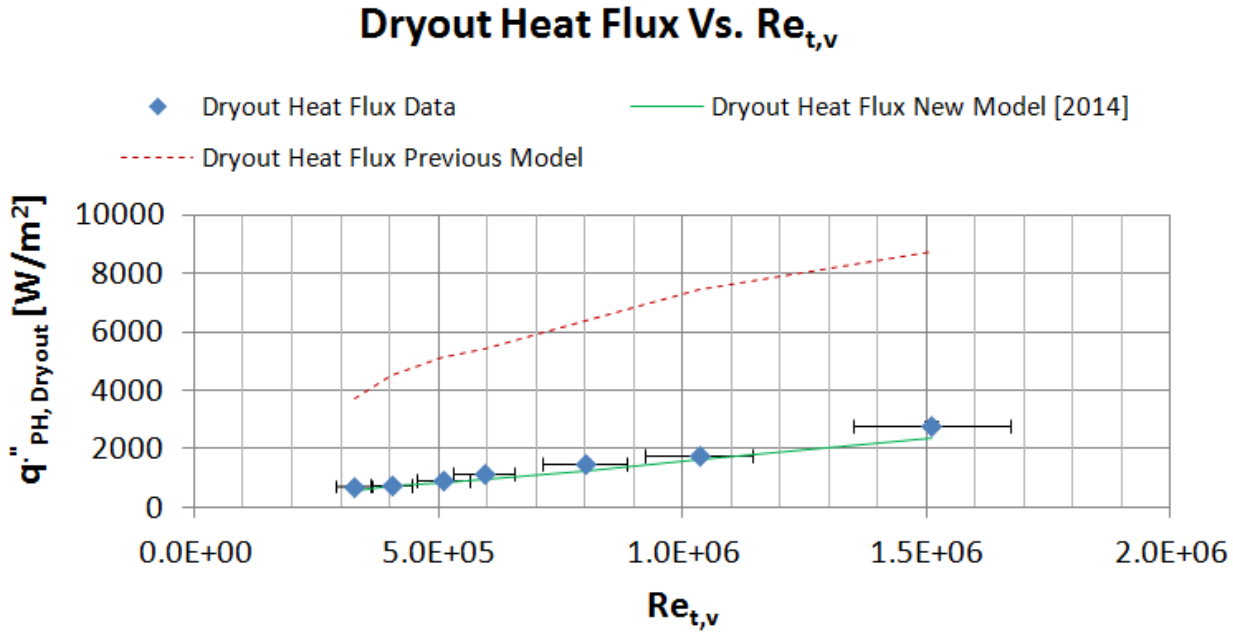

Figure 69: Dryout Heat Flux Experimental data compared with the new models and previous models.

8 Discussion

The flow parameters, including heat transfer coefficient, pressure drop gradient, and dryout heat flux, for high Reynolds number ($Re_{t,v}$ = 3.2e5 to 1.51e6) two phase helium up-flows with flow qualities between 0 and 0.3 were investigated for this research.

The heat transfer coefficient data obtained indicates that the heat transfer coefficient does increase for the studied qualities with Reynolds number. However, large increases in Reynolds numbers are needed for substantial increases in heat transfer coefficient. The boiling mechanism appears to change at about x≈0.1-0.2 for all the Reynolds numbers and the heat transfer coefficient drops substantially. At qualities above x≈0.3-0.4 the flow appears to dryout for all the Reynolds numbers so two-phase heat transfer coefficients are not measured above this quality using this experiment hardware. There does not appear to be a substantial change in heat transfer coefficient with quality probably because the latent heat of helium is very small and this limits the boiling component of the heat transfer. The heat transfer due to the convection portion of the flow does not change with quality very much because the thermophysical properties of liquid and vapor helium are very similar. It is interesting to note how low the heat transfer coefficient of helium is compared to other room temperature liquids where heat transfer coefficients often range into thousands of W/(m^2 K). It is possible that this behavior is a result of helium's very low latent heat of vaporization.

The pressure drop gradient data obtained indicates that the pressure drop increases with Reynolds number. Here again it does appear that the boiling mechanism changes at x≈0.1-0.2. At the lower Reynolds numbers, of up to 5e5 the total pressure drop gradient keeps falling at the intermediate quality of 0.3. At a Reynolds numbers of 5.92e5 and above it is observed that the total pressure drop gradient starts rising again at increasing qualities after hitting a minimum.

This phenomenon appears to be driven by the variation of frictional pressure drop with quality for the various Reynolds numbers. For instance, at a Reynolds number of 5.09e5, the calculated friction pressure drop gradient according to the new separated flow model drops from 9816 Pa/m to 6640 Pa/m as the total pressure drop gradient drops from 10523 Pa/m to 7049 Pa/m, as the quality increases from 0.1 to 0.3. However, for a Reynolds number of 8.01e5, the calculated friction pressure drop gradient according to the new separated flow model drops from 11310 Pa/m at a quality of 0.1 to 8420 Pa/m at a quality of 0.2 before rising to 10522 Pa/m at a quality of 0.3.For the Reynolds number of 8.01e5 the total pressure drop gradient drops from 12233 Pa/m at a quality of 0.1 to 8991 Pa/m at a quality of 0.2 before rising to 10957 Pa/m at a quality of 0.3. A physical interpretation of this could be the following: Initially as more vapor is formed because of the reduction in viscosity the frictional pressure drop falls with increasing quality. However above a Reynolds number of 5.93e5 at a quality of 0.3 there is sufficient vapor moving at higher velocities to start increasing the frictional pressure drop again. Since the viscosity of vapor helium is unusually large compared to the viscosity of liquid helium the small reduction in viscosity due to quality increase is more than compensated for by the increase in vapor velocity thus leading to an overall increase in pressure drop at higher Reynolds numbers and higher qualities.

The dryout heat flux data was obtained for flow in the copper foam filled pre-heater. As might be expected the dryout heat flux increases with increasing Reynolds number. However, it is interesting to note that the dryout quality seems to be independent of the Reynolds number. Figure 70 shows the minimal variation of the dryout quality with Reynolds number. This lack of variation of the dryout quality with Reynolds number may be indicating that the dryout heat flux is a function of the available wetted area. This theory is consistent with the observation that was

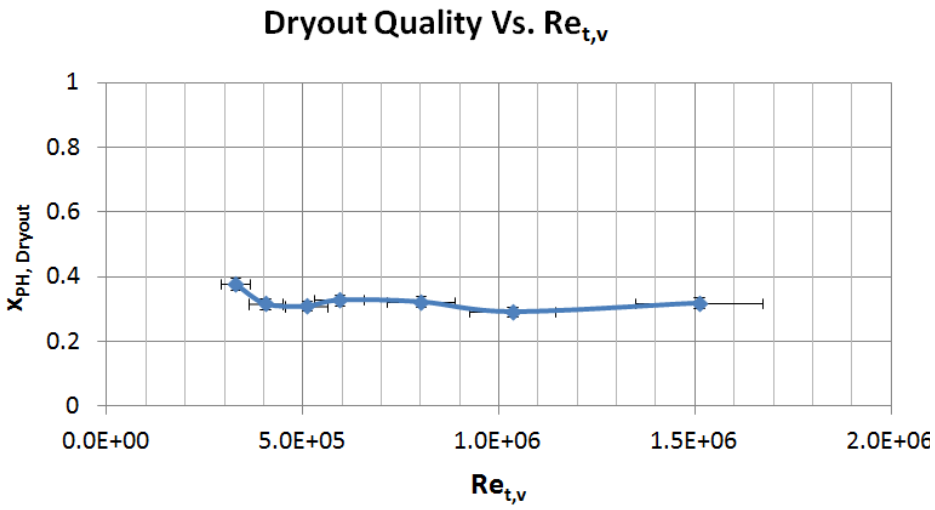

Figure 70: Dryout quality variation with Reynolds Number.

made that changing the pre-heater to include copper foam inserts (and thereby increasing the potential wetted area) appeared to allow the collection of data at higher qualities than what was possible with just a simple hollow tube pre-heater.

There appears to be some similarity between what is observed for helium flows and pressure drop in other near-critical flow studies. At the very low qualities according to the new separated flow momentum pressure drop correlation substantially large momentum pressure drops are calculated. This is similar to observations of large momentum pressure drops in near-critical flow studies. However the calculated friction pressure drop from the new separated flow correlation is also a major fraction of the pressure drop and this appears to be different from what is observed in near-critical flow studies for other fluids. It is also not unusual to see oscillation behavior for near-critical flows and thermal acoustic oscillations were noticed in and resolved in this experiment. [30]

New correlations have been proposed in this research for the heat transfer coefficient, separated flow pressure drop, homogeneous flow pressure drop and the dryout heat flux. These new correlations have been compared with the output of previous correlations in graphs in

Section 7. A qualitative assessment of these graphs indicates that these new correlations fit the collected data substantially better than previous correlations. A quantitative assessment of this should also do the same.

Equation (104) and equation (105) provide the mean deviation and the average deviation of the experiment data from the correlation being investigated. The mean deviation gives an assessment of the average magnitude of the deviation of the data from the correlation, and the average deviation gives an assessment of the average magnitude of the over-prediction or under-prediction of the correlation.

$$\text{Mean Deviation} = \frac{1}{\text{N}} \sum_{i=1}^{N} \frac{\left| \text{Value}_{\text{correlation}} - \text{Value}_{\text{experiment}} \right|}{\text{Value}_{\text{experiment}}} \times 100\% \tag{104}$$

$$\text{Average Deviation} = \frac{1}{\text{N}} \sum_{i=1}^{N} \frac{\left[\text{Value}_{\text{correlation}} - \text{Value}_{\text{experiment}} \right]}{\text{Value}_{\text{experiment}}} \times 100\% \tag{105}$$

Table 18 compares the mean deviation and average deviation of each of the correlations that have been proposed in this dissertation with the previous correlations that were available in the literature.

	Mean Deviation [%]		Average Deviation [%]	
	Prior Correlation	New Correlation [2014]	Prior Correlation	New Correlation [2014]
Heat Transfer Coefficient	579.5	5.9	579.5	-0.1
Pressure Drop Gradient-Separated	51.0	17.2	-51.0	0.7
Pressure Drop Gradient - Homogeneous	83.3	31.6	-83.3	2.3
Dryout Heat Flux	605.3	28.4	605.3	28.4

Table 18: Mean and Average Deviation of Experimental Data from Previous and New Correlations

The new heat transfer coefficient correlation performs significantly better than the prior Ogato and Sato correlation reducing the mean deviation of the correlation from the experimental data by over a factor of 98. The prior Ogato and Sato correlation considerably over predicted the heat transfer coefficient. This new heat transfer coefficient correlation slightly over predicts the heat transfer coefficient.

The new separated flow pressure drop gradient correlation and the new homogeneous flow pressure drop gradient correlation perform significantly better than the prior pressure drop gradient correlations. The new separated flow correlation reduces the mean deviation with the experimental data by about a factor of 3 and new homogeneous flow correlation reduces the mean deviation with the experimental data by more than a factor of 2. The prior separated flow and homogeneous flow correlations significantly under-predicted the observed pressure drop gradient. The new pressure drop correlations slightly over predict the pressure drop on the average. The new separated flow correlation provides a slightly better agreement with the experimental data than the new homogenous flow correlation.

The new dryout heat flux correlation also performs significantly better than the prior Kutateladze dryout heat flux correlation reducing the mean deviation of the correlation from the experimental data by more than a factor of 21. The prior correlation considerably over predicted the dryout heat flux. This new dryout heat flux correlation also over predicts the dryout heat flux but by a significantly reduced factor.

9 Future Work

This dissertation has been a first attempt to study the flow parameters in vertical up-flows of two phase helium I for high Reynolds number ($Re_{t,v}$ = 3.27e5 to 1.51e6) with flow qualities between 0 and 0.3. There are considerable gaps in knowledge that still need to be filled for flows of this type.

The study of the two-phase helium up-flows was limited in this study to qualities below 0.4 because of the significantly low dryout heat fluxes that are experienced in helium up-flows. Indications are that the dryout heat flux could be modified by modifying the flow geometry and available surface area in the pre-heater. It may also be possible to obtain higher quality data by introducing a sufficiently long mixing section in between the pre-heater and the test-section inlet so that the superheated vapor gets an additional opportunity to heat exchange with entrained droplets so that the vapor temperature drops back down to saturated conditions at the test section inlet. If it is possible to obtain data at a quality of 1 and density wave oscillations described in Section 4.4.2 are observed it might become possible to study and model this phenomenon in greater detail for cryogenic fluids.

The boiling mechanism of the liquid helium was inferred and not visualized in this study in order to maximize the accuracy of the data collected. Any attempt to do flow visualization would compromise on the accuracy of the measurements on helium because of the extremely low latent heat of vaporization and boiling point of helium. The transitions in the boiling mechanisms and the flow regimes were inferred to happen at considerably lower qualities than what is seen in other non –quantum fluids. Future studies that solely focus on flow visualization of helium will provide valuable insights into the transitions in the boiling mechanisms and flow regimes for liquid helium.

The effect of adding the copper foam to the pre-heater was to increase the dryout heat flux that enabled data collection at higher qualities. It would be interesting to study the heat transfer coefficient and the pressure drop by introducing the copper foam into the test section. It is theorized that the heat transfer coefficient would be increased and the pressure drop would also be increased, however having accurate data on this would be valuable in the design of future cryogenic two-phase heat exchangers. In addition to this effort it would be useful to investigate the effect of tube diameters and the potential for heat transfer enhancements and the related pressure drop issues in high Reynolds number flows of helium in microchannels. [31]

The data collected in these experiments was for liquid helium. However there is also a gap in similar data for the other two quantum fluids - hydrogen and neon. It would be beneficial to do this research for these other quantum fluids as well so that the resulting correlations can be compared. In fact the helium that is being studied here is just an inert substitute for hydrogen which is the fluid of interest for the TCS heat exchanger application described in section 1.2. Helium is a challenging cryogen to work with; however hydrogen's combustible characteristics mean that experiments with hydrogen would require additional levels of complexity. Neon, like helium, is inert. However, liquid neon is very expensive because of the rarity of available neon.

All of the measurements that were performed at the test section were at operating pressures near 1 atm. However, it is possible that the two–phase heat exchangers could have operating pressures that are lower or higher than the ambient. In fact the operating pressure in the TCS heat exchanger application is only about 0.1 atm. It would be valuable to understand the effect of varying the pressure in the test section and pre-heater on the flow parameters.

The boundary condition that was investigated in these experiments was a constant wall heat flux boundary condition. It would be valuable to do this experiment with a constant wall temperature boundary condition and a wall temperature boundary condition that varies along the length of the wall. In the TCS heat exchanger application the two phase heat exchanger will experience a temperature gradient of 20 K to 15 K along the length of the heat exchanger.

This research was performed to investigate high Reynolds number vertical up-flows of two-phase helium. However, there is also a knowledge gap for high Reynolds number vertical down-flows and horizontal flows of two-phase helium. Future investigations of higher Reynolds number vertical up-flows, and high Reynolds number vertical down-flows and horizontal flows would be beneficial in the design of high flow rate two-phase cryogenic heat exchangers that operate in different orientations and that may also be considered for the TCS or other applications.

10 Concluding Remarks

The body of research presented in this document represents a first attempt to investigate two phase helium I up-flows at Reynolds numbers above 3e5. The Reynolds number range studied for this research was 3.27e5≤ $Re_{t,v}$≤1.51e6 for vapor qualities up to around 0.3. Three parameters of the flow were investigated: heat transfer coefficient, pressure drop, and the dryout heat flux.

Since no correlations for heat transfer coefficient, pressure drop and dryout heat flux existed for vertical up-flows of helium at these Reynolds numbers any predictions of these parameters were dependent on prior correlations that were tested at lower Reynolds numbers, models that were based on correlations for other fluids, or a combination of these two characteristics. As a quantum fluid, the thermophysical properties of helium I, such as the density, viscosity, boiling point and latent heat of vaporization are significantly different from that of most other fluids; therefore the capability of these prior models in predicting experimental observations were severely limited. This research begins the fundamental investigation of a new regime for two-phase helium I flows at Reynolds numbers above 3e5. The techniques described in this document will hopefully enable future work to address other gaps in knowledge for helium I flows that still remain.

The prior model for heat transfer coefficient that was closest to the Reynolds number range that has been studied was proposed by Ogato and Sato (1974) and was only tested for $Re_{t,v}$≤1.85e5. This model considerably over-predicted the observed heat transfer coefficient in the data that was collected for this research. A new correlation for heat transfer coefficient has been proposed in this research that improves the agreement with data by more than a factor of 98.

Two prior models for pressure drop, the separated flow model and the homogeneous flow model were compared with the data obtained for this research. Both these models under-predict the observed pressure drop. Newer versions of these correlations have been proposed for this research. The newer version of the separated flow correlation improves agreement with the data by about a factor of 3 and the newer version of the homogeneous flow correlation improves agreement with the data by more than a factor of 2.

The unusually low dryout heat flux of the helium posed a significant challenge in data collection for this experiment. The previous dryout heat flux correlation proposed by Kutateladze (1959) considerably over predicts the dryout heat flux. As a result significant changes had to be made to the experiment hardware to get additional data. Using copper foam helped to increase the dryout heat flux sufficiently to get data up to qualities around 0.3. The new correlation proposed in this research improves agreement with the data by more than a factor of 21.

Having defined the heat transfer coefficient, pressure drop and dryout heat flux parameters for high Reynolds number vertical up-flows of helium; it is now possible to design a vertical two phase heat exchanger for helium up-flows with Reynolds numbers up to 1.51e6 with operating qualities up to 0.3. This information may also be used for preliminary design of two-phase heat exchangers for hydrogen for applications such as subcooling for long term storage of hydrogen. However, it is also recognized that a significant amount of future research should be performed to better characterize and enhance the performance of such two-phase heat exchangers.

Significant cryogenic challenges were overcome to collect the data that is the basis of this research. The techniques described in this document for surmounting the diverse challenges such as thermal acoustic oscillations, parasitic heat loads, solid air plugs, cold leaks, and low dryout

heat flux could also be used by future researchers who will face the difficulties of conducting two-phase flow boiling experiments in a vacuum at temperatures that are about 290 K below the ambient room temperature. Figure 71 is a picture of the experiment operating nominally and collecting data.

Figure 71: Experiment operating nominally and collecting data.

11 Appendix A: Experiment Procedure

Please use Addendum 1-3 and Figures 1-4 located at the end of this document to follow this procedure.

1 Preparing Room Temperature System for Cooldown (skip if system contains some LHe and only needs refilling)

1.1 This procedure shall be performed by at least a level 2 certified cryogenic operators.

1.2 Conduct a pre-task briefing, discussing the procedure and emergency response at the end of the document (***Addendum 1***).

1.3 Discuss the hazards of handling cryogens and speak up immediately if you notice something wrong.

1.4 Ensure that relief valves are in place the LHe reservoir in the Precision Cryogenic Services (PCS) Test Dewar, and the vacuum jacket chamber of the PCS Test Dewar cryostat. Inspect all relief valves and fitting to ensure that they seat properly and that they do not have visibly damaged gaskets. (***Figure 1*****)**

2 Hazard Analysis

2.1 ***Before proceeding, go through the hazard analysis checklist at the end of this document (Addendum 2) to ensure that all of its requirements are met.***

2.2 Ensure that operators have clear paths to the equipment and to egress.

2.3 Mark off a “keep out” area around the dewar of at least a 2 meter radius.

2.4 ***Ensure that operators have the proper protective equipment - Gloves, eye protection, closed top shoes, long-sleeved shirt, and long pants.***

3 Instrumentation (Figure 3 and 4)

3.1 Measuring Temperature

The Temperatures will be measured using Cernox Thermometers

3.2 Measuring Pressure

The pressures are measured using Baratrons. Make sure that the baratrons are heated for at least an hour prior to conducting the experiment.

3.3 Measuring Flow Rate

The flow rate will be measured by measuring the pressure drop in a venturi. A spreadsheet program will be used to convert the pressure drop into a flow rate. A Toshiba Variable Frequency Drive is used to control the flow rate of the pump.

3.4 Liquid Level Detector

The liquid level detectors will be read with liquid level detector readout.

3.5 Power

Power witll be applied to two heaters: the Pre-Heater and the Test Section Heater. The power source for the pre-heater is a Kepco KLP 75-33 power supply. The power source the test section is a HP3616 A DC Power Supply

4 Pump and Purge Experiment (Figure 3)

Before putting in liquid helium into the PCS Test Dewar and running the experiment each time conduct the following pump and purge procedure. This reduces the possibility of air being present in the experiment that could form solid air plugs:

4.1 Connect the pump to the PCS Test Dewar Vacuum chamber valve and pump out the vacuum chamber.

4.2 Hook up a pump to the Helium Vent valve on the PCS Test Dewar.

4.3 Hook up a stainless steel hose from the vent port of the ***Clean Helium Supply Gas Bottle*** to the Helium Purge valve on the PCS Test Dewar.

4.4 Cap the fill and the outlet ports on the PCS Test Dewar with a quick connect cap.

4.5 Monitor the pressure in the experiment volume with the experiment pressure monitors.

4.6 Pump out the PCS Test Dewar and the transfer line to a pressure reading of 0.1 Torr (13.3 Pascal) or lower on all pressure monitors.

4.7 Close the Helium Vent Valve on the PCS Test dewar

4.8 Purge the PCS Test Dewar and the experiment with helium from the LHe Supply dewar by opening valve S-V2 on the LHe Supply dewar

4.9 When the pressure very slightly exceeds 1 atm., stop the helium vapor flow by turning off the regulator on the ***Clean Helium Supply Gas Bottle.***

4.10 Close the Helium Purge Valve on the PCS Test Dewar.

4.11 Repeat steps 4.5 – 4.10 three times.

4.12 Remove the stainless steel transfer line to the helium purge valve on the PCS Test Dewar.

4.13 Disconnect the pump connection from the PCS Test Dewar from the Helium Vent Valve

4.14 The PCS Test Dewar is now ready for Liquid Helium Transfer.

5 Liquid Helium Storage Dewar and Transfer Line Preparation

5.1 Make sure that the experiment is ready to run (method in Step 7) before continuing with rest of the steps in Section 5.

5.2 **Storage Dewar Preparation (Figures 1 and 2.)**

5.2.1 Verify that the dewar compound pressure gauge reads approximately zero (atmospheric pressure). Note that light tapping of the gauge may be necessary to get an accurate reading. If it reads above zero, verify that the relief valve shut off valve, S-V1 is open. If it is not open, stand clear of the relief valve and slowly open S-V1 to relieve pressure in the tank.

5.2.2 Verify that vent valve, S-V2, and transfer valve, S-V3 are closed. If so, skip the next step.

5.2.3 If either S-V2 or S-V3 have been open for many minutes, it is possible that air may have condensed in the central tube, possibly blocking the transfer tube path into the storage dewar. Close S-V2 and S-V3 and proceed to ***Addendum 3: "Troubleshooting a Possibly Plugged Supply Dewar."***

5.2.4 Verify that the amount of liquid in the storage dewar is sufficient for the test. If necessary, measure the liquid level using the section on Storage Dewar Liquid Level Measurement.

5.3 **Transfer Line Preparation**

5.3.1 Ensure that the transfer line is in good physical condition. The rigid tubes should be relatively straight, round cross-section, and free of foreign matter including water.

5.3.2 Ensure that the transfer line vertical section is 1/2” o.d. rigid tube and that it will reach the bottom of the storage dewar.

5.3.3 Ensure that any attachments, such as extension tubes on the vertical leg(s) are secure.

5.3.4 Verify that any quick connect couplings necessary to mate with either the storage dewar (1/2” quick connect nut, rubber o-ring and ferule) or the test dewar are in place on the transfer line legs.

5.4 **Liquid Helium Transfer**

5.4.1 Ensure that operators have clear paths to the equipment and to egress.

5.4.2 Mark off a “keep out” area around the dewar of at least a 2 meter radius.

5.4.3 Ensure a temperature read-out system is attached to the Test Dewar cryostat and the thermometers are operating correctly.

5.4.4 ***Ensure that operators have the proper protective equipment - Gloves, eye protection.***

5.4.5 Ensure that a hand-held oxygen monitor near the PCS Test Dewar is operational and is indicating an acceptable amount of oxygen.

5.4.6 Test conductor will brief the operators on the steps to be followed during the cooldown.

5.4.7 Make sure that the experiment is ready to run (method in Section 7) before continuing with rest of the steps in Section 5.

5.4.8 While standing out of the vent path, slowly open the vent valve, S-V2.

5.4.9 When the flow out of S-V2 has settled down, slowly open transfer valve S-V3.

5.4.10 Insert the long, rigid transfer tube slowly into the liquid helium storage dewar through S-V3. During this insertion, as soon as practical, move the 1/2” quick connect parts down on top of the storage dewar and make a seal against the transfer tube.

5.4.11 Continue lowering the rigid transfer tube. If the tube reaches the bottom of the storage dewar, raise it up about 1/2”. If extra pressure is desired to begin the transfer, close S-V2 and S-V1. Monitor the pressure gauge. If the pressure rises too high (typically > 5psi, but this is application specific) lower the pressure by slowly opening either S-V1, S-V2, or both, while standing out of the way of the venting cold gas.

6 Transfer of LHe into the PCS Test Dewar

6.1 Make sure that the experiment is ready to run (Step 7) before continuing with rest of the steps in Section 6.

6.2 Monitor the temperature using the thermometers on the experiment [Step 3.1].

6.3 ***Note: The following three steps must be done such that there is gas flowing out of the transfer line and PCS Test Dewar at all times during which it is not sealed from ambient air. Read the steps carefully before proceeding. If outward flow stops during these steps, stop the process and re-do the pump and purge steps in Section 4.***

6.4 Carefully uncap the fill port on the PCS Test Dewar, insert the LHe transfer line into it, and seal the quick connect onto the transfer line.

6.5 Immediately crack the PCS Test Dewar vent valve. If there is gas flowing out of the vent valve, open the valve to provide a slight flow impedence and proceed with the transfer. If not, close the PCS Test Dewar vent valve, wait 10 seconds, and try opening it again. Continue until there is positive outward gas flow from the vent valve.

6.6 Regulate the transfer rate by maintaining a low positive pressure on the storage dewar. If initially cooling down the PCS Test dewar, the transfer rate should be slow, with the gas tank's regulator pressure set to well below 1 psig.

6.7 If needed, aid the flow of LHe from the storage dewar by attaching a helium gas tank (with regulator) to the S-V2 port. Set the regulator outlet pressure to zero. Open S-V2. Slowly start flow LHe through transfer line. When the plume looks like a small flame, carefully insert the transfer line into the PCS Test Dewar LHe fill port.

6.8 Confirm that gas is venting out of the PCS Test Dewar vent valve.

6.9 Ensure that temperature critical parts on the top of the PCS Test dewar (such as the rubber o-rings on the vacuum fitting and relief valves) do not get too cold. Use a hand held heat gun to maintain proper temperature.

6.10 ***When the vent plume suddenly increases indicating that the PCS Test dewar is full to the desired level perform the following steps. Check the Liquid Level Detector to ensure that the vacuum chamber inside the PCS Test Dewar is submerged under helium.***

6.11 ***Perform the following steps to remove the transfer line, out of the PCS Test Dewar and the Supply Dewar.***

6.12 Close SV-2 and valve off and remove the GHe tank from the outlet of S-V2 if present.

6.13 Slowly open S-V2 to lower the pressure. Don't allow the pressure to drop to zero; it's important to keep gas flowing outward to prevent an air plug inside the supply dewar. Stand clear of the cold venting gas.

6.14 Partially close the PCS Test Dewar vent valve so that very little gas is venting from it.

6.15 Remove the transfer line from the PCS Test dewar and immediately cap the PCS Test dewar fill port. **Note that the line will be very cold and should be kept away from exposed skin and clothing.**

6.16 Uncouple the 1/2” quick connect seal to the transfer line at the top of the LHe Supply dewer.

6.17 Slowly slide the transfer line up out of the LHe Supply dewer. **Note that the line will be very cold and should be kept away from exposed skin and clothing.**

6.18 When the transfer line has been removed from the LHe Supply dewer and hung in its safe storage location, close S-V3.

6.19 Close S-V2 and open S-V1.

6.20 Check the liquid helium level in the PCS Test dewar using the liquid level detector.

6.21 Make sure that the the PCS Test Dewar Helium Chamber Relief Valves at the top of the PCS Test dewar cryostat are functional and make sure the Helium Relief Valves are closed.

7 Conducting Experiment (Figure 3 and Figure 4)

During the operation of the experiment, helium is nominally pumped from the PCS Test Dewar through the experiment assembly in the vacuum chamber and out the exit port of the PCS Test Dewar cryostat into a vented hood. The maximum mass flow rate of helium will be about 12g/s. This volumetric flow rate at around 4-5 K as a vapor is about 0.6 liters/second and as a liquid is about 0.1 liters/second. [***Step 3.3***] See Figure 3 to get an indication of the geometry of the experiment and the PCS Test Dewar. Ensure that the vented hood has the capability to accept and withdraw the above flow rate.

7.1 Increase the flow rate in the experiment by using the pump drive control.

7.2 Monitor the thermodynamic condition of the flow by reading the Temperature ($T_{Ven\text{-}F\text{-}In}$) and Absolute Pressure (P_{Venl}) just prior to the Venturi

7.3 Control the flow rate in the experiment by reading the Differential Pressure across the Venturi (ΔP_{Ven}). Use the spreadsheet CLVHE Experiment.xls to determine the mass flow rate from ΔP_{Ven}. This is how the Reynolds number for the flow is set.

7.4 Monitor the thermodynamic condition of the flow after the Venturi and before the Pre-Heater by reading the Temperature ($T_{PH\text{-}f\text{-}In}$) and Absolute Pressure on Pressure Channel (P_{PH})

7.5 Calculate the Required Heater Power to reach the desired Quality in the Pre-Heater.

7.6 Use the KEPCO Power supply to input the appropriate power into the Pre-Heater Section for the desired flow quality.

7.7 Wait for the temperature readings on Pre-Heater Thermometers ($T_{PH\text{-}W\text{-}Control}$ and $T_{PH\text{-}W}$) to reach equilibrium. If $T_{PH\text{-}W\text{-}Control}$ reads a temperature greater than 100 K, the Pre-Heater will should be shut down.

7.8 Monitor the thermodynamic condition of the flow after the Pre-Heater and before the Test-Section by reading the Temperature ($T_{TS\text{-}F\text{-}In}$) and Absolute Pressure (P_{TS1})

7.9 Monitor the power input needed in the Test Section to maintain the temperature recorded ($T_{TS\text{-}W}$ and $T_{TS\text{-}W\text{-}Control}$ at 0.5 K above $T_{TS\text{-}F\text{-}In}$. This power input and temperature difference will be used to calculate the heat transfer coefficient for the Reynolds number and Flow Quality. If $T_{TS\text{-}W\text{-}Control}$ reads a temperature greater than10 K, the Test Section heater should be shut down.

7.10 Record the differential pressure drop between for the Test Section (ΔP_{TS}). This is the pressure drop for the Reynolds number and Flow Quality.

7.11 Monitor the thermodynamic condition of the flow after the Test Section ($T_{TS\text{-}F\text{-}Out}$) and Absolute Pressure ($P_{TS2} = P_{TS1} - \Delta P_{TS}$). Make sure that fluid is not superheated.(i.e. make sure that $T_{TS\text{-}F\text{-}Out} > T_{saturation} @ P_{TS2}$), unless heat transfer properties are being investigated at a quality =1.

7.12 During the experiment make sure that temperature critical parts on the top of the PCS Test dewar (such as the rubber o-rings on the vacuum fitting and relief valves) do not get too cold. Use a hand held heat gun to maintain proper temperature.

8 Post Experiment Procedure

8.1 Slow the pump so that there is a low flow of helium out into the vent hood

8.2 Put a relief valve on at the end of the hose from the exit port to the vent hood to prevent back flow of air into the experiment.

8.3 Shut down the pump

9 Storage Dewar Liquid Level Measurement

9.1 **Ensure that operators have proper protective equipment: one glove and eye protection.**

9.2 Obtain a “Thumper” (device which uses the thermoacoustic oscillation (TAO) observed in gases spanning a large factor in absolute temperature). Make sure it is long enough to reach the bottom of the storage dewar.

9.3 Slowly open S-V2 while standing away from the venting gas.

9.4 Open S-V3.

9.5 Insert the Thumper into the storage dewar until it touches the bottom of the helium tank. Mark this position. (A convenient way to mark the thumper tube is to attach an alligator clip at the top of the storage dewar transfer port above S-V3.)

9.6 Cover the top of the Thumper with a thumb either directly or over an elastomeric diaphragm (such as a finger cot or part of a balloon).

9.7 Raise the thumper slightly off the bottom of the tank and note the frequency of the oscillations. Continue raising the thumper until the oscillation frequency suddenly increases. Localize this vertical location by slowly lowering and raising the thumper. Mark this position. Note that this position could be as much as 24” below the first mark, so allow personnel access to this higher location. If no change is seen then the dewar is probably empty.

9.8 Remove the thumper from the storage dewar and close S-V3 and S–V2. Verify that S-V1 is open.

9.9 Measure the distance between marks on the thumper and compare with the depth versus volume calibration on the storage dewar. This table is usually in inches vs. liters. This is the remaining liquid in the storage dewar. Note the volume of remaining liquid on the supply dewar's paper tag.

10 Removing LHe from PCS dewar back into supply dewar

In the event of an air plug liquid helium might have to be extracted back out from the PCS Test dewar and put into the supply dewar to assist in a more rapid warm up of the dewar to unplug the dewar without the risk of having large quantities of cryogen present in the PCS Test dewar. The strategy for extraction will depend on the location of the air plug.

10.1 Fluid Transfer from the experiment dewar to the Receiving LHe Supply Dewar

Make sure valve S-V1 is open in the ***Receiving*** LHe Supply dewar

10.1.1 Verify that the ***Receiving*** LHe Supply dewar compound pressure gauge reads approximately zero (atmospheric pressure). Note that light tapping of the gauge may be necessary to get an accurate reading. If it reads above zero, verify that the relief valve shut off valve, S-V1 is open. If it is not open, stand clear of the relief valve and slowly open S-V1 to relieve pressure in the tank.

10.1.2 Make sure that a rubber hose is attached from the vent port connected to S-V2 to a fume hood, to direct out the excess Helium vapor from the experiment.

10.1.3 Verify that in the ***Receiving*** LHe Supply dewar the vent valve, S-V2, is closed and transfer valve, S-V3 has a transfer line between the the ***Receiving*** LHe supply dewar and the PCS Test Dewar. If so, skip the next step.

10.1.4 For the ***Receiving*** LHe Supply dewer, if either S-V2 or S-V3 have been open or if there has been no transfer tube venting out helium vapor from the LHe supply dewar through the valve S-V3 for many minutes, it is possible that air may have condensed in the central tube, possibly blocking the transfer tube path into the storage dewar. Close S-V2 and S-V3 and proceed to ***Addendum 3: "Troubleshooting a Possibly Plugged Supply Dewar."***

10.2 Raise the transfer tube

10.3 ***The helium may be pumped out of the exit port side with a pump or the fill port side by pressurizing with gaseous helium. If the air plug is downstream of the pump then the helium will have to be extracted from the fill port side. If the air plug is upstream of the pump (such as in the fill port side) then the pump can be used to extract the liquid from the PCS Test dewar.***

10.3.1 ***If the helium is being extracted out of the fill port side of the PCS test dewar then the test dewar can be pressurized from the dewar helium purge valve and the cryogen can be extracted using a transfer line placed inside the fill port. The flow rate can be monitored using the liquid level detectector. Crack SV2, verify flow outward, then open SV2 to maintain a small flow impedence.***

10.3.2 ***If the helium is being extracted out of the exit port side of the PCS test dewar, start a slow flow of Helium through the transfer line by pumping helium through the experiment at a low rate. The flow rate can be monitored using the venturi pressure***

drop and the liquid level detector as described in Step 3. Crack SV2, verify flow outward, then open SV2 to maintain a small flow impedence.

10.4 During the experiment make sure that temperature critical parts on the top of the PCS Test dewar (such as the rubber o-rings on the vacuum fitting and relief valves) do not get too cold. Use a hand held heat gun to maintain proper temperature.

Addendum 1: Emergency Procedures

1. In case of a cryogen spill that does not trigger the Oxygen (O_2) monitor alarm:
All personnel working in the area shall move away from the immediate area of the spill and stay away until the cryogen has evaporated and the area has sufficiently warmed

2. If the oxygen monitor alarm sounds:
Stop the flow of cryogens and all personnel working in the area shall leave the area until the alarm ceases. If the alarm does not cease in a reasonable amount of time, contact the lab Manager and notify the appropriate Branch staff. A no-entry sign shall be posted at entrances to the area and shall remain in place until the area is deemed safe to return. The Lab Manager will check the area for good ventilation and safe oxygen level using a separate O2 monitor and will confirm that the cause of the problem is no longer an issue

3. If the fire alarm sounds during cryogen testing:
Personnel shall shut off flow of cryogens and make an attempt at precluding the backflow of air onto cold surfaces before evacuating the area.

4. In the case of personnel injury (cryo burns, etc.):

Immediately take the injured personnel to the Health Facility, or call 911 if the situation requires it.

Addendum 2: Hazard Analysis Checklist

The following checklist identifies the hazards associated with cryogenic systems, and itemizes the required steps to mitigate the hazards. The hazard assessment for cryogenic systems can be completed by indicating compliance with controls for each relevant class of hazards.

Asphyxiation (applicable to all systems using solid or liquid cryogens)

- ❑ Oxygen monitors are located in the work area and properly calibrated
- ❑ Work areas are properly ventilated to regularly refresh room air, especially during periods of cryogen transfer
- ❑ Procedures limit the generation of boiloff gas to levels that maintain safe oxygen levels

Exposure to cold (applies to the handling of solid or liquid cryogens, or cryogenically cooled components)

- ❑ Personal protective equipment is readily available and used during operations, and operators are instructed in proper clothing requirements
- ❑ Procedures for handling cryogens are written, and cryogen tank vents are configured to minimize the possibility that cold gas or liquid venting from the dewar will impinge on personnel or sensitive surfaces (includes both nominal and emergency situations)

Trapped Volumes (applicable to all cryogenic systems)

- ❑ All cryogen tanks have redundant vent paths (For tanks with a single fill/vent port, the port shall have an insert that provides two independent paths along the portion of the vent that is warmer than the triple point of air [65 K].)
- ❑ All fill/vent paths are equipped with pressure relief devices or flow restrictors that prevent the backflow of air into the tank
- ❑ All volumes within the cryogenic system that operate at sub-atmospheric pressures have passive pressure relief devices. (Exceptions can be made for volumes specifically designed for high pressure.) (Note that cryocooler manufacturers provide pressure relief for the internal volumes of the cold head, so this volume need not be considered.)

Combustion (applies to non-combustible cryogens; combustible cryogens require separate certification and assessment)

- ❑ Formation of liquid air on cold external surfaces is prevented from dripping or splashing onto combustible materials.

Addendum 3: Troubleshooting a Possibly Plugged Supply Tank

- Wait several minutes after closing S-V2 and S-V3.
- Slowly open S-V2 while standing clear of any venting gas.
- If no gas is released, assume that the storage dewar is plugged. Close S-V2, verify that S-V1 is open and consult with Code 552 personnel on appropriate safety steps.
- If some gas is released reclose S-V2, wait several minutes, and slowly open S-V3 while avoiding the vent path.
- If no gas is released, reclose S-V3 and verify that S-V1 is open. The dewar probably has a plug in the central tube. This is a safe condition in that the dewar can still vent without overpressurization, however, transfer from this dewar will not be possible. Consult with Code 552 personnel on appropriate steps to remove the plug.
- If some gas is released a transfer may be attempted.

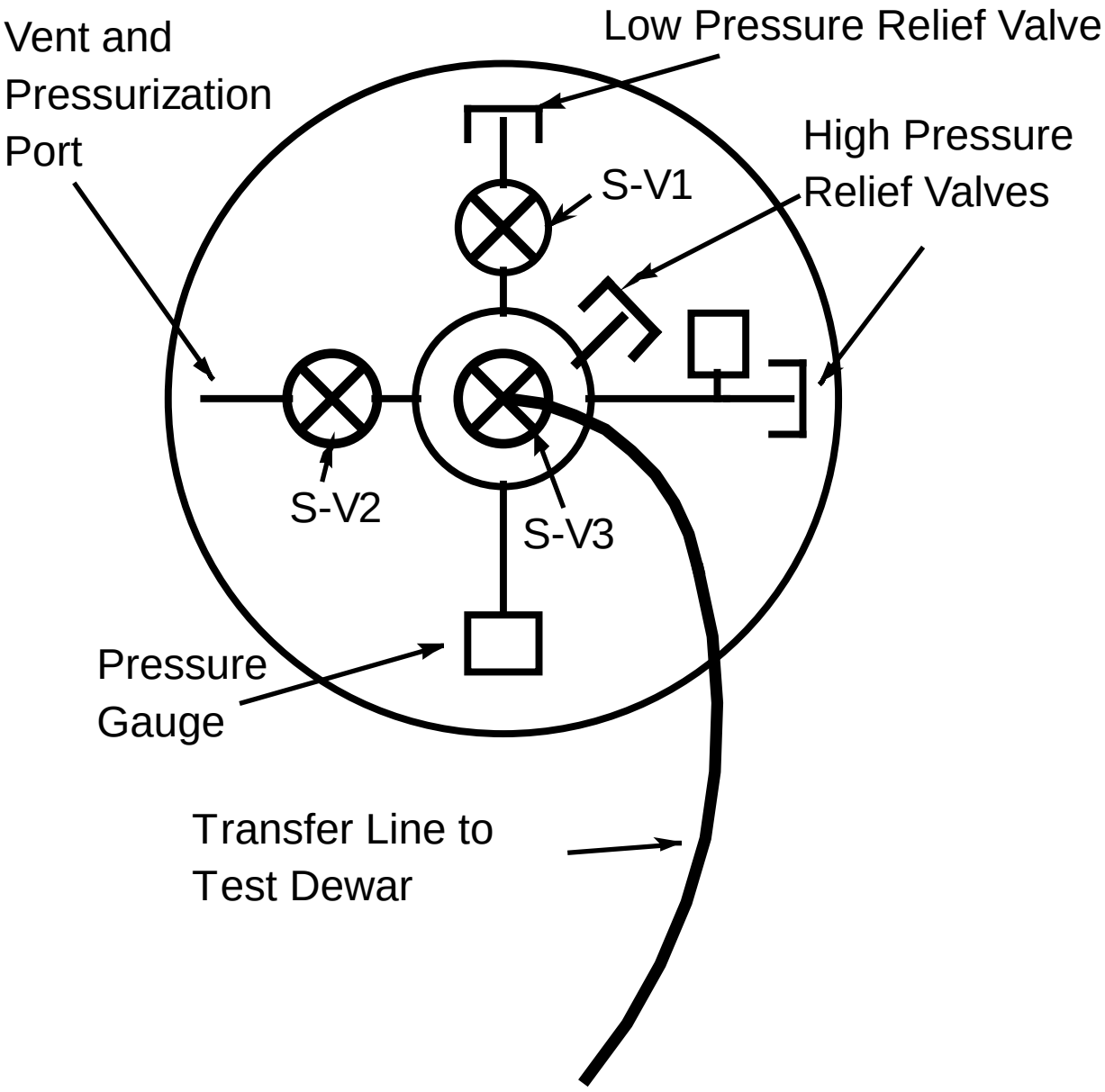

Figure 1. Schematic of 100 Liter LHe Storage Dewar

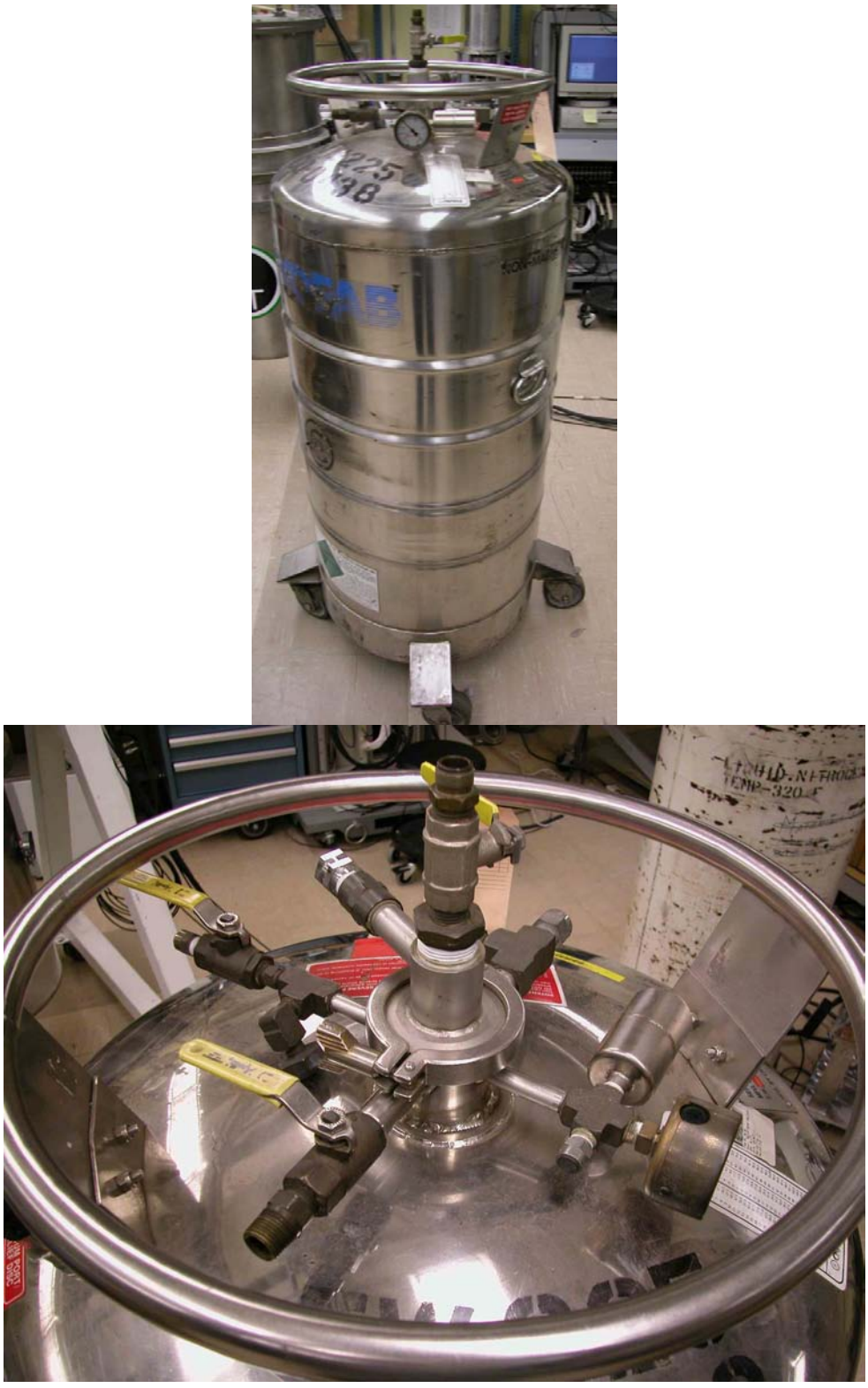

Figure 2. Typical 100 Liter LHe Storage dewar with detail of top.

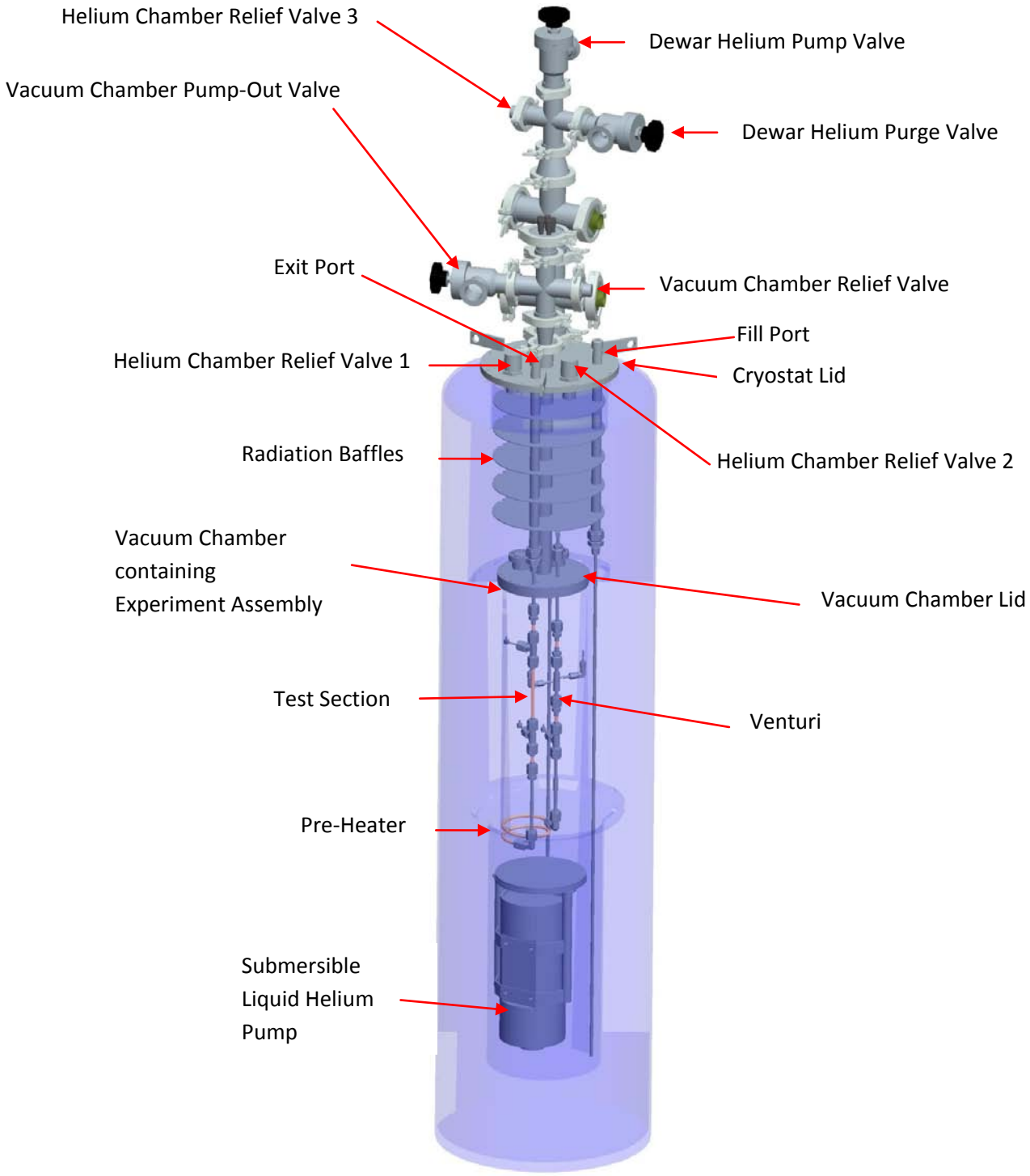

Figure 3. Two Phase Flow Parameters Experiment

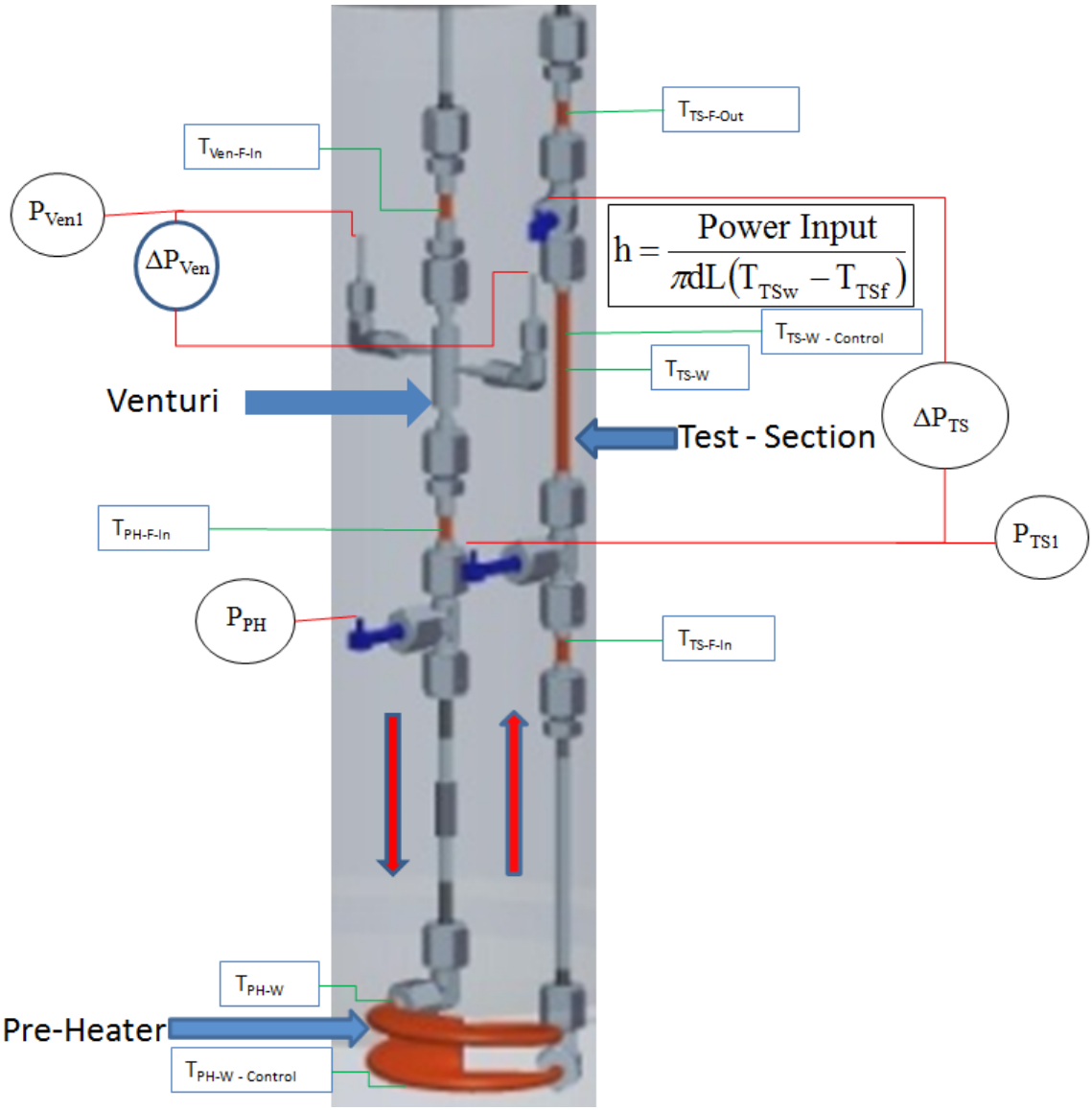

Figure 4. Experiment Instrumentation

References

1. Mustafi, S., et al, "Subcooling Cryogenic Propellants for Long Duration Space Exploration," AIAA2009-6584.

2. Mustafi, S., et al, "Subcooling for Long Duration In-Space Cryogenic Propellant Storage," AIAA2010-8869.

3. Flynn, T.M., *Cryogenic Engineering,2nd Edition*, Taylor & Francis, Boca Raton, FL, 2005.

4. Carey, V., *Liquid-Vapor Phase-Change Phenomena*, Taylor & Francis, Philadelphia, PA, 1992.

5. Barron, R., *Cryogenic Heat Transfer*, Taylor & Francis, Philadelphia, PA, 1999.

6. Van Dresar, N.T., Siegwarth, J., and M. Hassan, "Convective heat transfer coefficients for near-horizontal two-phase flow of nitrogen and hydrogen at low mass and heat flux," *Cryogenics* **41**, 805-811, 2002.

7. Van Dresar, N.T., and Siegwarth, J., *Near-Horizontal, Two-Phase Flow Patterns of Nitrogen and Hydrogen at Low Mass and Heat Flux*, NASA/TP-2001-210380, NASA Glenn Research Center, Cleveland, OH, 2001.

8. Liu, Z., and Winterton, R.H.S., "A general correlation for saturated and subcooled flow boiling in tubes and annuli, based on a nucleate pool boiling equation," *International Journal of Heat and Mass Transfer* **34**, 2759-2766, 1991.

9. Shah, M., "Prediction of heat transfer during boiling of cryogenic fluids flowing in tubes," *Cryogenics* **24**, 231-236, 1984.

10. Steiner, D., "Heat transfer during flow boiling of cryogenic fluids in vertical and horizontal tubes," *Cryogenics* **26**, 309-318, 1986.

11. Gungor, K.E., and Winterton, R.H.S., "A general correlation for flow boiling in tubes and annuli," *International Journal of Heat and Mass Transfer* **29**, 351-358, 1986.

12. Li, W., and Wu, Z.., "A general correlation for evaporative heat transfer in micro/mini-channels," *International Journal of Heat and Mass Transfer* **53**, 1778-1787, 2010

13. Klimenko, V.V., “A generalized correlation for two-phase forced flow heat transfer,” *International Journal of Heat and Mass Transfer* **31**, 2759-2766, 1991.

14. Klimenko, V.V., “Heat transfer intensity at forced flow boiling of cryogenic liquids in tubes,” *Cryogenics*, 569-576, 1982.

15. Keilin, V.E., Likov, V.V., Pozvonkov, M.M.,“Forced Convection heat transfer to liquid helium I in the nucleate boiling region,” *Cryogenics*, 141-145, 1975.

16. Ogato, H., Sato, S, “Forced Convection heat transfer to boiling helium in a tube,” *Cryogenics*, 375-380, 1974.

17. Rivetti, A., Martini, G., Birello, G., “LHe Venturi Flowmeters: Practical Design Criteria and Calibration Method,”*Cryogenics* **34** *ICEC Supplement*, 449-452, 1994.

18. Liang, S.C., “On the calculation of thermal transpiration,” *Canadian Journal of Chemistry*, 279-285, 1955.

19. Bennett, M.J.,Tompkins,F.C. “Thermal Transpiration: Application of Liang’s Equation,” *Canadian Journal of Chemistry*, 185-192, 1957.

20. Yazaki, T., et al, “Experiments on Thermally Driven Acoustic Oscillations of Gaseous Helium,” Journal of Low Temperature Physics Vol. **41**, 805-811, 1980.

21. Fuerst, J.D., “An Investigation of Thermally Driven Acoustical Oscillations in Heliu Systems,” *Fermi National Accelerator Laboratory, TM-1676*, Published in the proceedings of the *Low Temperature Engineering and Cryogenics Conference*, 1990

22. Gu, Y.F., Timmerhaus, K.D., “Damping criteria for thermal acoustic oscillations in slush and liquid hydrogen system,” *Cryogenics* **32**, 194-198, 1992.

23. Vaidyai, H.A., et al, “Numerical simulations of swirling pipe flows-decay of swirl and occurrence of vortex structures,” *13th European Turbulence Conference, IOP Journal of Physics: Conference Series* **318**, 2011.

24. Parchen, R.R., “Decay of Swirl in Turbulent Pipe Flows,” *Ph.D. Dissertation*, 1993.

25. Bald, W.B., Hands, B.A., “Cryogenic heat transfer research at Oxford Part 2 – Flow boiling,” *Cryogenics*, 179-197, 1974.

26. Coleman, H.G., Steele, W.G., *Experimentation Validation, and Uncertainty Analysis for Engineers, Third edition*, John Wiley & Sons, Inc., NJ, 2009.

27. Arp, V.D., McCarty, R.D., Friend, D.G., “Thermophysical Properties of Helium-4 from 0.8 to 1500K with Pressures to 2000 MPa,” *NIST Technical Note 1334 (revised)*, 1998.

28. McCarty, R.D., Arp, V.D., “A New Wide Range Equation of State for Helium,” *Advances in Cryogenic Engineering* **35**, 1465-1475, 1990.

29. Kathedar, H. Süsser, M., “Discharge Coefficient of a classical venturi tube for measuring liquid helium flow,” *Cryogenics* **29**, 1067-1069, 1989.

30 Hendricks, R.C., Simoneau, R.J., and Smith, R.V. *Survey of Heat Transfer to Near-Critical Fluids* , NASA/TN D-5886, NASA Lewis Research Center, Cleveland, OH, 1970.

31 Ohadi, M., Choo, K.., Dessiatoun, S., Cetegen, E. *Next Generation Microchannel Heat Exchangers, Third edition*, Springer., NY, 2013.